Density Model for Pilot Whales (*Globicephala spp.*) for the U.S. East Coast: Supplementary Report

Duke University Marine Geospatial Ecology Lab*

Model Version 4.3 - 2015-09-30

Citation

When referencing our methodology or results generally, please cite our open-access article:

Roberts JJ, Best BD, Mannocci L, Fujioka E, Halpin PN, Palka DL, Garrison LP, Mullin KD, Cole TVN, Khan CB, McLellan WM, Pabst DA, Lockhart GG (2016) Habitat-based cetacean density models for the U.S. Atlantic and Gulf of Mexico. Scientific Reports 6: 22615. doi: 10.1038/srep22615

To reference this specific model or Supplementary Report, please cite:

Roberts JJ, Best BD, Mannocci L, Fujioka E, Halpin PN, Palka DL, Garrison LP, Mullin KD, Cole TVN, Khan CB, McLellan WM, Pabst DA, Lockhart GG (2015) Density Model for Pilot Whales (*Globicephala spp.*) for the U.S. East Coast Version 4.3, 2015-09-30, and Supplementary Report. Marine Geospatial Ecology Lab, Duke University, Durham, North Carolina.

Copyright and License

Revision History

Version	Date	Description of changes
1	2014-09-01	Initial version.
2	2014-10-23	Added Palka (2006) survey-specific g(0) estimates. Updated distance to eddy predictors using Chelton et al.'s 2014 database. Removed distance to eddy predictors from shelf model; added distance to canyon predictor. Removed wind speed predictor from all models. Fixed missing pixels in several climatological predictors, which led to not all segments being utilized. Eliminated Cape Cod Bay subregion (combined it with Shelf).
3	2014-11-19	Reconfigured detection hierarchy and adjusted NARWSS detection functions based on additional information from Tim Cole. Removed CumVGPM180 predictor. Updated documentation.
4	2014-12-04	Fixed bug that applied the wrong detection function to segments NE_narwss_1999_widgeon_hapo dataset. Refitted model. Updated documentation.
4.1	2015-03-06	Updated the documentation. No changes to the model.
4.2	2015-05-14	Updated calculation of CVs. Switched density rasters to logarithmic breaks. No changes to the model.
4.3	2015-09-30	Updated the documentation. No changes to the model.

*For questions, or to offer feedback about this model or report, please contact Jason Roberts (jason.roberts@duke.edu)

Survey Data

Survey	Period	Length (1000 km)	Hours	Sightings
NEFSC Aerial Surveys	1995-2008	70	412	171
NEFSC NARWSS Harbor Porpoise Survey	1999-1999	6	36	2
NEFSC North Atlantic Right Whale Sighting Survey	1999-2013	432	2330	431
NEFSC Shipboard Surveys	1995-2004	16	1143	124
NJDEP Aerial Surveys	2008-2009	11	60	0
NJDEP Shipboard Surveys	2008-2009	14	836	0
SEFSC Atlantic Shipboard Surveys	1992-2005	28	1731	95
SEFSC Mid Atlantic Tursiops Aerial Surveys	1995-2005	35	196	0
SEFSC Southeast Cetacean Aerial Surveys	1992-1995	8	42	0
UNCW Cape Hatteras Navy Surveys	2011-2013	19	125	65
UNCW Early Marine Mammal Surveys	2002-2002	18	98	0
UNCW Jacksonville Navy Surveys	2009-2013	66	402	11
UNCW Onslow Navy Surveys	2007-2011	49	282	7
UNCW Right Whale Surveys	2005-2008	114	586	3
Virginia Aquarium Aerial Surveys	2012-2014	9	53	0
Total		895	8332	909

Table 2: Survey effort and sightings used in this model. Effort is tallied as the cumulative length of on-effort transects and hours the survey team was on effort. Sightings are the number of on-effort encounters of the modeled species for which a perpendicular sighting distance (PSD) was available. Off effort sightings and those without PSDs were omitted from the analysis.

Season	Months	Length (1000 km)	Hours	Sightings
All_Year	All	897	8332	909

Table 3: Survey effort and on-effort sightings having perpendicular sighting distances.

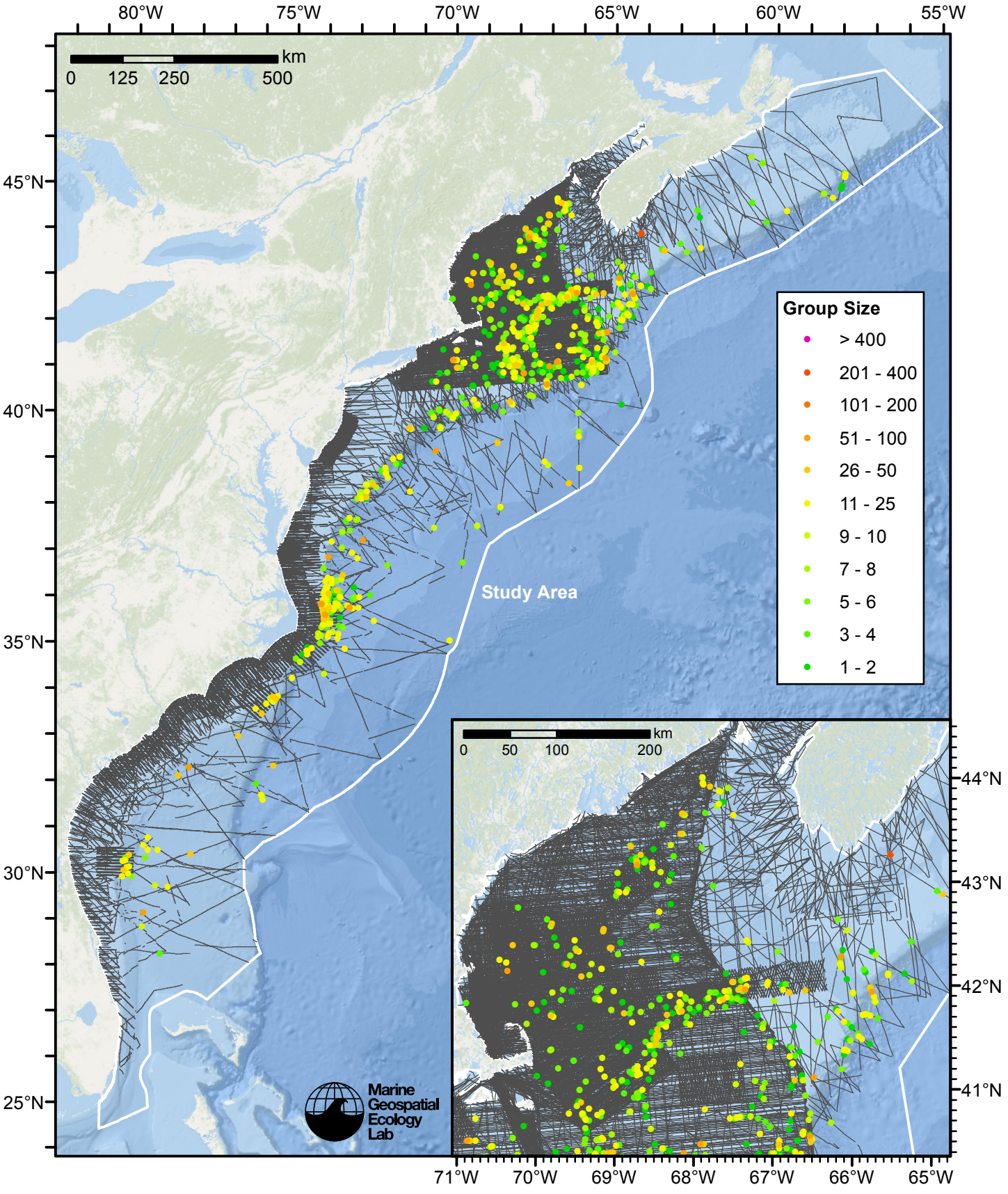

Figure 1: Pilot whales sightings and survey tracklines.

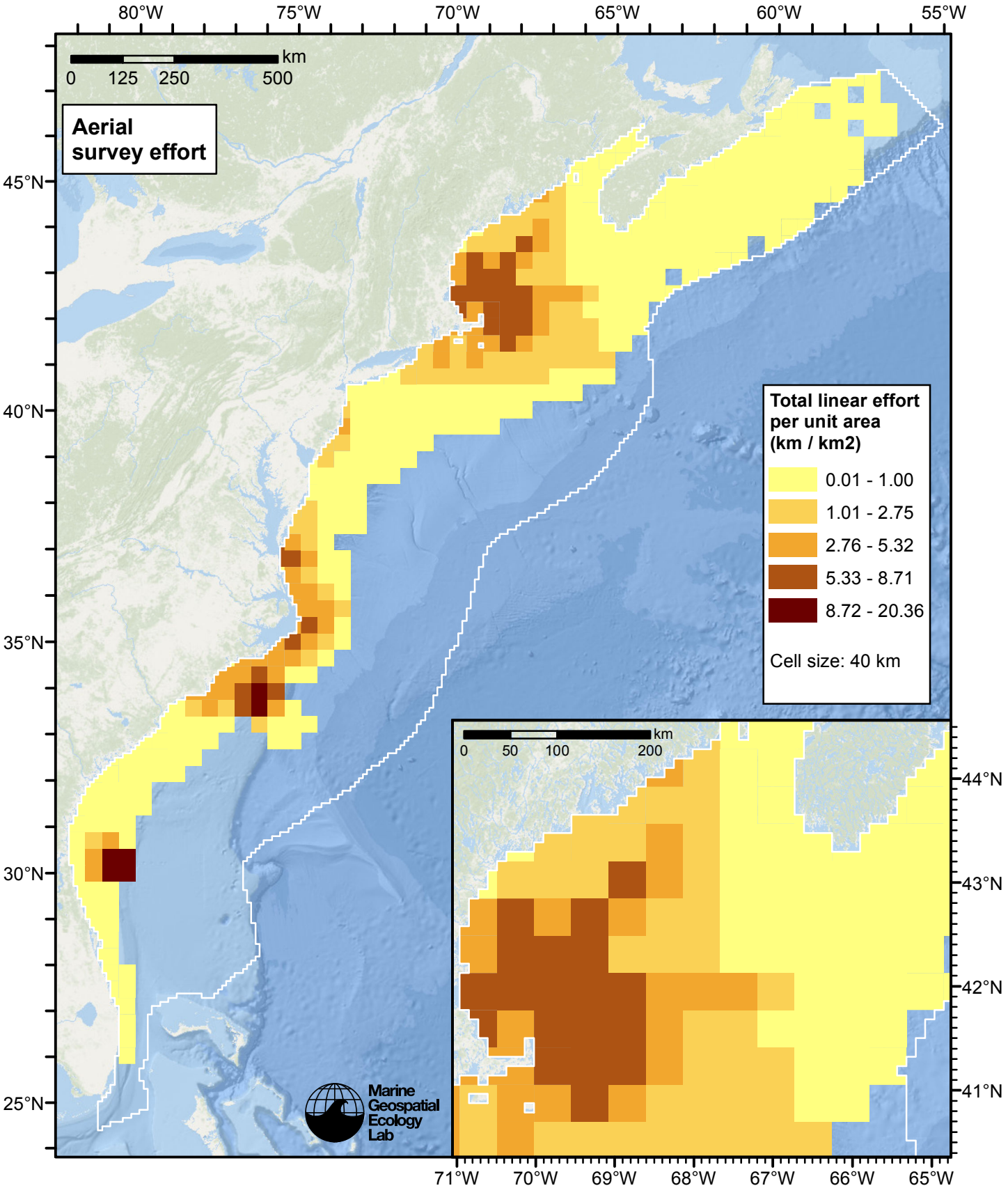

Figure 2: Aerial linear survey effort per unit area.

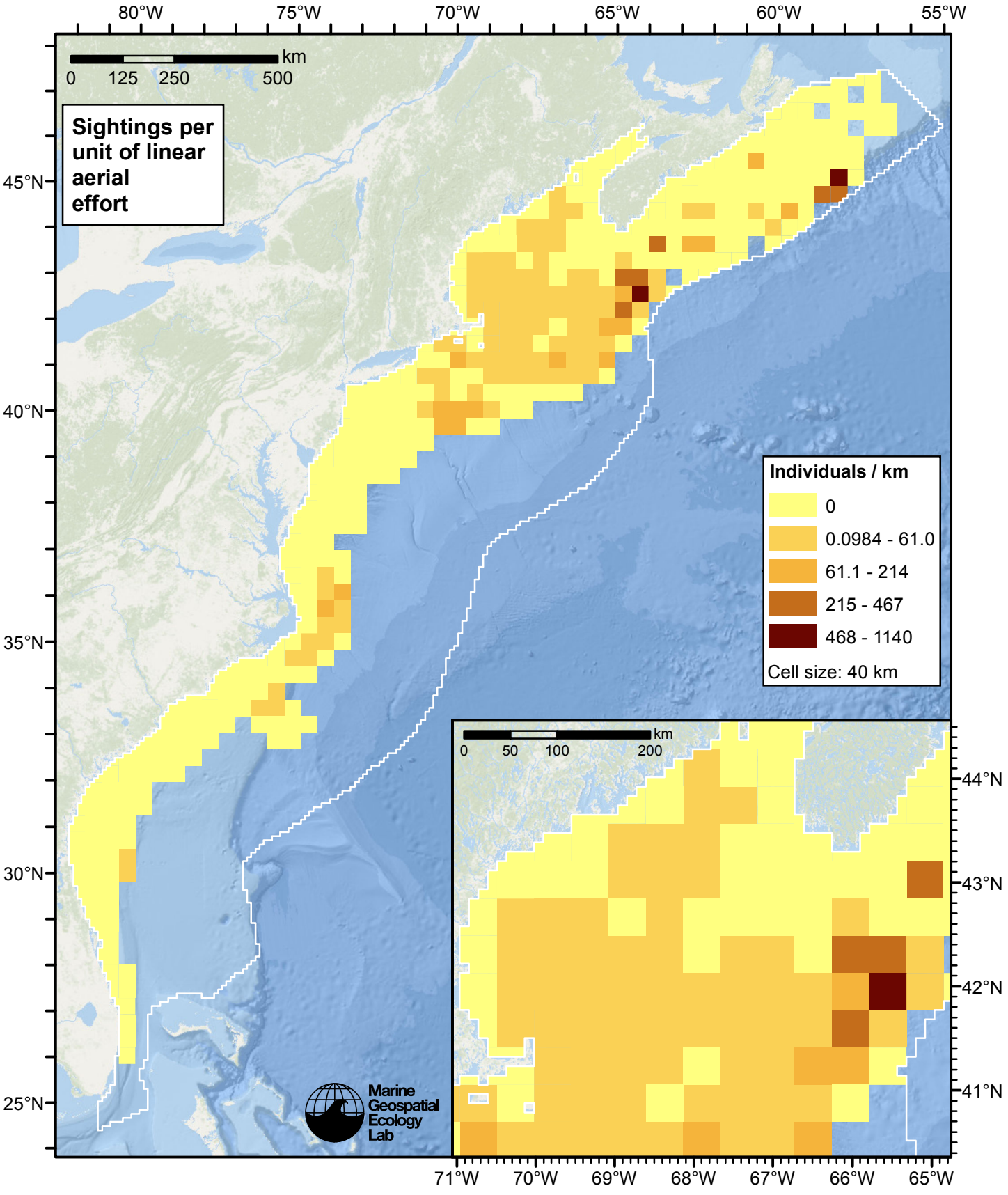

Figure 3: Pilot whales sightings per unit aerial linear survey effort.

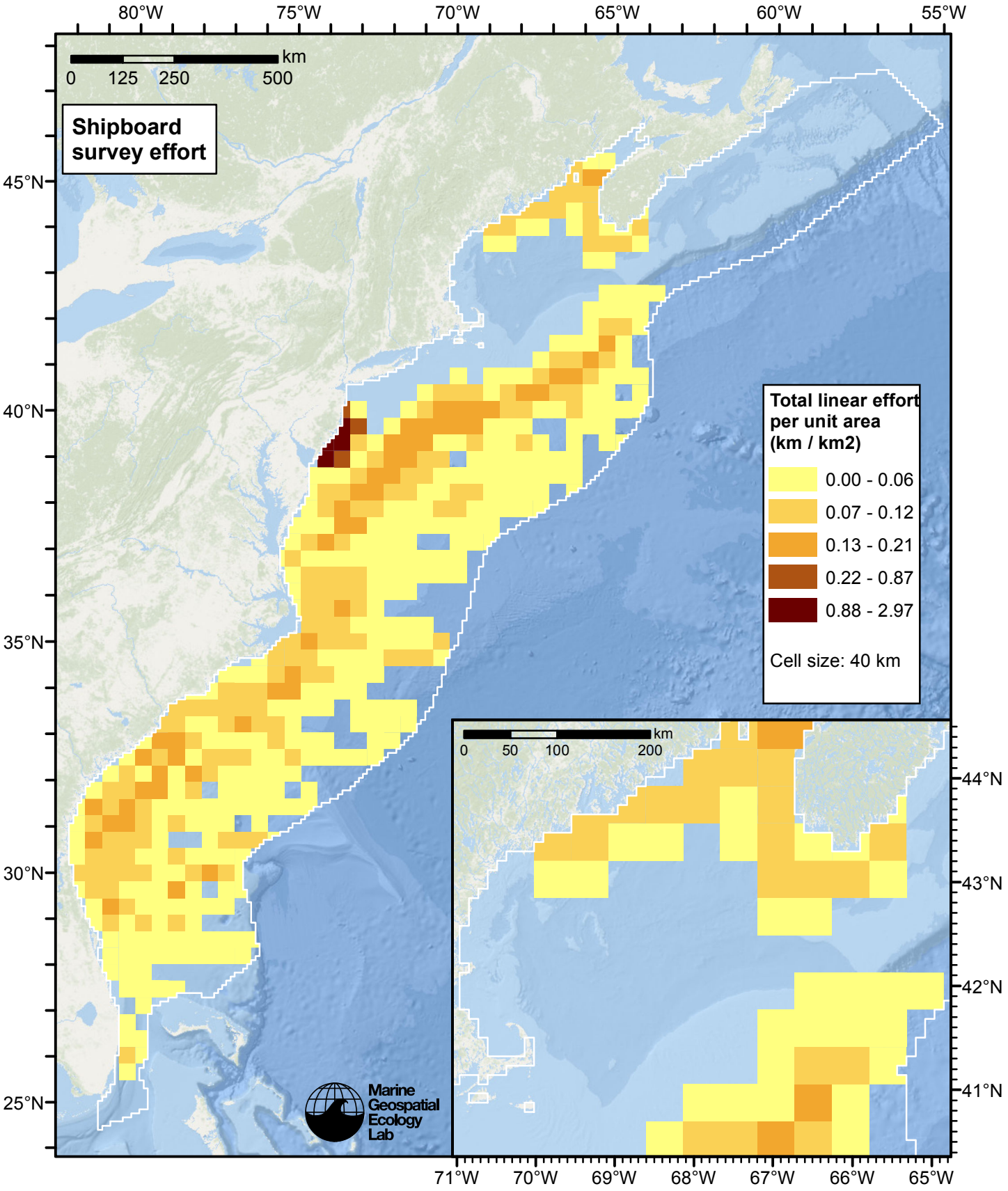

Figure 4: Shipboard linear survey effort per unit area.

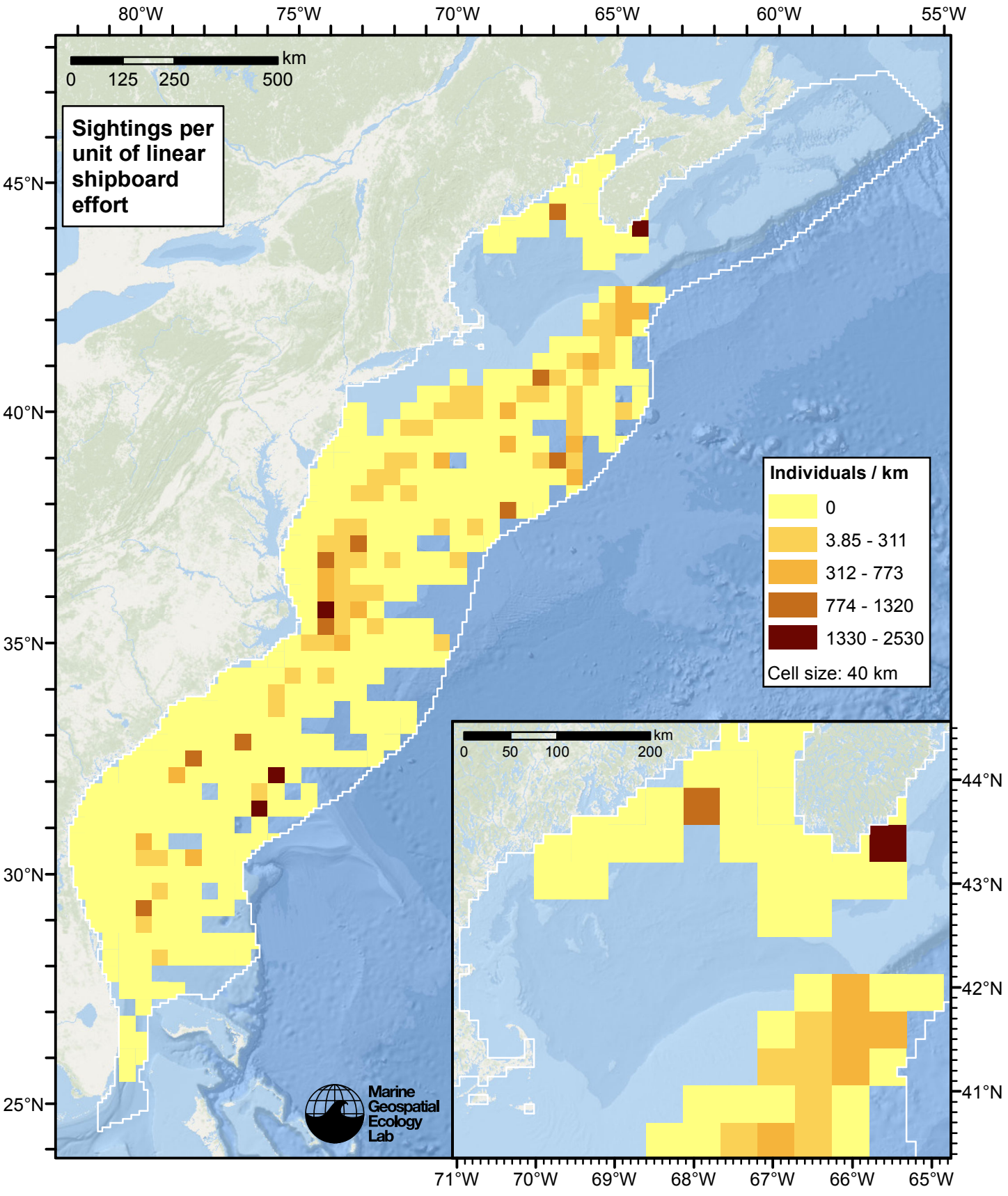

Figure 5: Pilot whales sightings per unit shipboard linear survey effort.

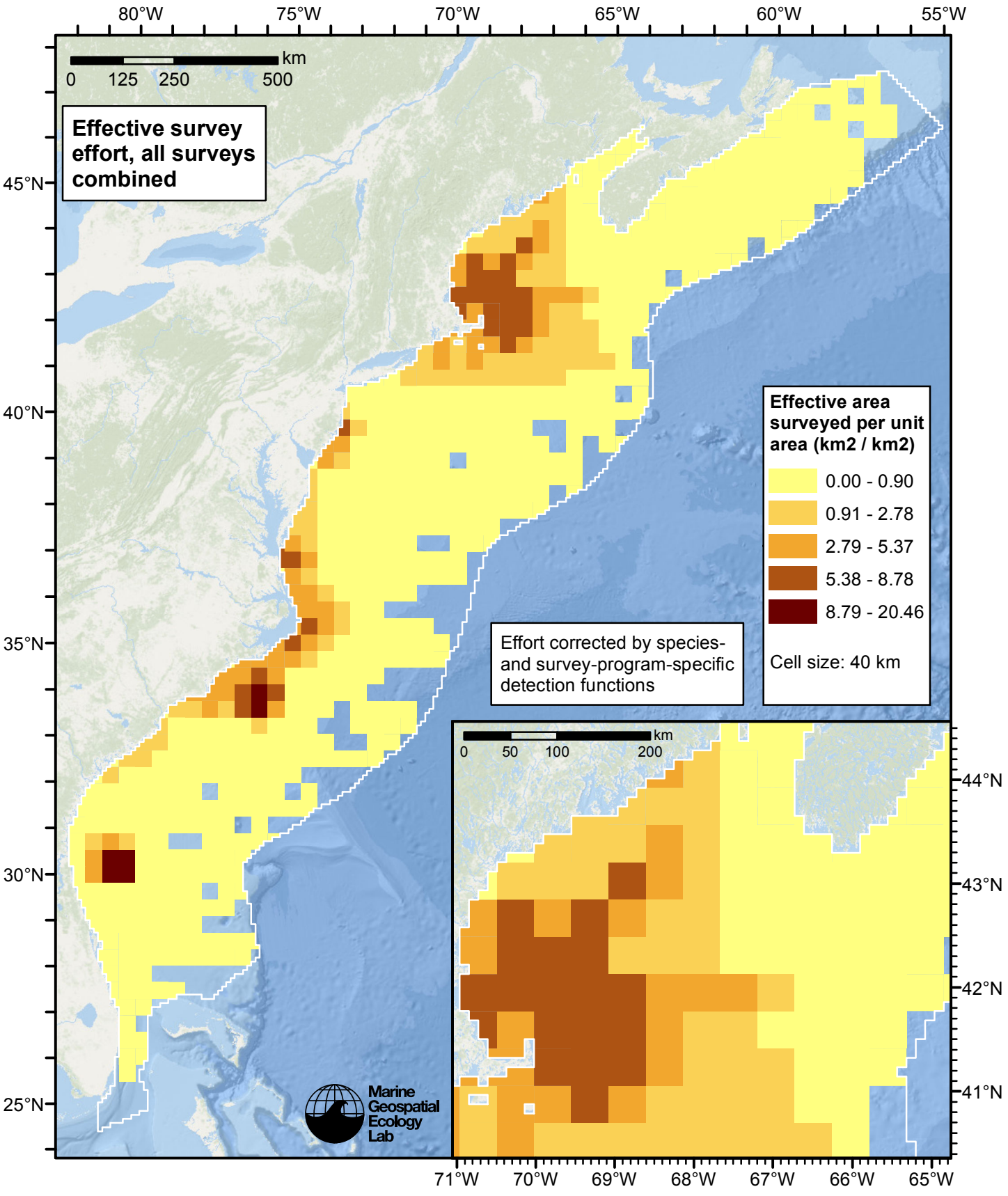

Figure 6: Effective survey effort per unit area, for all surveys combined. Here, effort is corrected by the species- and survey-program-specific detection functions used in fitting the density models.

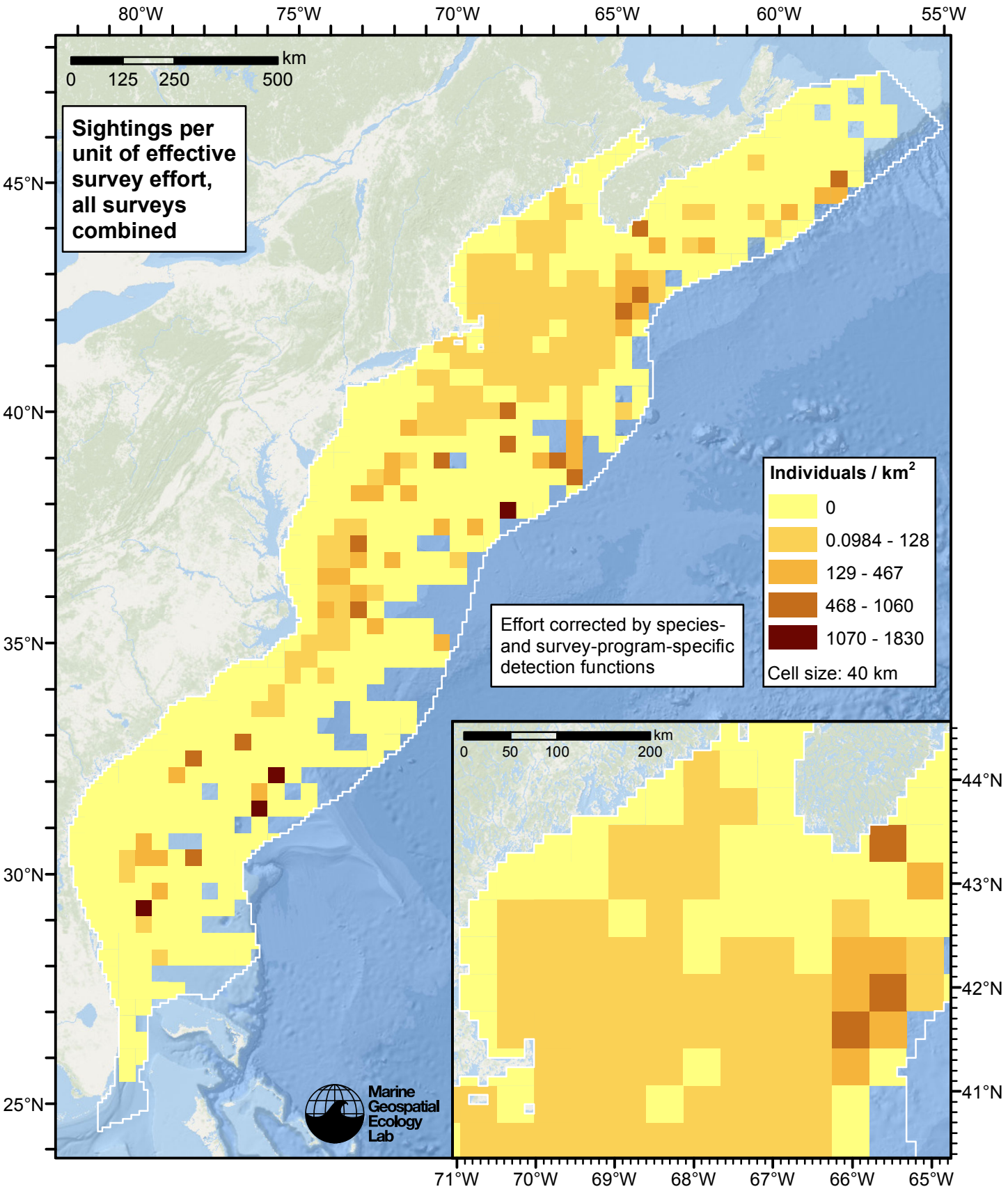

Figure 7: Pilot whales sightings per unit of effective survey effort, for all surveys combined. Here, effort is corrected by the species- and survey-program-specific detection functions used in fitting the density models.

Detection Functions

The detection hierarchy figures below show how sightings from multiple surveys were pooled to try to achieve Buckland et. al's (2001) recommendation that at least 60-80 sightings be used to fit a detection function. Leaf nodes, on the right, usually represent individual surveys, while the hierarchy to the left shows how they have been grouped according to how similar we believed the surveys were to each other in their detection performance.

At each node, the red or green number indicates the total number of sightings below that node in the hierarchy, and is colored green if 70 or more sightings were available, and red otherwise. If a grouping node has zero sightings–i.e. all of the surveys within it had zero sightings–it may be collapsed and shown as a leaf to save space.

Each histogram in the figure indicates a node where a detection function was fitted. The actual detection functions do not appear in this figure; they are presented in subsequent sections. The histogram shows the frequency of sightings by perpendicular sighting distance for all surveys contained by that node. Each survey (leaf node) recieves the detection function that is closest to it up the hierarchy. Thus, for common species, sufficient sightings may be available to fit detection functions deep in the hierarchy, with each function applying to only a few surveys, thereby allowing variability in detection performance between surveys to be addressed relatively finely. For rare species, so few sightings may be available that we have to pool many surveys together to try to meet Buckland's recommendation, and fit only a few coarse detection functions high in the hierarchy.

A blue Proxy Species tag indicates that so few sightings were available that, rather than ascend higher in the hierarchy to a point that we would pool grossly-incompatible surveys together, (e.g. shipboard surveys that used big-eye binoculars with those that used only naked eyes) we pooled sightings of similar species together instead. The list of species pooled is given in following sections.

Shipboard Surveys

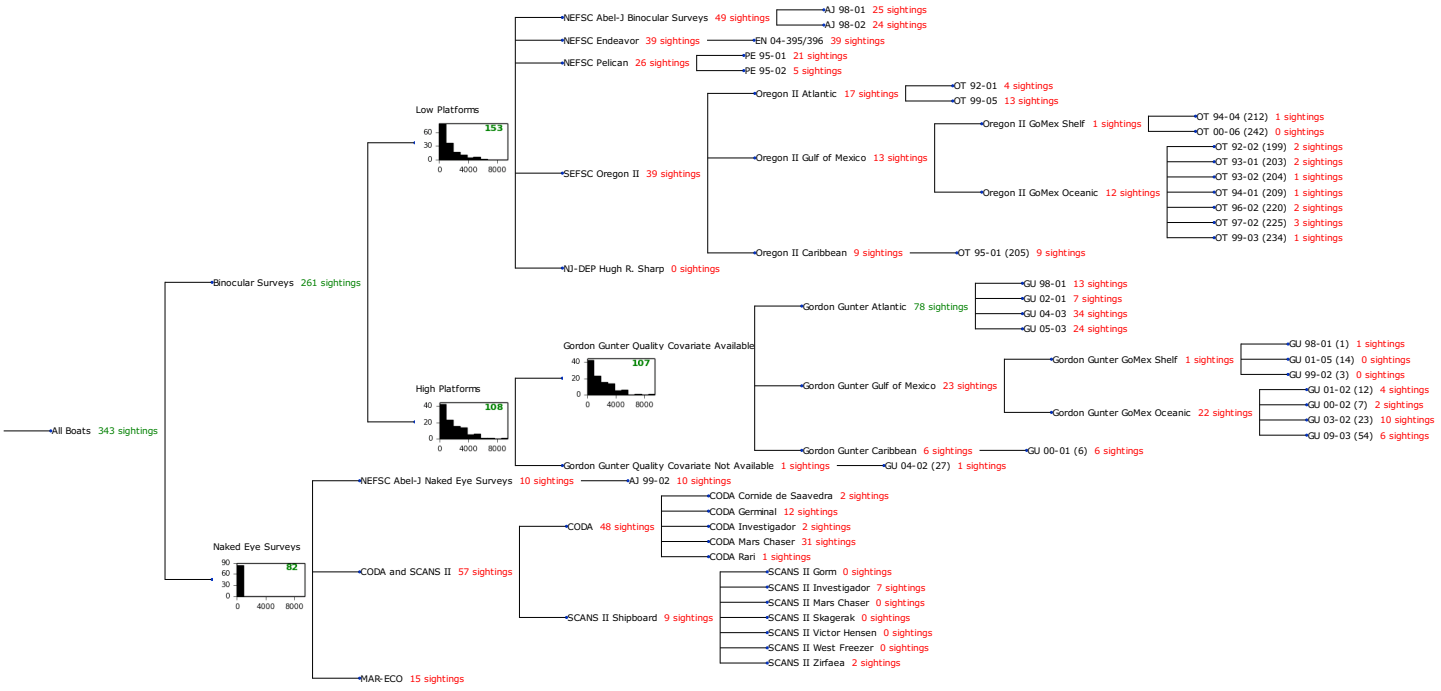

Figure 8: Detection hierarchy for shipboard surveys

Low Platforms

The sightings were right truncated at 7000m.

Covariate	Description

beaufort	Beaufort sea state.
size	Estimated size (number of individuals) of the sighted group.

Table 4: Covariates tested in candidate "multi-covariate distance sampling" (MCDS) detection functions.

Key	Adjustment	Order	Covariates	Succeeded	Δ AIC	Mean ESHW (m)
hr	poly	2		Yes	0.00	1685
hr	poly	4		Yes	0.12	1739
hr			beaufort	Yes	0.32	1804
hn	cos	2		Yes	0.86	1979
hr				Yes	1.07	1815
hr			beaufort, size	Yes	2.30	1801
hn	cos	3		Yes	2.87	1824
hn			beaufort	Yes	12.76	2408
hn				Yes	12.89	2415
hn	herm	4		Yes	14.72	2412
hr			size	No		
hn			size	No		
hn			beaufort, size	No		

Table 5: Candidate detection functions for Low Platforms. The first one listed was selected for the density model.

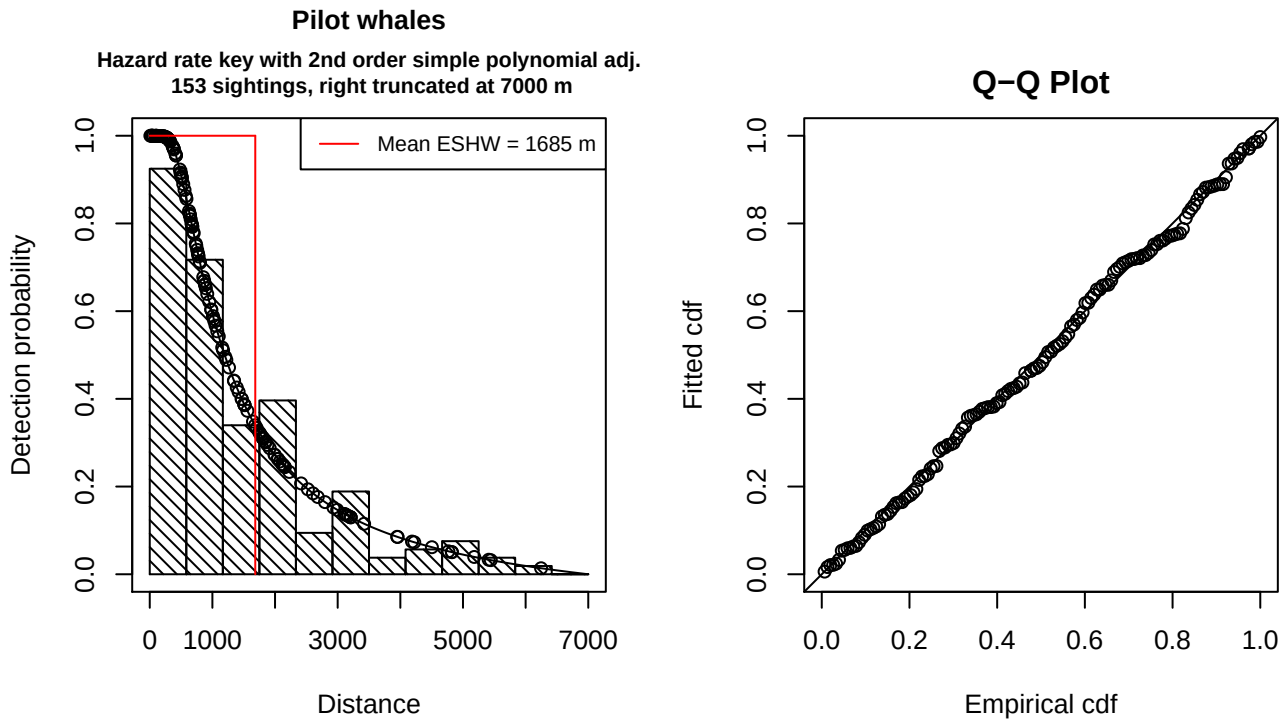

Figure 9: Detection function for Low Platforms that was selected for the density model

Statistical output for this detection function:

```
Summary for ds object
Number of observations :  153
Distance range         :  0  -  7000
AIC                    :  2525.03

Detection function:
 Hazard-rate key function with simple polynomial adjustment term of order 2

Detection function parameters
Scale Coefficients:
            estimate       se
(Intercept) 6.857564 0.2694695

Shape parameters:
             estimate        se
(Intercept) 0.3448006 0.2271376

Adjustment term parameter(s):
                estimate        se
poly, order 2 -0.9999998 0.2895039


Monotonicity constraints were enforced.
                       Estimate          SE        CV
Average p              0.2406467  0.03362653 0.1397340
N in covered region 635.7868377 99.49339784 0.1564886

Monotonicity constraints were enforced.
```

Additional diagnostic plots:

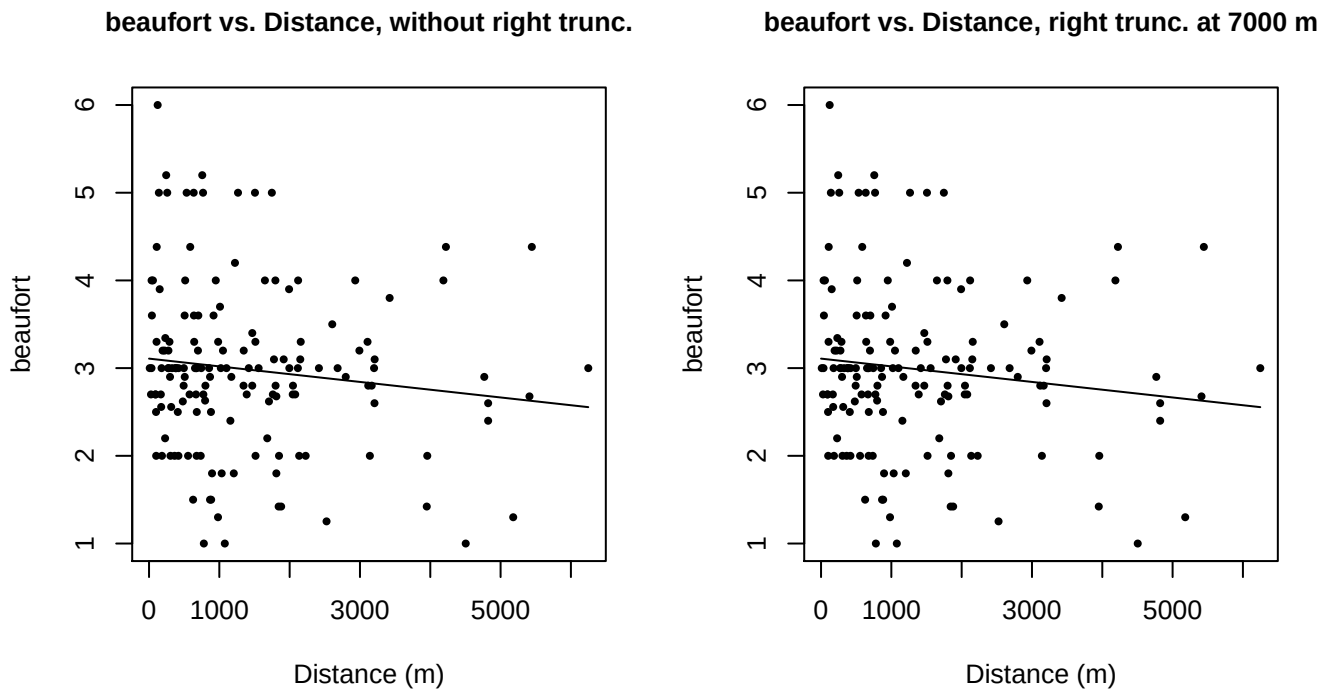

Figure 10: Scatterplots showing the relationship between Beaufort sea state and perpendicular sighting distance, for all sightings (left) and only those not right truncated (right). The line is a simple linear regression.

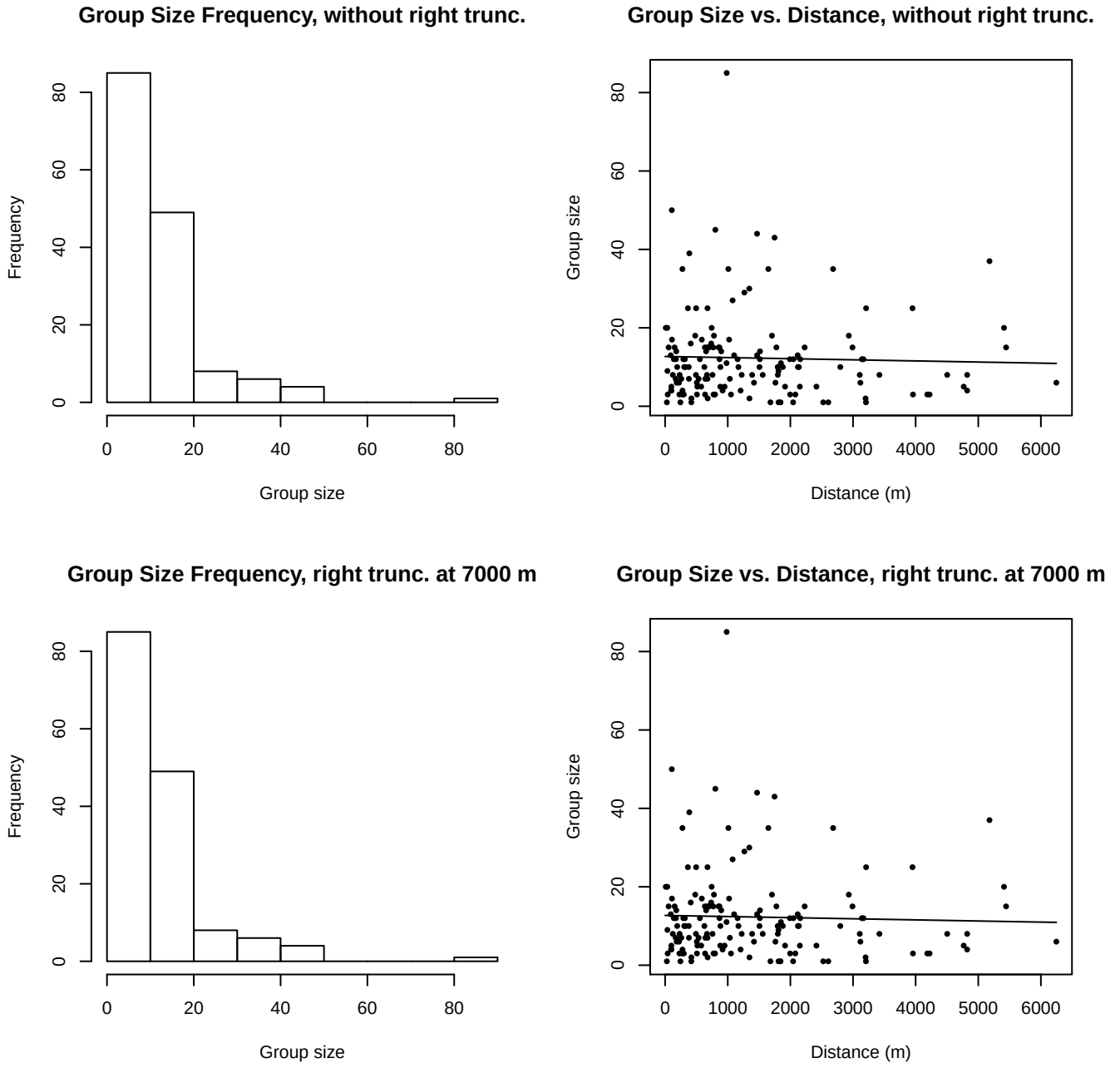

Figure 11: Histograms showing group size frequency and scatterplots showing the relationship between group size and perpendicular sighting distance, for all sightings (top row) and only those not right truncated (bottom row). In the scatterplot, the line is a simple linear regression.

High Platforms

The sightings were right truncated at 8000m.

Covariate	Description
beaufort	Beaufort sea state.
size	Estimated size (number of individuals) of the sighted group.

Table 6: Covariates tested in candidate "multi-covariate distance sampling" (MCDS) detection functions.

Key	Adjustment	Order	Covariates	Succeeded	Δ AIC	Mean ESHW (m)
hn			beaufort, size	Yes	0.00	2966
hn			beaufort	Yes	2.07	3008
hr			beaufort, size	Yes	9.84	3298
hr			beaufort	Yes	10.82	3450
hn			size	Yes	11.22	3031
hn	cos	3		Yes	16.30	2439
hr	poly	2		Yes	16.47	1910
hr			size	Yes	17.32	2828
hn	cos	2		Yes	17.90	2681
hr	poly	4		Yes	17.95	1994
hn				Yes	18.60	3042
hn	herm	4		Yes	20.54	3037
hr				Yes	21.05	2508

Table 7: Candidate detection functions for High Platforms. The first one listed was selected for the density model.

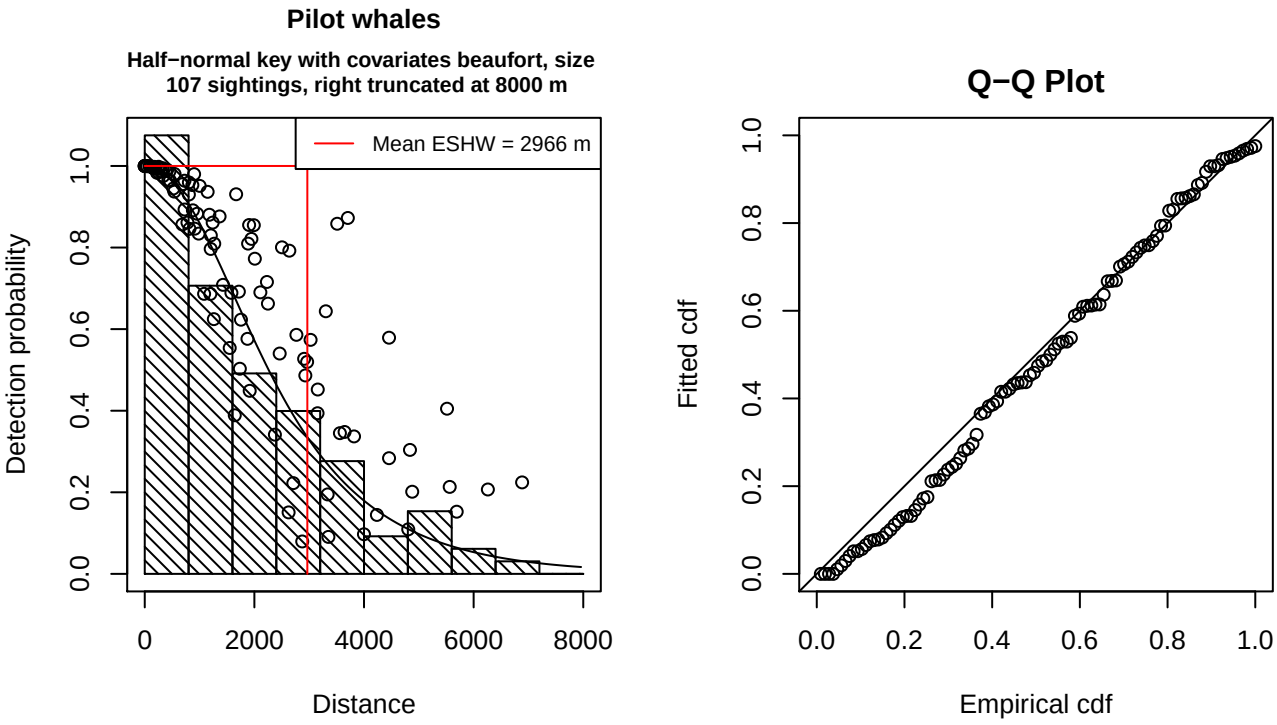

Figure 12: Detection function for High Platforms that was selected for the density model

Statistical output for this detection function:

```
Summary for ds object
```

```
Number of observations :  107
Distance range         :  0  -  8000
AIC                    :  1805.5

Detection function:
 Half-normal key function

Detection function parameters
Scale Coefficients:
              estimate         se
(Intercept)  8.0763226 0.27050263
beaufort    -0.2024908 0.06367844
size         0.1829904 0.10562413

                       Estimate          SE         CV
Average p             0.3286587  0.02660151 0.08093961
N in covered region 325.5657017 37.43191402 0.11497499
```

Additional diagnostic plots:

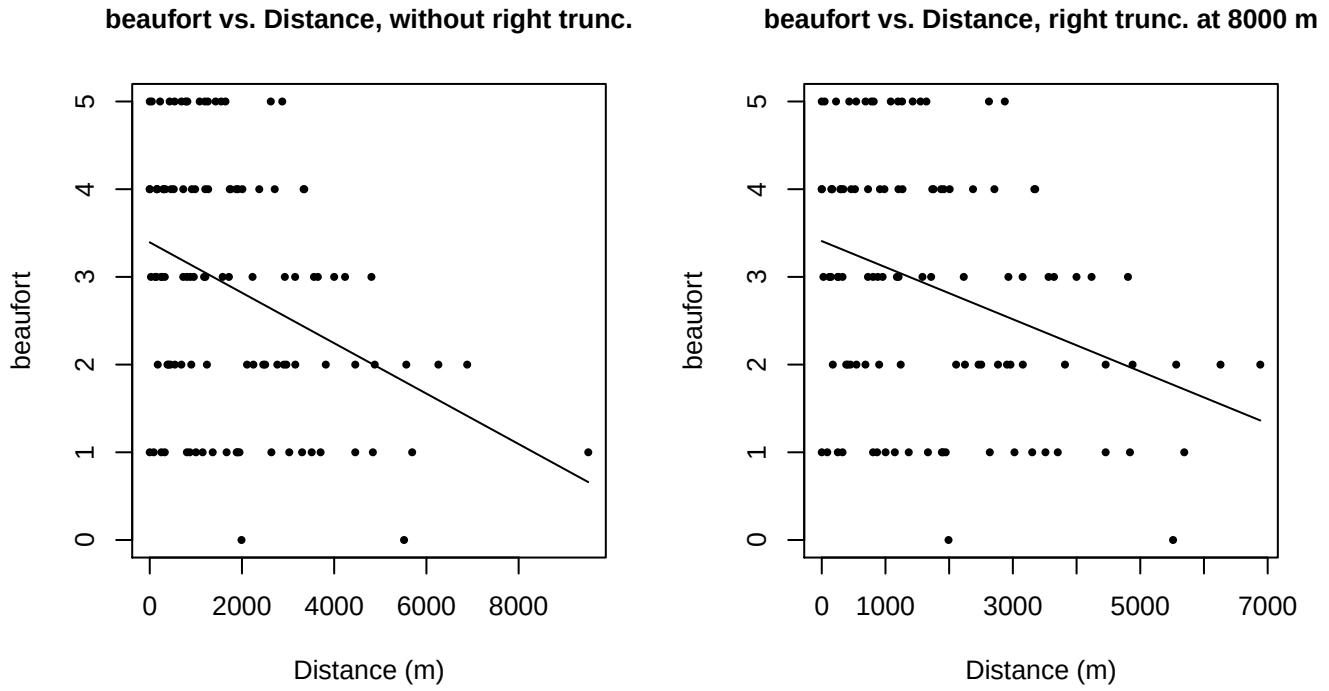

Figure 13: Scatterplots showing the relationship between Beaufort sea state and perpendicular sighting distance, for all sightings (left) and only those not right truncated (right). The line is a simple linear regression.

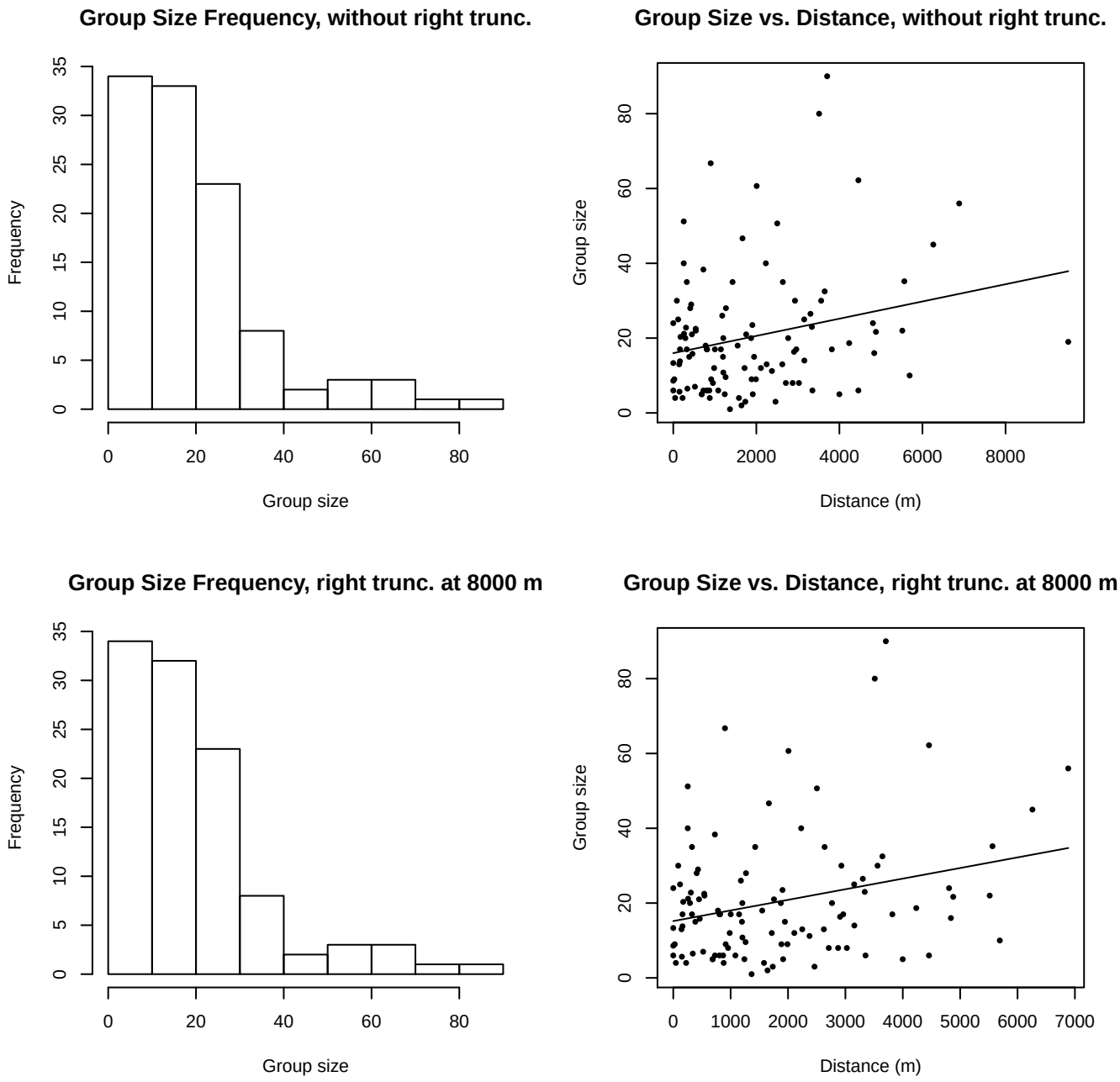

Figure 14: Histograms showing group size frequency and scatterplots showing the relationship between group size and perpendicular sighting distance, for all sightings (top row) and only those not right truncated (bottom row). In the scatterplot, the line is a simple linear regression.

Gordon Gunter Quality Covariate Available

The sightings were right truncated at 8000m.

Covariate	Description
beaufort	Beaufort sea state.
quality	Survey-specific index of the quality of observation conditions, utilizing relevant factors other than Beaufort sea state (see methods).
size	Estimated size (number of individuals) of the sighted group.

Table 8: Covariates tested in candidate "multi-covariate distance sampling" (MCDS) detection functions.

Key	Adjustment	Order	Covariates	Succeeded	Δ AIC	Mean ESHW (m)
hn			beaufort, quality	Yes	0.00	2858
hn			beaufort, size	Yes	0.44	2885
hn			beaufort, quality, size	Yes	0.56	2830
hn			beaufort	Yes	1.24	2911
hn			quality, size	Yes	3.88	2842
hn			quality	Yes	5.01	2873
hr			beaufort, quality, size	Yes	6.84	3482
hr			beaufort, quality	Yes	7.12	3556
hr			quality, size	Yes	9.41	3505
hr			beaufort, size	Yes	9.90	3269
hr			beaufort	Yes	9.97	3427
hn			size	Yes	11.48	2942
hr			quality	Yes	12.65	3382
hn	cos	3		Yes	14.41	2400
hr	poly	2		Yes	15.83	1867
hn				Yes	16.28	2955
hn	cos	2		Yes	16.42	2664
hr			size	Yes	17.39	2798
hr	poly	4		Yes	17.56	2062
hn	herm	4		Yes	18.23	2951
hr				Yes	20.48	2538

Table 9: Candidate detection functions for Gordon Gunter Quality Covariate Available. The first one listed was selected for the density model.

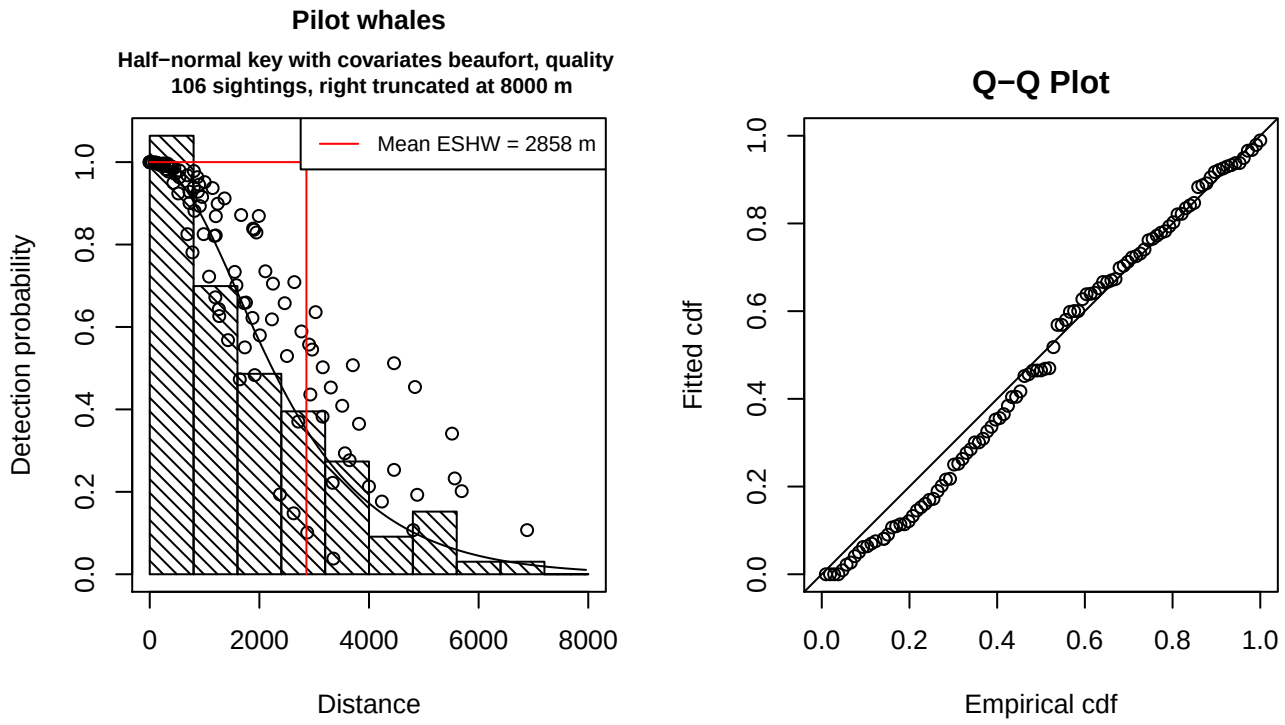

Figure 15: Detection function for Gordon Gunter Quality Covariate Available that was selected for the density model

Statistical output for this detection function:

```
Summary for ds object
Number of observations :  106
Distance range         :  0  -  8000
AIC                    :  1784.977

Detection function:
 Half-normal key function

Detection function parameters
Scale Coefficients:
             estimate         se
(Intercept)  8.4240449 0.21281649
beaufort    -0.1676876 0.07913117
quality     -0.1149824 0.06080005

                     Estimate          SE         CV
Average p            0.3222397  0.02598744 0.08064632
N in covered region 328.9476699 37.83382097 0.11501471
```

Additional diagnostic plots:

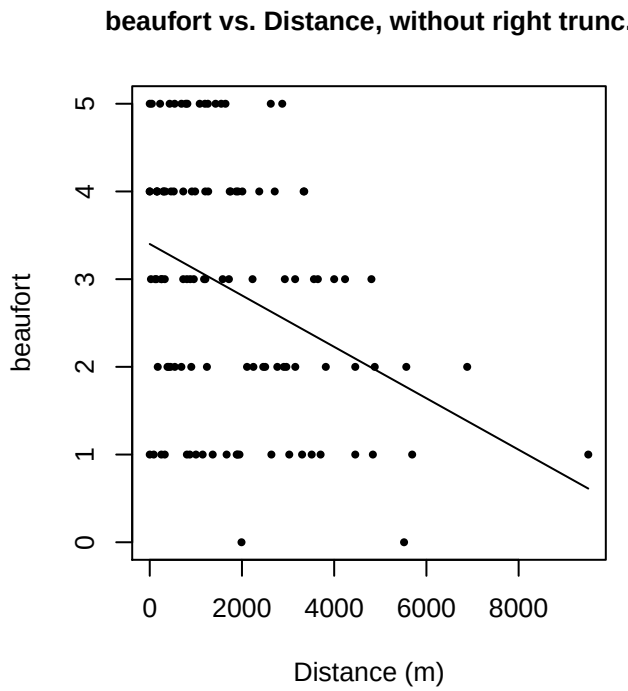

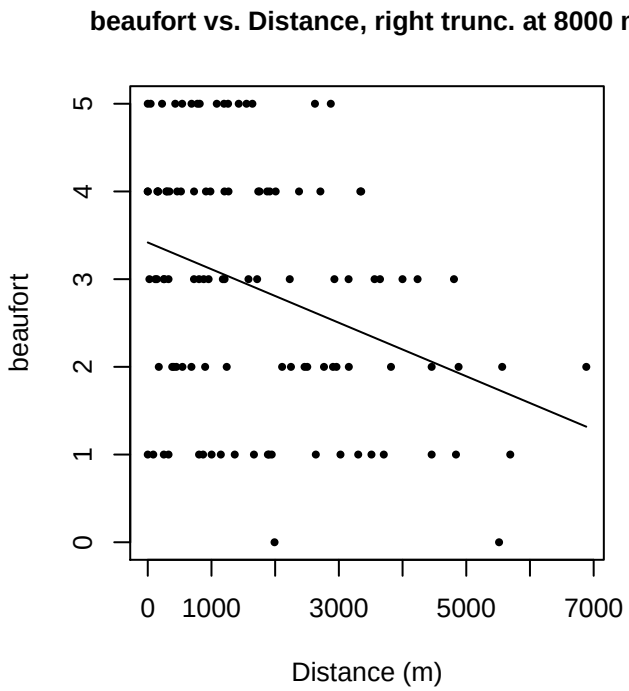

Figure 16: Scatterplots showing the relationship between Beaufort sea state and perpendicular sighting distance, for all sightings (left) and only those not right truncated (right). The line is a simple linear regression.

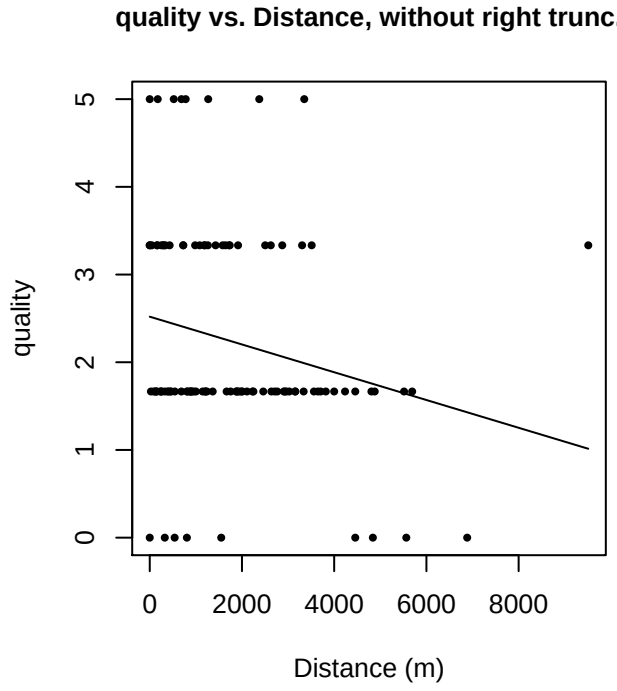

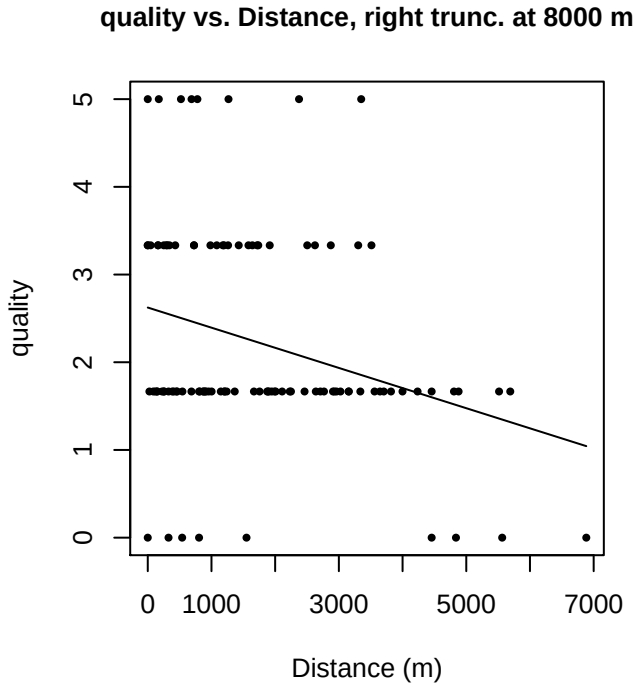

Figure 17: Scatterplots showing the relationship between the survey-specific index of the quality of observation conditions and perpendicular sighting distance, for all sightings (left) and only those not right truncated (right). Low values of the quality index correspond to better observation conditions. The line is a simple linear regression.

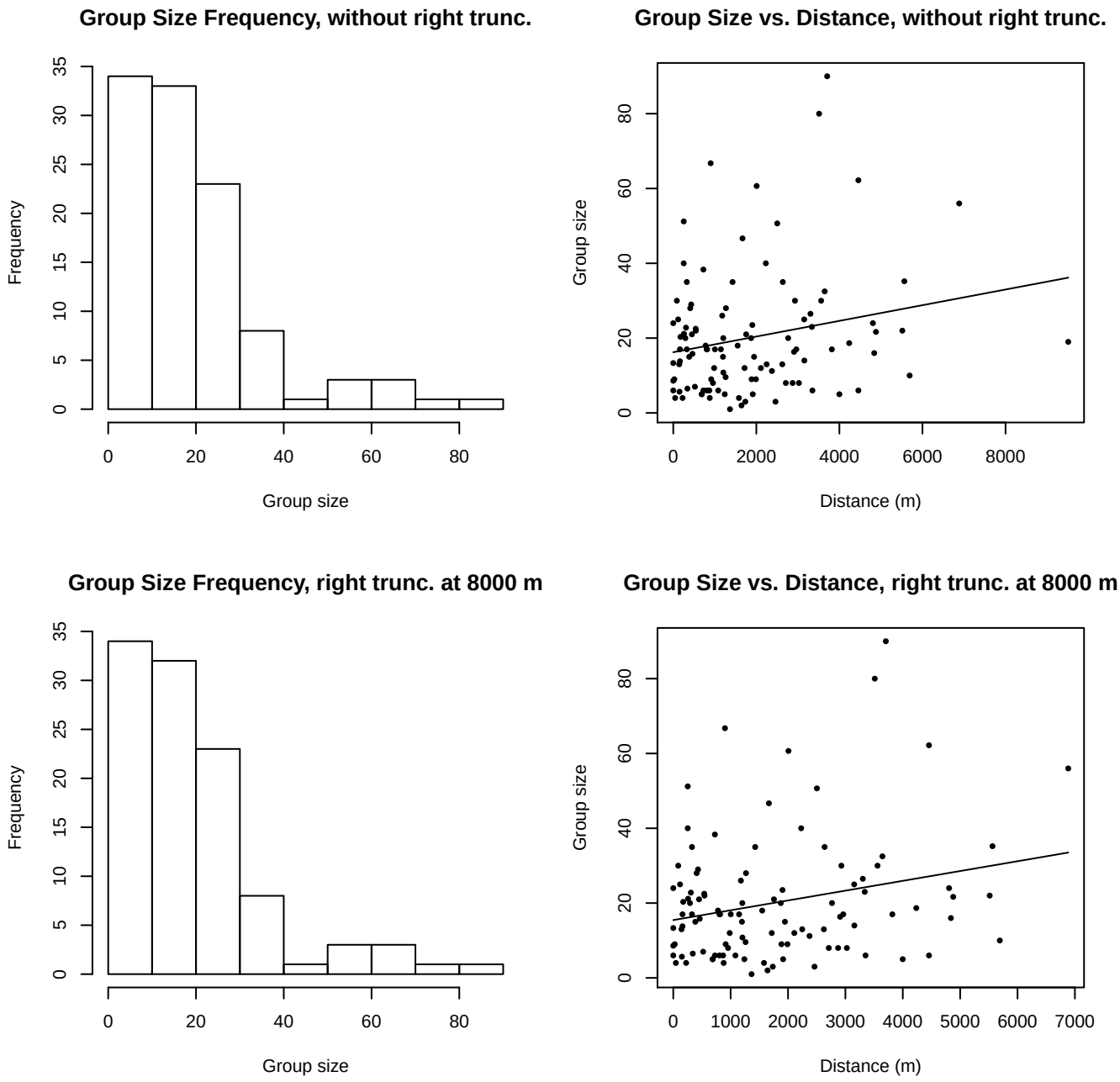

Figure 18: Histograms showing group size frequency and scatterplots showing the relationship between group size and perpendicular sighting distance, for all sightings (top row) and only those not right truncated (bottom row). In the scatterplot, the line is a simple linear regression.

Naked Eye Surveys

The sightings were right truncated at 1000m.

Covariate	Description
beaufort	Beaufort sea state.
size	Estimated size (number of individuals) of the sighted group.

Table 10: Covariates tested in candidate "multi-covariate distance sampling" (MCDS) detection functions.

Key	Adjustment	Order	Covariates	Succeeded	Δ AIC	Mean ESHW (m)
hr			beaufort	Yes	0.00	417
hn			beaufort	Yes	7.25	483
hr				Yes	10.28	176
hr	poly	2		Yes	14.55	139
hn	cos	2		Yes	15.47	356
hn	cos	3		Yes	16.91	327
hn				Yes	22.12	465
hn	herm	4		Yes	23.94	464
hr	poly	4		No		
hr			size	No		
hn			size	No		
hr			beaufort, size	No		
hn			beaufort, size	No		

Table 11: Candidate detection functions for Naked Eye Surveys. The first one listed was selected for the density model.

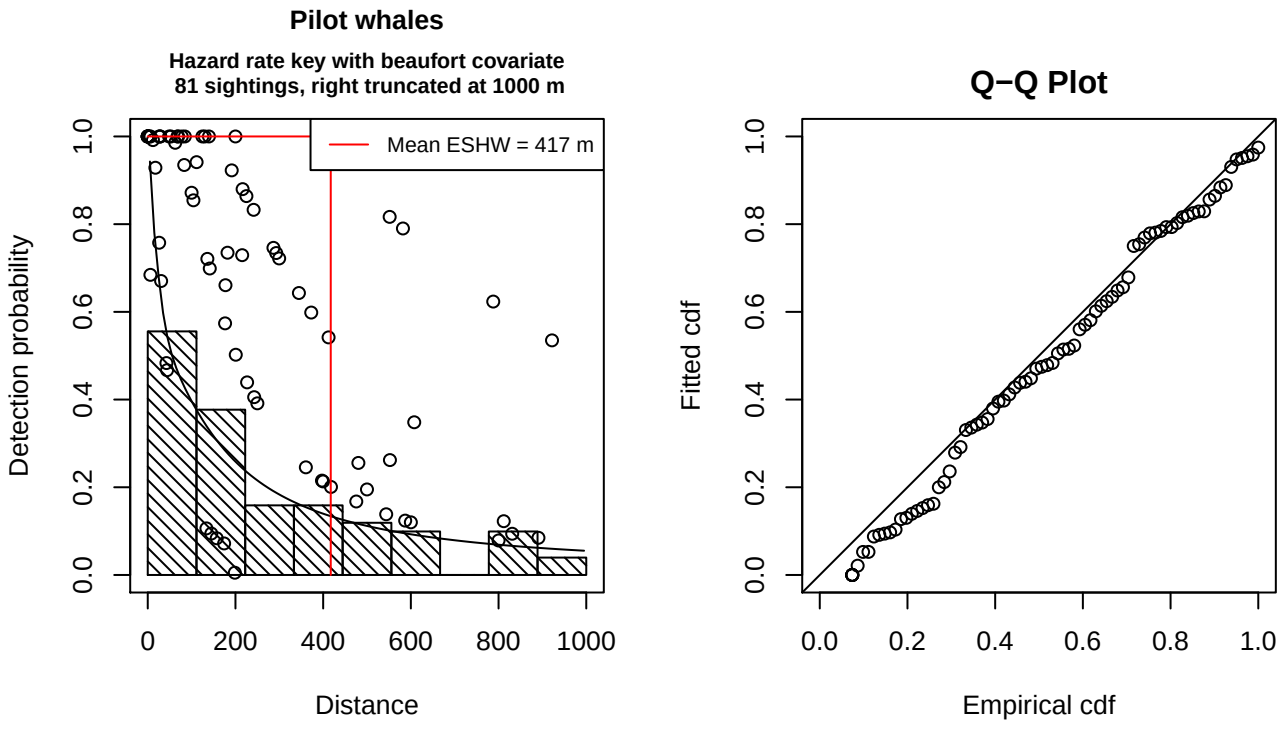

Figure 19: Detection function for Naked Eye Surveys that was selected for the density model

Statistical output for this detection function:

```
Summary for ds object
```

```
Number of observations :  81
Distance range         :  0  -  1000
AIC                    :  1051.085

Detection function:
 Hazard-rate key function

Detection function parameters
Scale Coefficients:
             estimate        se
(Intercept)  9.823252 1.2208180
beaufort    -1.584524 0.4261818

Shape parameters:
             estimate        se
(Intercept) 0.4375463 0.2096068

                      Estimate           SE        CV
Average p             0.178549   0.07676947 0.4299629
N in covered region 453.656872 201.84260200 0.4449235
```

Additional diagnostic plots:

Figure 20: Scatterplots showing the relationship between Beaufort sea state and perpendicular sighting distance, for all sightings (left) and only those not right truncated (right). The line is a simple linear regression.

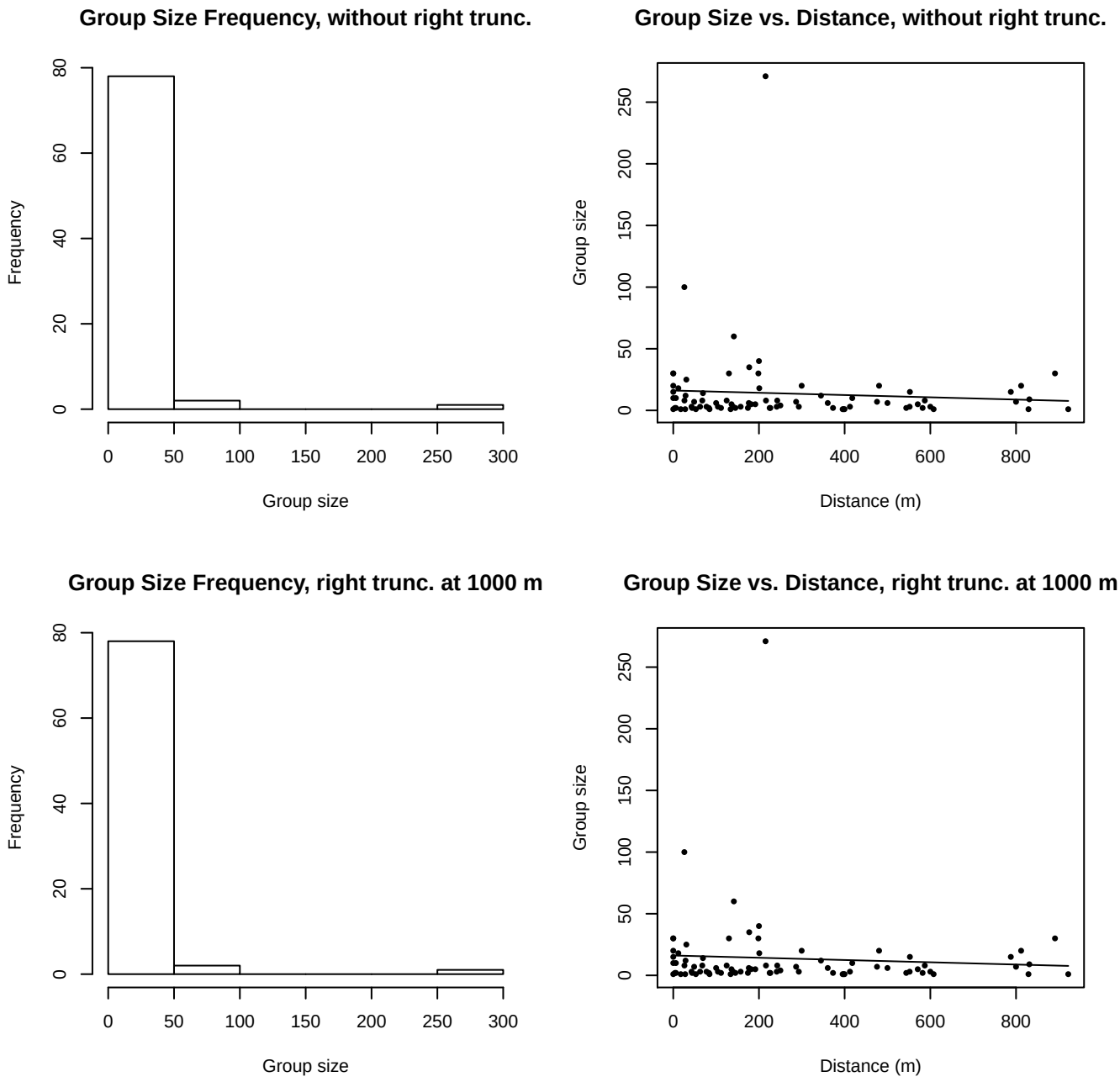

Figure 21: Histograms showing group size frequency and scatterplots showing the relationship between group size and perpendicular sighting distance, for all sightings (top row) and only those not right truncated (bottom row). In the scatterplot, the line is a simple linear regression.

Aerial Surveys

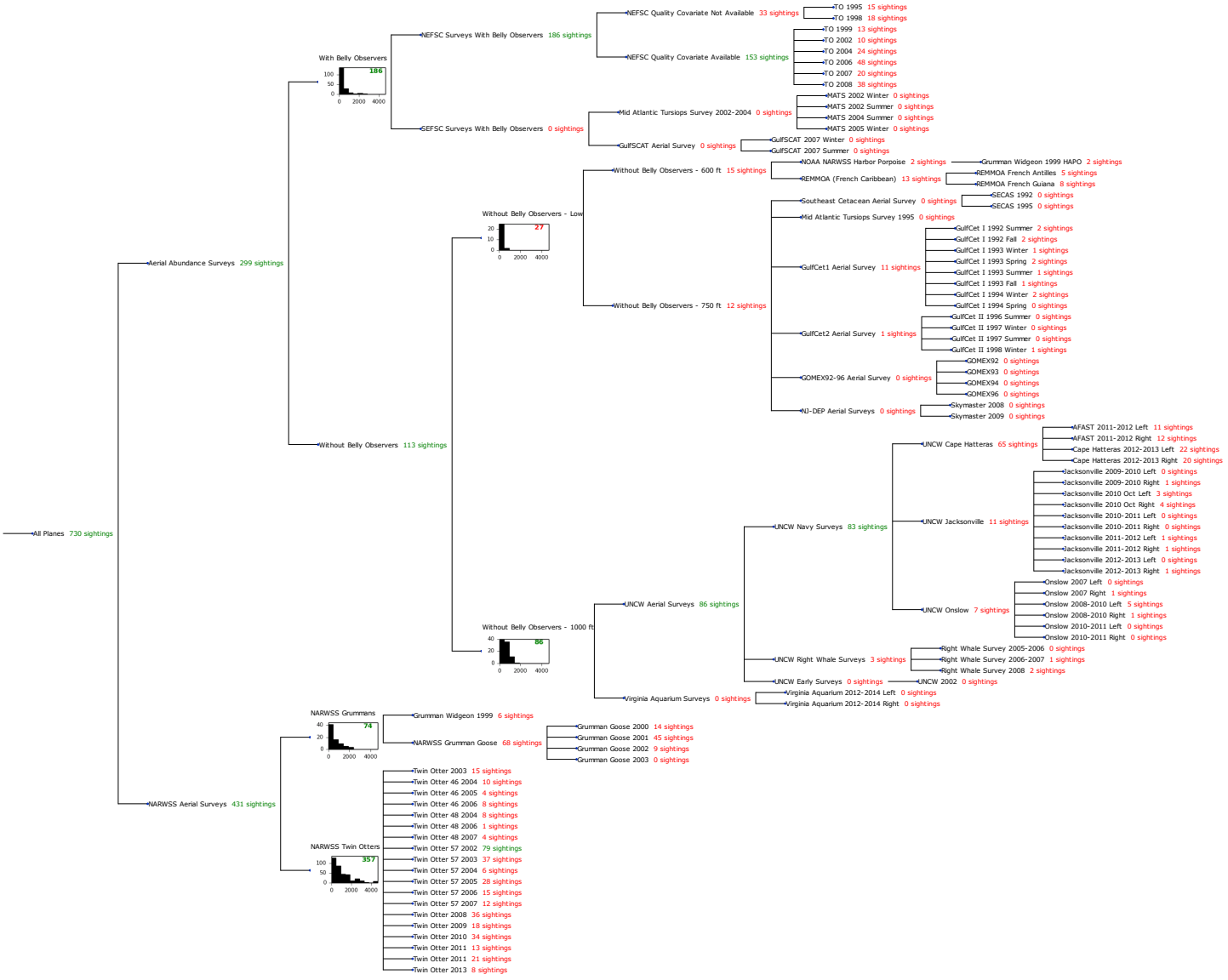

Figure 22: Detection hierarchy for aerial surveys

With Belly Observers

The sightings were right truncated at 1500m.

Covariate	Description
beaufort	Beaufort sea state.
size	Estimated size (number of individuals) of the sighted group.

Table 12: Covariates tested in candidate “multi-covariate distance sampling” (MCDS) detection functions.

Key	Adjustment	Order	Covariates	Succeeded	Δ AIC	Mean ESHW (m)

hr			size	Yes	0.00	394
hr			beaufort, size	Yes	1.78	398
hr				Yes	5.86	396
hr			beaufort	Yes	7.58	399
hr	poly	2		Yes	7.86	396
hr	poly	4		Yes	7.86	396
hn	cos	2		Yes	11.98	434
hn	cos	3		Yes	22.90	411
hn			size	Yes	24.93	596
hn				Yes	34.60	553
hn	herm	4		Yes	36.11	552
hn			beaufort	No		
hn			beaufort, size	No		

Table 13: Candidate detection functions for With Belly Observers. The first one listed was selected for the density model.

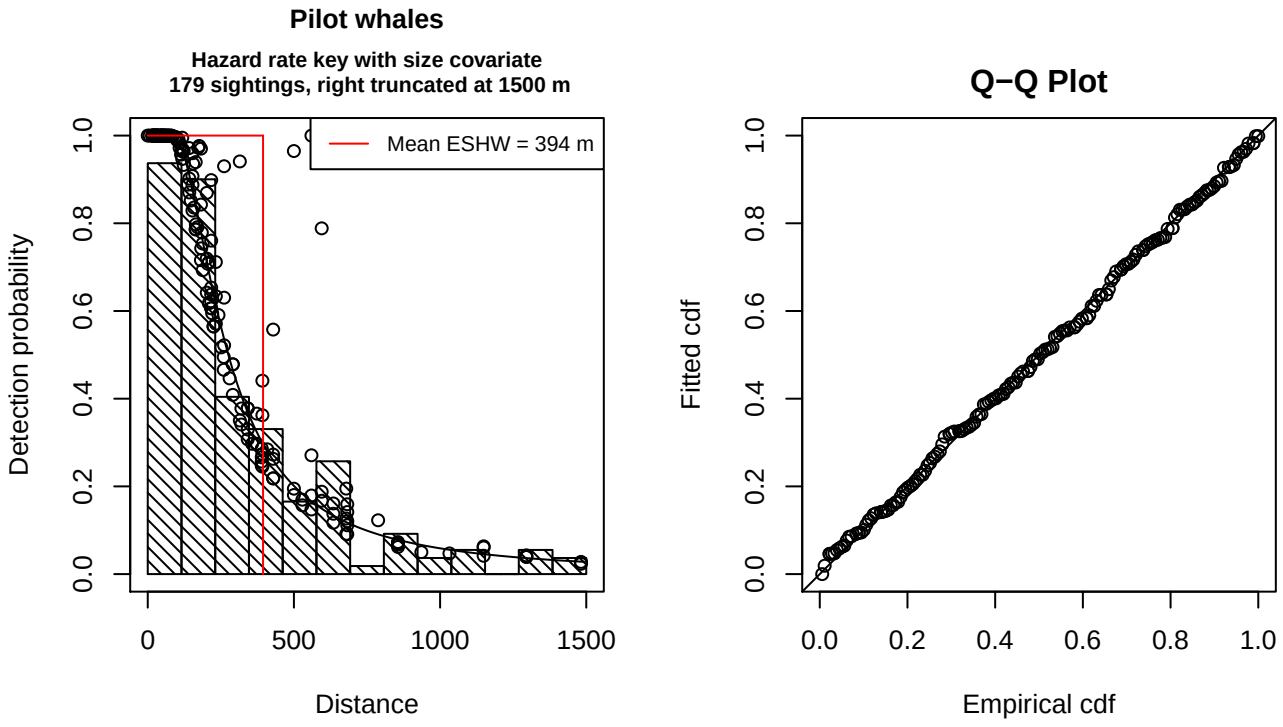

Figure 23: Detection function for With Belly Observers that was selected for the density model

Statistical output for this detection function:

```
Summary for ds object
Number of observations :  179
```

```
Distance range         :  0  -  1500
AIC                    :  2405.616

Detection function:
 Hazard-rate key function

Detection function parameters
Scale Coefficients:
             estimate        se
(Intercept) 5.2999331 0.1854678
size        0.2491643 0.1862108

Shape parameters:
             estimate        se
(Intercept) 0.6689847 0.1239738

                        Estimate         SE        CV
Average p               0.2529798  0.0258198 0.1020627
N in covered region 707.5664222 85.6297480 0.1210201
```

Additional diagnostic plots:

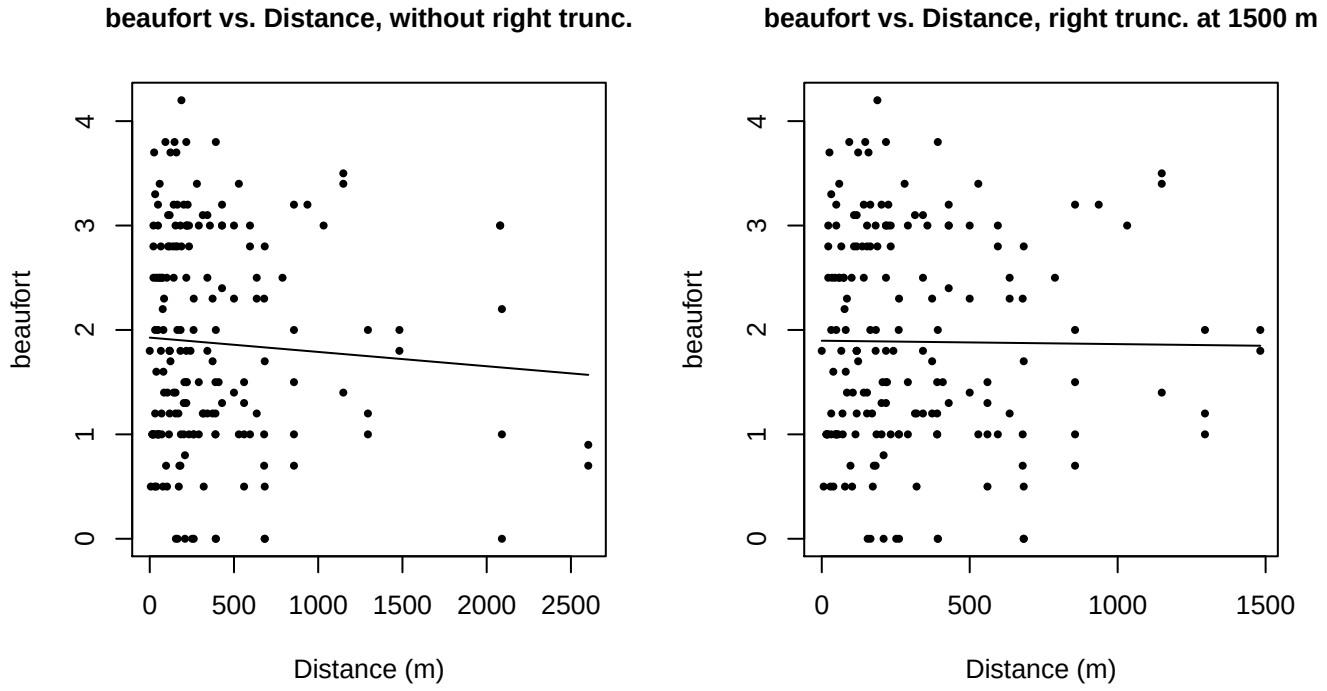

Figure 24: Scatterplots showing the relationship between Beaufort sea state and perpendicular sighting distance, for all sightings (left) and only those not right truncated (right). The line is a simple linear regression.

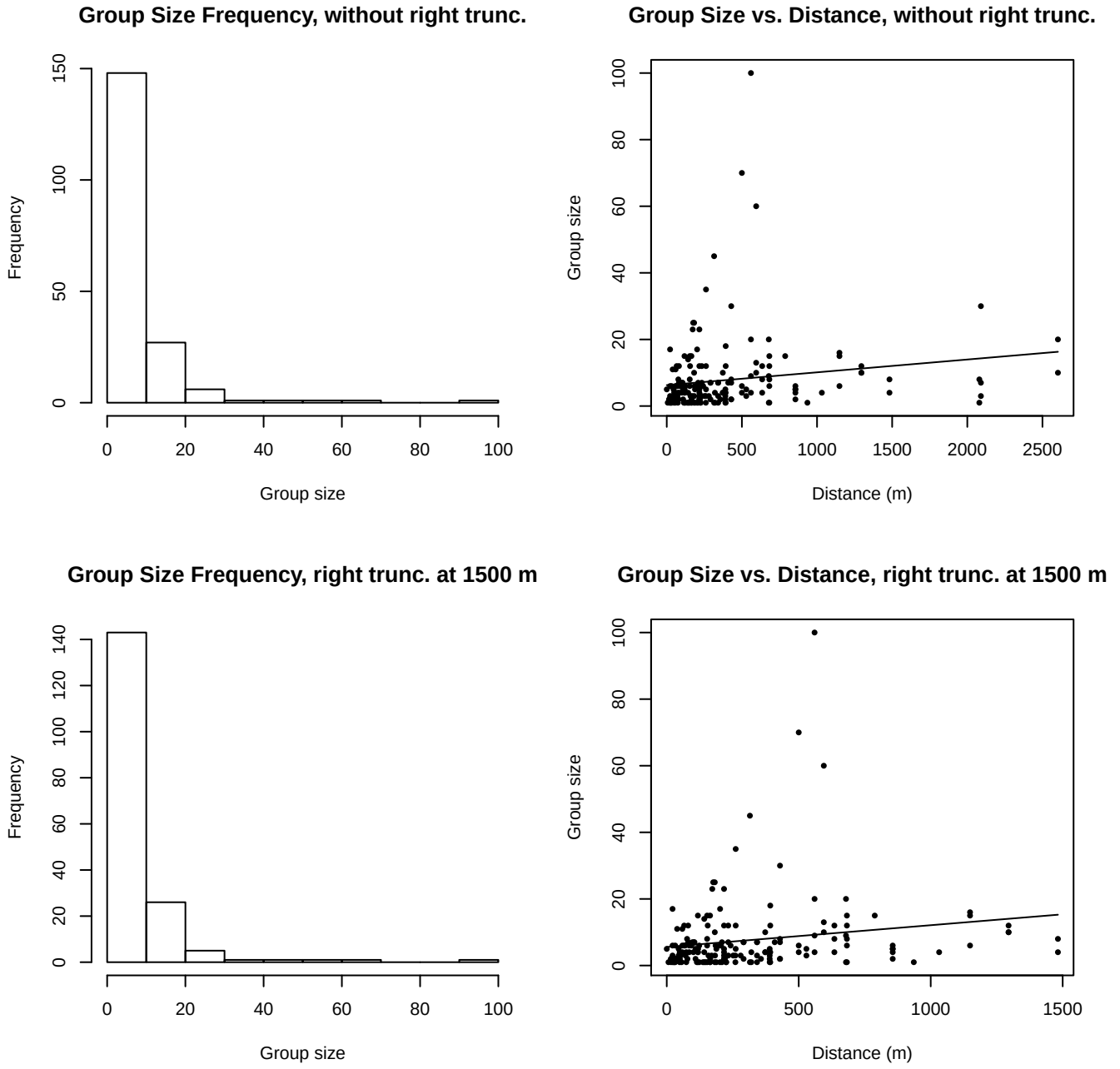

Figure 25: Histograms showing group size frequency and scatterplots showing the relationship between group size and perpendicular sighting distance, for all sightings (top row) and only those not right truncated (bottom row). In the scatterplot, the line is a simple linear regression.

Without Belly Observers - Low

The sightings were right truncated at 800m. Due to a reduced frequency of sightings close to the trackline that plausibly resulted from the behavior of the observers and/or the configuration of the survey platform, the sightings were left truncted as well. Sightings closer than 83 m to the trackline were omitted from the analysis, and it was assumed that the the area closer to the trackline than this was not surveyed. This distance was estimated by inspecting histograms of perpendicular sighting distances.

Key	Adjustment	Order	Covariates	Succeeded	Δ AIC	Mean ESHW (m)

hn			Yes	0.00	235
hr			Yes	0.13	301
hn	cos	3	Yes	1.25	269
hn	cos	2	Yes	1.91	265
hn	herm	4	Yes	1.99	234
hr	poly	4	Yes	2.13	301
hr	poly	2	Yes	2.13	301

Table 14: Candidate detection functions for Without Belly Observers - Low. The first one listed was selected for the density model.

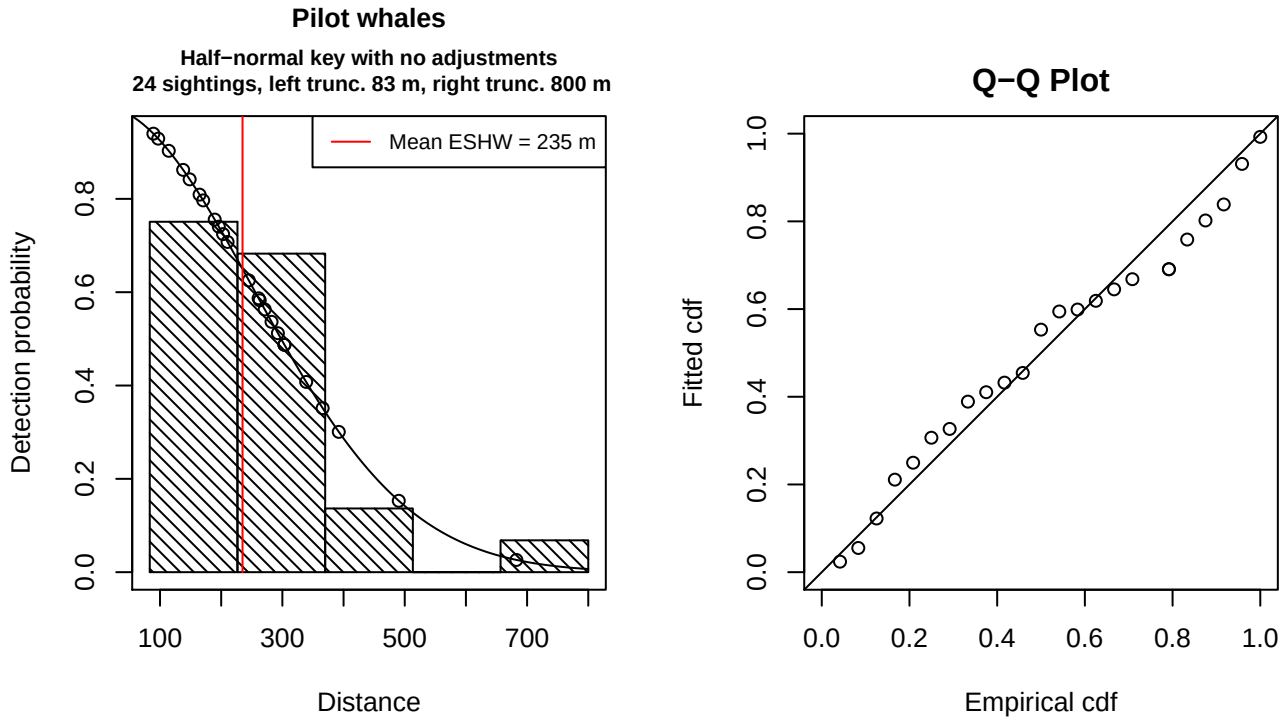

Figure 26: Detection function for Without Belly Observers - Low that was selected for the density model

Statistical output for this detection function:

```
Summary for ds object
Number of observations :  24
Distance range         :  83.2036  -  800
AIC                    :  295.5364

Detection function:
 Half-normal key function

Detection function parameters
Scale Coefficients:
            estimate        se
```

```
(Intercept) 5.533402 0.1369899

                       Estimate          SE        CV
Average p             0.2935847  0.05279273 0.1798211
N in covered region 81.7481219 20.31726236 0.2485349
```

Additional diagnostic plots:

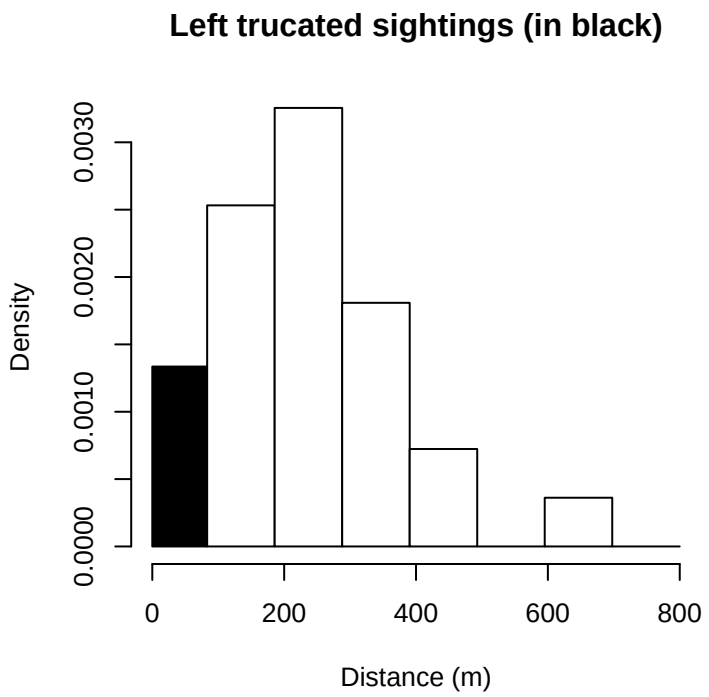

Figure 27: Density of sightings by perpendicular distance for Without Belly Observers - Low. Black bars on the left show sightings that were left truncated.

Without Belly Observers - 1000 ft

The sightings were right truncated at 1600m.

Covariate	Description
beaufort	Beaufort sea state.
quality	Survey-specific index of the quality of observation conditions, utilizing relevant factors other than Beaufort sea state (see methods).
size	Estimated size (number of individuals) of the sighted group.

Table 15: Covariates tested in candidate "multi-covariate distance sampling" (MCDS) detection functions.

Key	Adjustment	Order	Covariates	Succeeded	Δ AIC	Mean ESHW (m)
hr				Yes	0.00	1074
hr			beaufort	Yes	1.48	1082

hr	poly	2		Yes	1.59	1013
hr	poly	4		Yes	1.99	1071
hn	cos	2		Yes	2.49	910
hn				Yes	2.84	821
hn			beaufort	Yes	4.10	821
hn	cos	3		Yes	4.82	807
hn	herm	4		No		
hn			quality	No		
hr			quality	No		
hn			size	No		
hr			size	No		
hn			beaufort, quality	No		
hr			beaufort, quality	No		
hn			beaufort, size	No		
hr			beaufort, size	No		
hn			quality, size	No		
hr			quality, size	No		
hn			beaufort, quality, size	No		
hr			beaufort, quality, size	No		

Table 16: Candidate detection functions for Without Belly Observers - 1000 ft. The first one listed was selected for the density model.

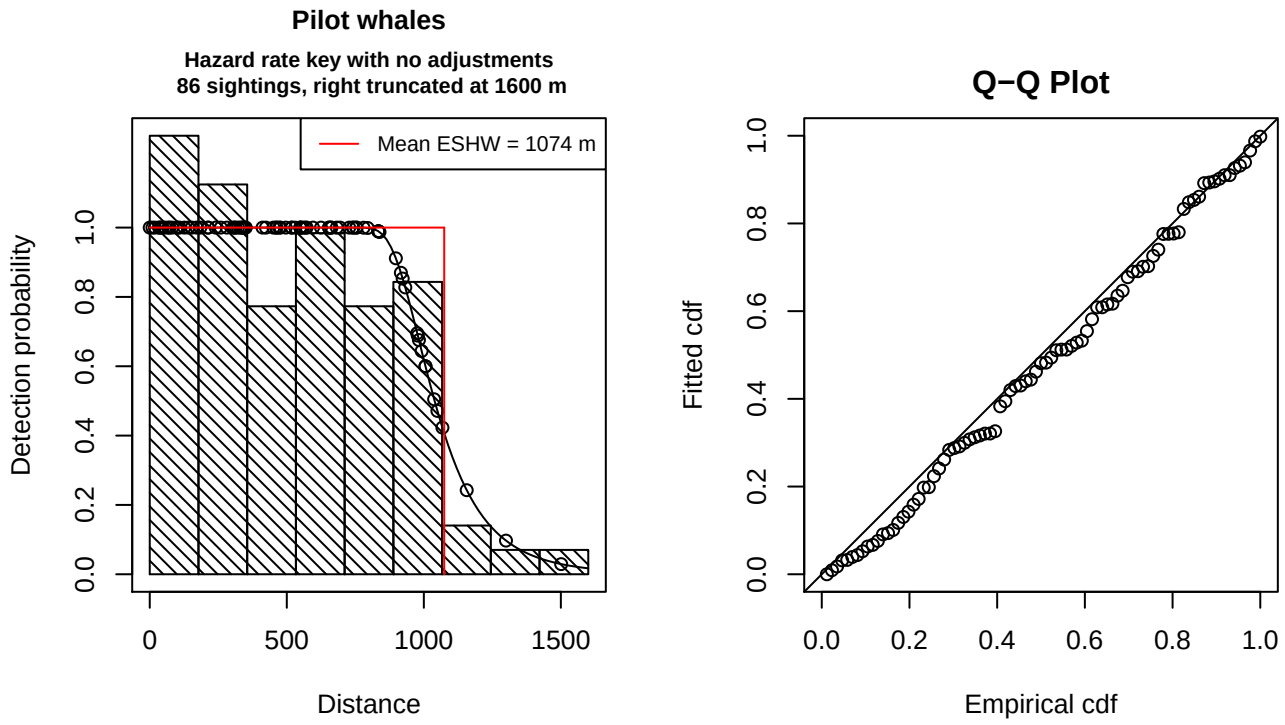

Figure 28: Detection function for Without Belly Observers - 1000 ft that was selected for the density model

Statistical output for this detection function:

```
Summary for ds object
Number of observations :  86
Distance range         :  0  -  1600
AIC                    :  1230.056

Detection function:
 Hazard-rate key function

Detection function parameters
Scale Coefficients:
            estimate         se
(Intercept) 6.903546 0.06408302

Shape parameters:
            estimate        se
(Intercept) 2.147213 0.2997496

                       Estimate          SE         CV
Average p              0.6714929  0.03470472 0.05168293
N in covered region 128.0728387 10.31839221 0.08056659
```

Additional diagnostic plots:

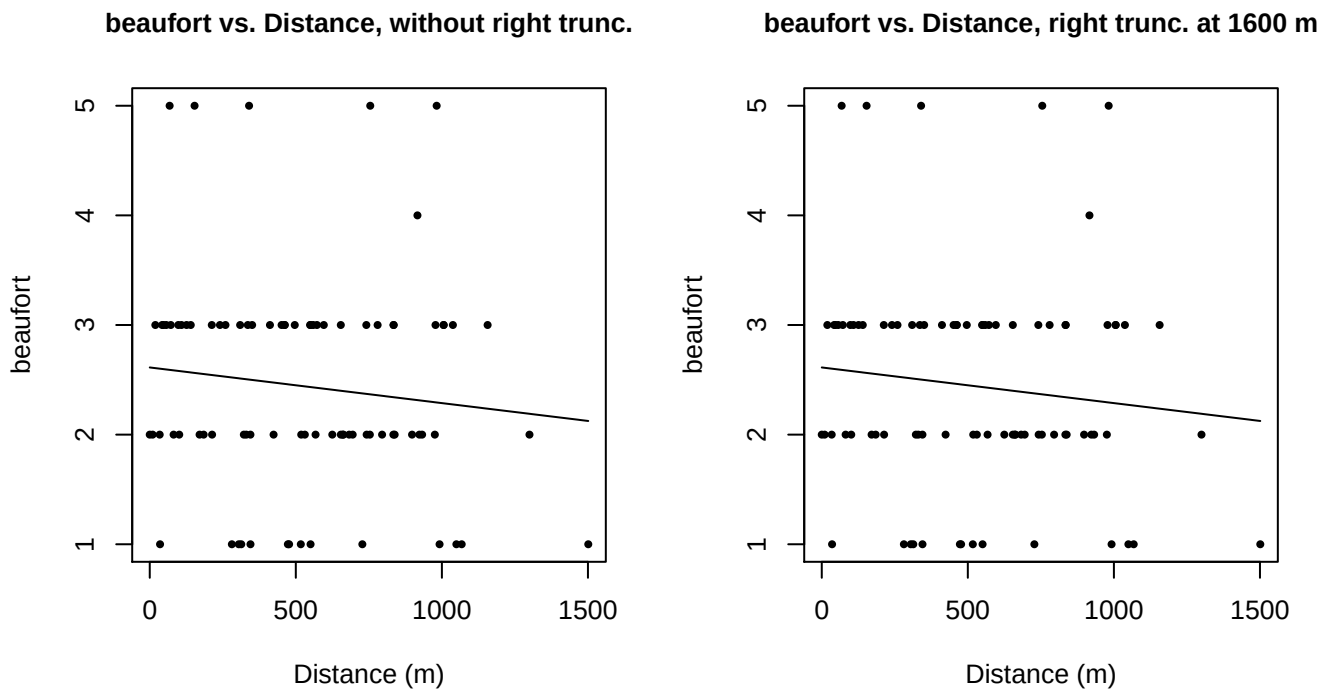

Figure 29: Scatterplots showing the relationship between Beaufort sea state and perpendicular sighting distance, for all sightings (left) and only those not right truncated (right). The line is a simple linear regression.

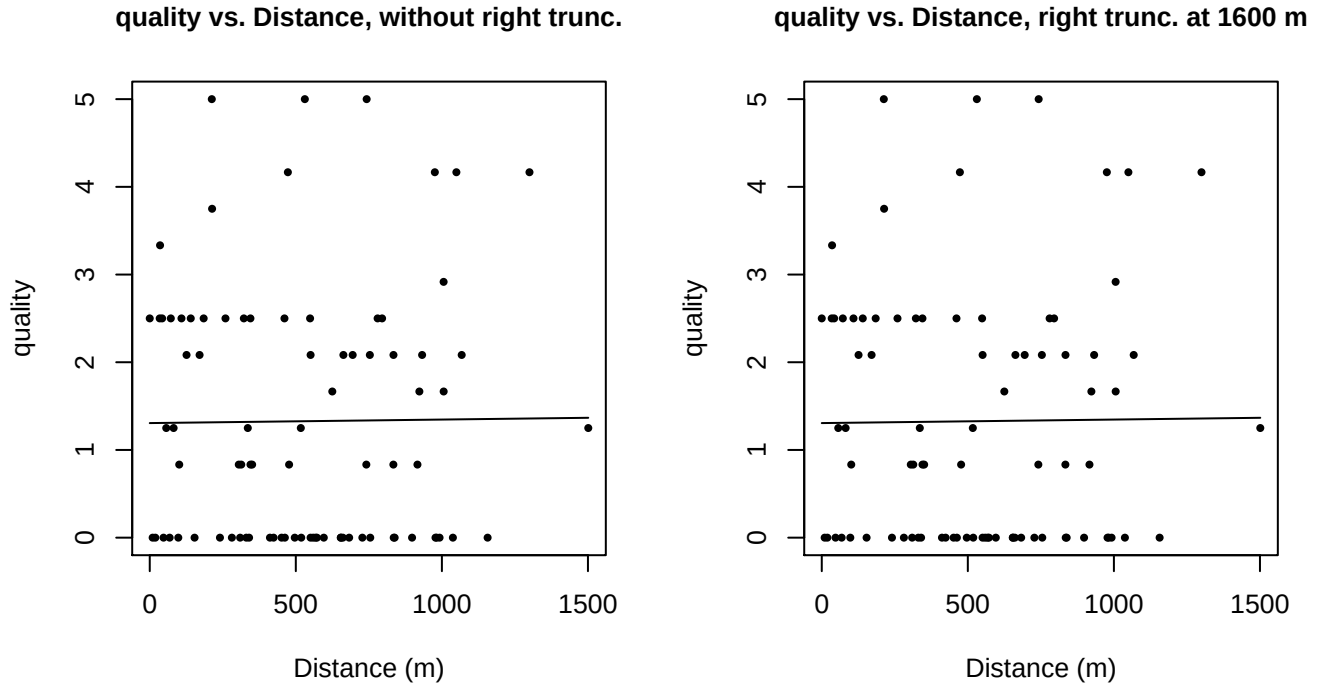

Figure 30: Scatterplots showing the relationship between the survey-specific index of the quality of observation conditions and perpendicular sighting distance, for all sightings (left) and only those not right truncated (right). Low values of the quality index correspond to better observation conditions. The line is a simple linear regression.

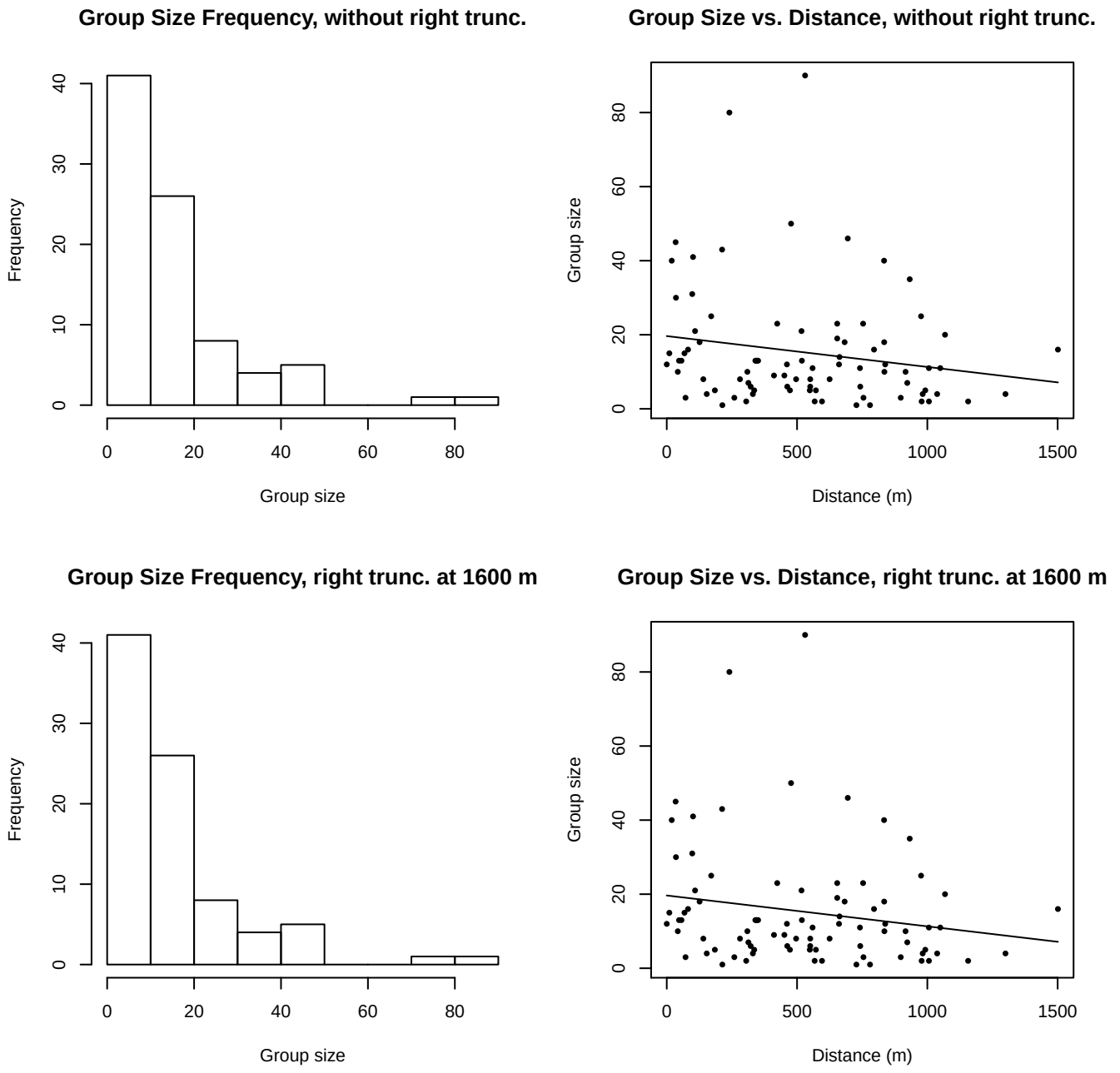

Figure 31: Histograms showing group size frequency and scatterplots showing the relationship between group size and perpendicular sighting distance, for all sightings (top row) and only those not right truncated (bottom row). In the scatterplot, the line is a simple linear regression.

NARWSS Grummans

The sightings were right truncated at 2500m. Due to a reduced frequency of sightings close to the trackline that plausibly resulted from the behavior of the observers and/or the configuration of the survey platform, the sightings were left truncted as well. Sightings closer than 107 m to the trackline were omitted from the analysis, and it was assumed that the the area closer to the trackline than this was not surveyed. This distance was estimated by inspecting histograms of perpendicular sighting distances.

Covariate	Description

beaufort	Beaufort sea state.
quality	Survey-specific index of the quality of observation conditions, utilizing relevant factors other than Beaufort sea state (see methods).
size	Estimated size (number of individuals) of the sighted group.

Table 17: Covariates tested in candidate "multi-covariate distance sampling" (MCDS) detection functions.

Key	Adjustment	Order	Covariates	Succeeded	Δ AIC	Mean ESHW (m)
hr			beaufort	Yes	0.00	701
hr				Yes	2.59	639
hn	cos	2		Yes	3.08	628
hr			quality	Yes	3.36	671
hr	poly	2		Yes	4.59	639
hr	poly	4		Yes	4.59	645
hn	cos	3		Yes	9.07	558
hn			beaufort	Yes	11.52	883
hn				Yes	13.75	885
hn			quality	Yes	15.62	885
hn	herm	4		No		
hn			size	No		
hr			size	No		
hn			beaufort, quality	No		
hr			beaufort, quality	No		
hn			beaufort, size	No		
hr			beaufort, size	No		
hn			quality, size	No		
hr			quality, size	No		
hn			beaufort, quality, size	No		
hr			beaufort, quality, size	No		

Table 18: Candidate detection functions for NARWSS Grummans. The first one listed was selected for the density model.

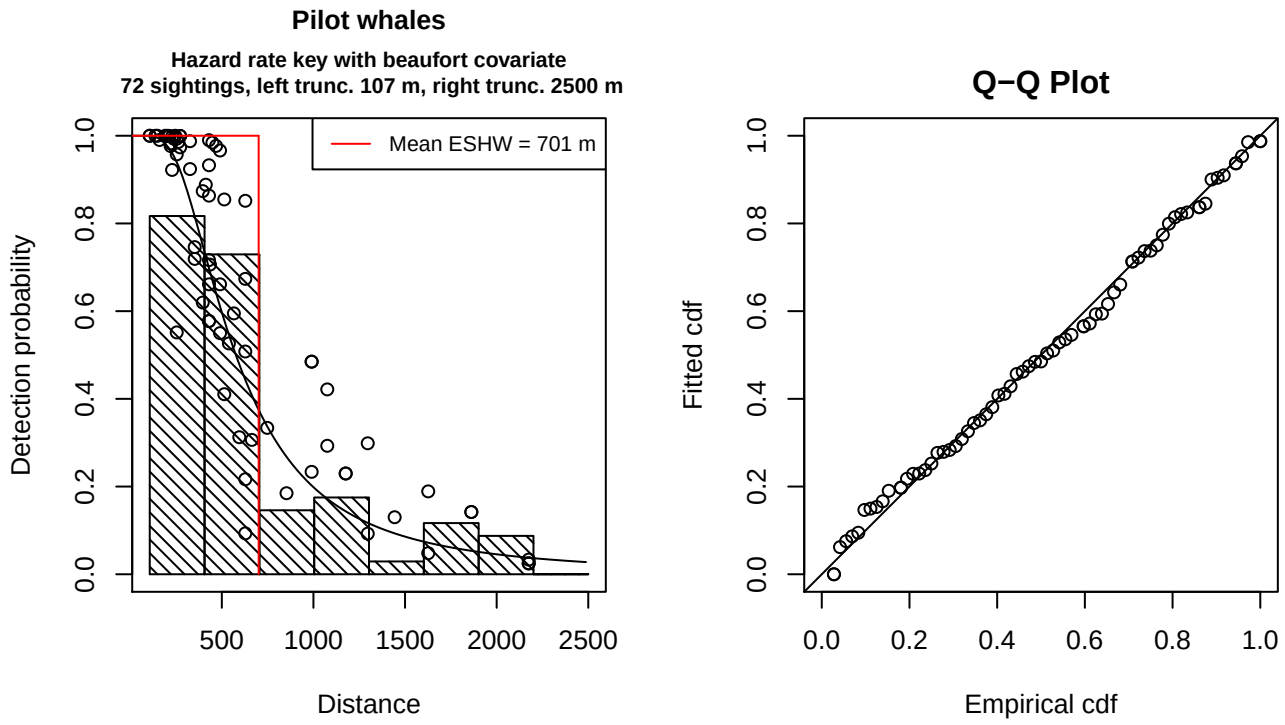

Figure 32: Detection function for NARWSS Grummans that was selected for the density model

Statistical output for this detection function:

```
Summary for ds object
Number of observations :  72
Distance range         :  106.5979  -  2500
AIC                    :  1044.564

Detection function:
 Hazard-rate key function

Detection function parameters
Scale Coefficients:
             estimate        se
(Intercept)  6.9834310 0.3634061
beaufort    -0.3279923 0.1586143

Shape parameters:
             estimate       se
(Intercept) 0.8421173 0.187872

                       Estimate          SE        CV
Average p             0.2513918  0.05159578 0.2052405
N in covered region 286.4055578 65.88835117 0.2300526
```

Additional diagnostic plots:

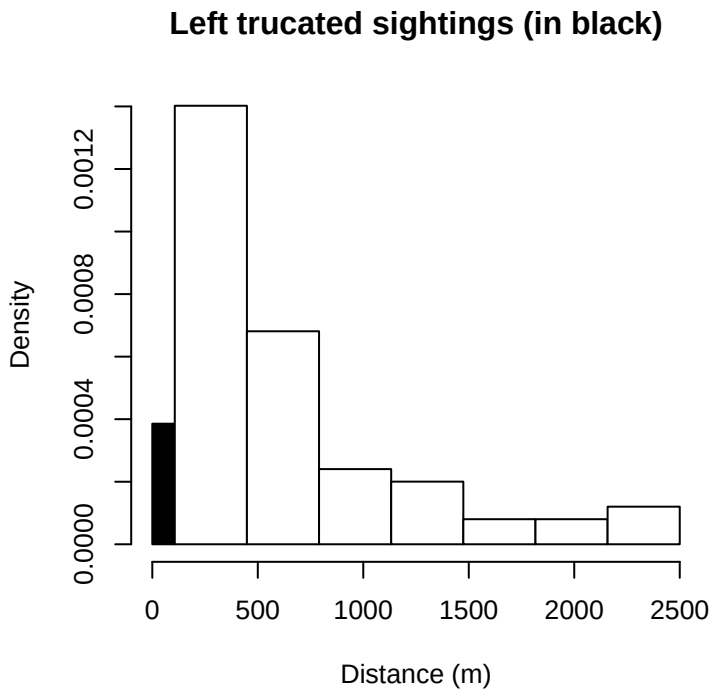

Figure 33: Density of sightings by perpendicular distance for NARWSS Grummans. Black bars on the left show sightings that were left truncated.

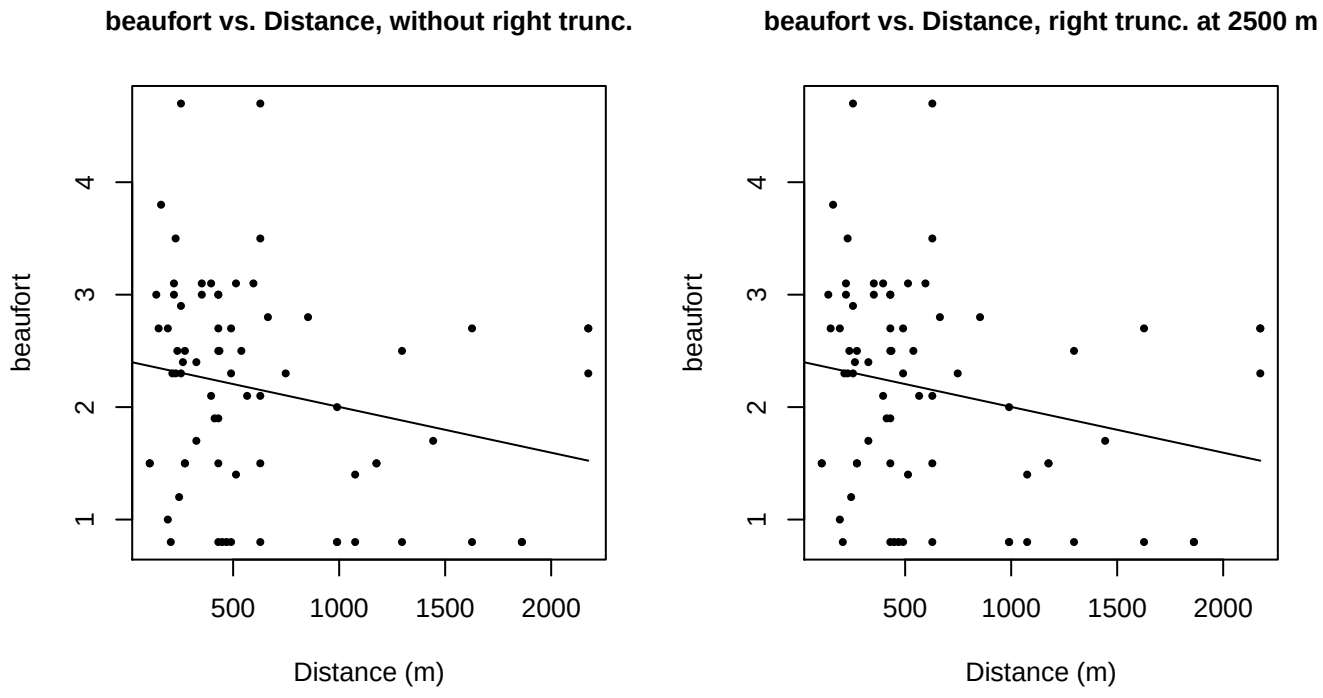

Figure 34: Scatterplots showing the relationship between Beaufort sea state and perpendicular sighting distance, for all sightings (left) and only those not right truncated (right). The line is a simple linear regression.

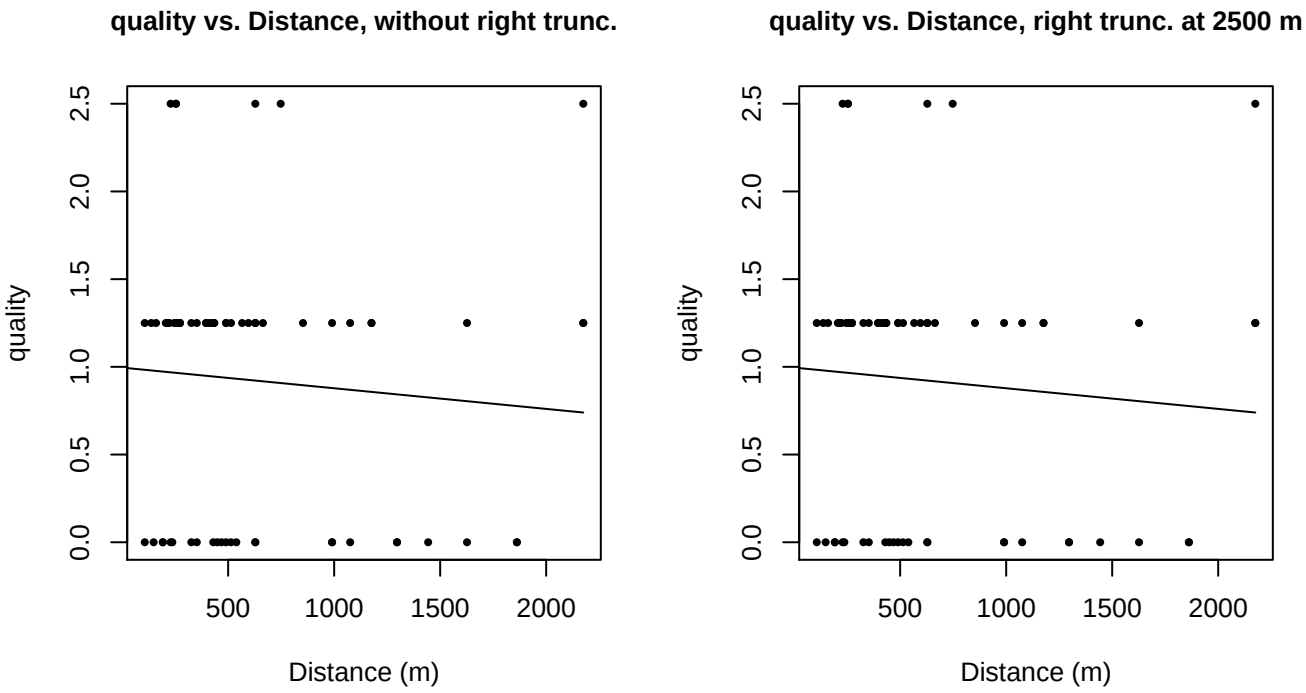

Figure 35: Scatterplots showing the relationship between the survey-specific index of the quality of observation conditions and perpendicular sighting distance, for all sightings (left) and only those not right truncated (right). Low values of the quality index correspond to better observation conditions. The line is a simple linear regression.

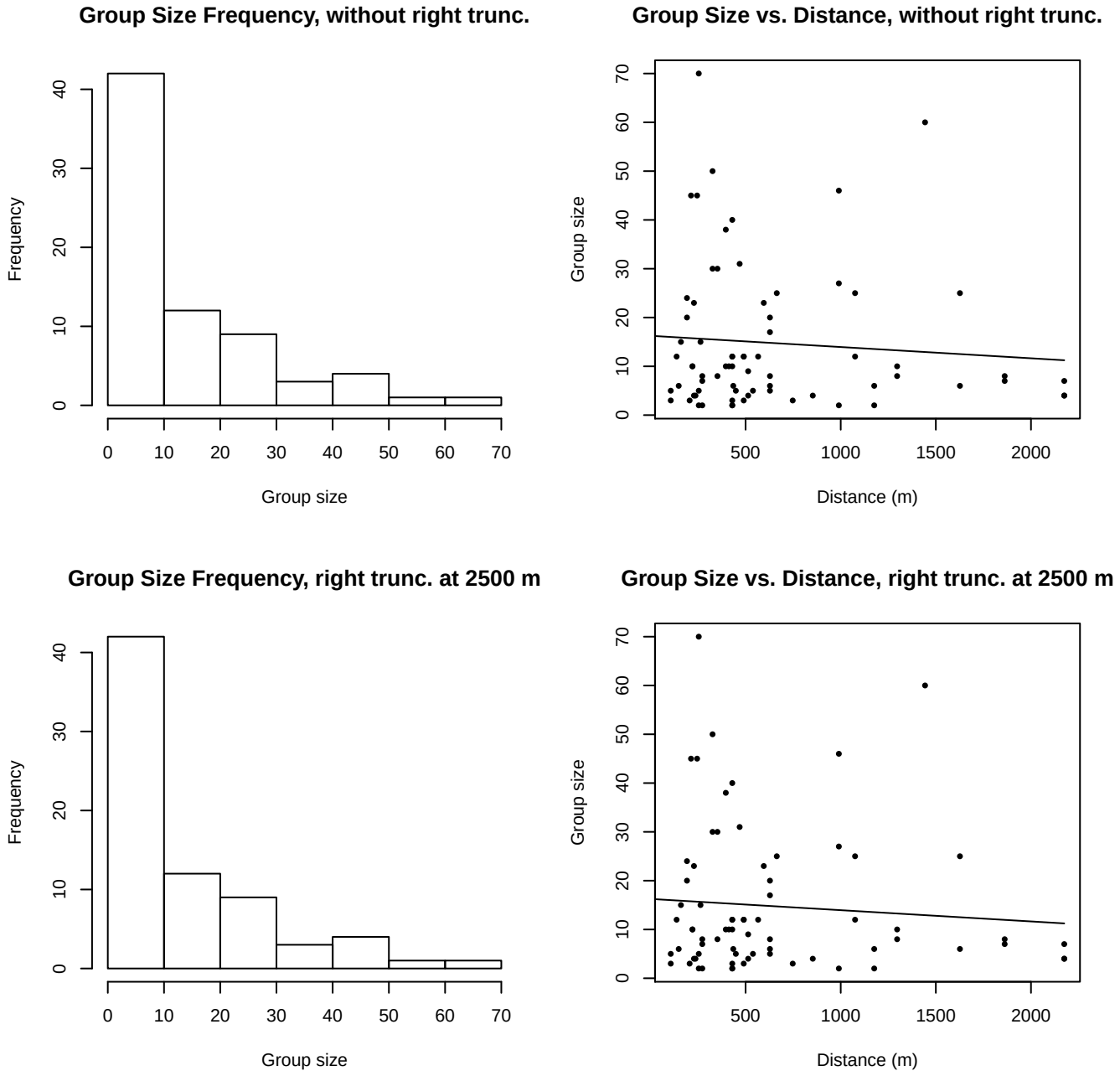

Figure 36: Histograms showing group size frequency and scatterplots showing the relationship between group size and perpendicular sighting distance, for all sightings (top row) and only those not right truncated (bottom row). In the scatterplot, the line is a simple linear regression.

NARWSS Twin Otters

The sightings were right truncated at 4000m. Due to a reduced frequency of sightings close to the trackline that plausibly resulted from the behavior of the observers and/or the configuration of the survey platform, the sightings were left truncted as well. Sightings closer than 61 m to the trackline were omitted from the analysis, and it was assumed that the the area closer to the trackline than this was not surveyed. This distance was estimated by inspecting histograms of perpendicular sighting distances. The vertical sighting angles were heaped at 10 degree increments up to 80 degrees and 1 degree increments thereafter, so the candidate detection functions were fitted using linear bins scaled accordingly.

Covariate	Description

beaufort	Beaufort sea state.
quality	Survey-specific index of the quality of observation conditions, utilizing relevant factors other than Beaufort sea state (see methods).
size	Estimated size (number of individuals) of the sighted group.

Table 19: Covariates tested in candidate "multi-covariate distance sampling" (MCDS) detection functions.

Key	Adjustment	Order	Covariates	Succeeded	Δ AIC	Mean ESHW (m)
hr	poly	2		Yes	0.00	1095
hn	cos	3		Yes	1.38	1116
hn	cos	2		Yes	3.49	1255
hr			quality	Yes	3.62	1192
hr				Yes	4.28	1199
hr			quality, size	Yes	4.97	1200
hr			size	Yes	5.39	1209
hr			beaufort, quality	Yes	5.61	1194
hr			beaufort	Yes	5.83	1210
hr			beaufort, size	Yes	6.88	1221
hr			beaufort, quality, size	Yes	6.94	1203
hn			quality	Yes	16.52	1543
hn			beaufort, quality	Yes	17.81	1542
hn			quality, size	Yes	18.38	1543
hn			beaufort, quality, size	Yes	19.70	1542
hn			beaufort	Yes	20.45	1544
hn				Yes	21.16	1544
hn			beaufort, size	Yes	22.32	1544
hn	herm	4		Yes	22.84	1541
hn			size	Yes	22.91	1543
hr	poly	4		Yes	5577.66	28

Table 20: Candidate detection functions for NARWSS Twin Otters. The first one listed was selected for the density model.

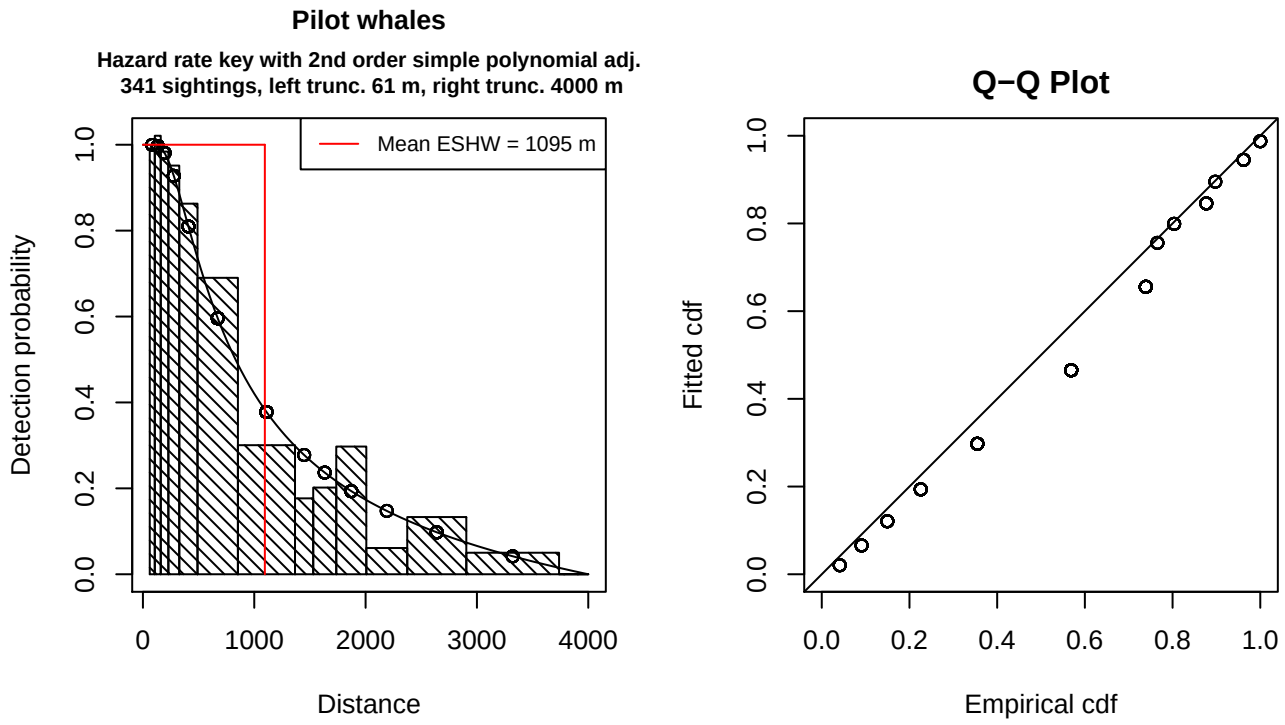

Figure 37: Detection function for NARWSS Twin Otters that was selected for the density model

Statistical output for this detection function:

```
Summary for ds object
Number of observations :  341
Distance range         :  61.25319  -  4000
AIC                    :  1614.624

Detection function:
 Hazard-rate key function with simple polynomial adjustment term of order 2

Detection function parameters
Scale Coefficients:
            estimate        se
(Intercept) 6.466549 0.2632679

Shape parameters:
             estimate        se
(Intercept) 0.1624016 0.2164028

Adjustment term parameter(s):
              estimate        se
poly, order 2       -1 0.2033083


Monotonicity constraints were enforced.
                        Estimate           SE        CV
Average p              0.2737477   0.03539637 0.1293029
N in covered region 1245.6724964 171.02049986 0.1372917

Monotonicity constraints were enforced.
```

Additional diagnostic plots:

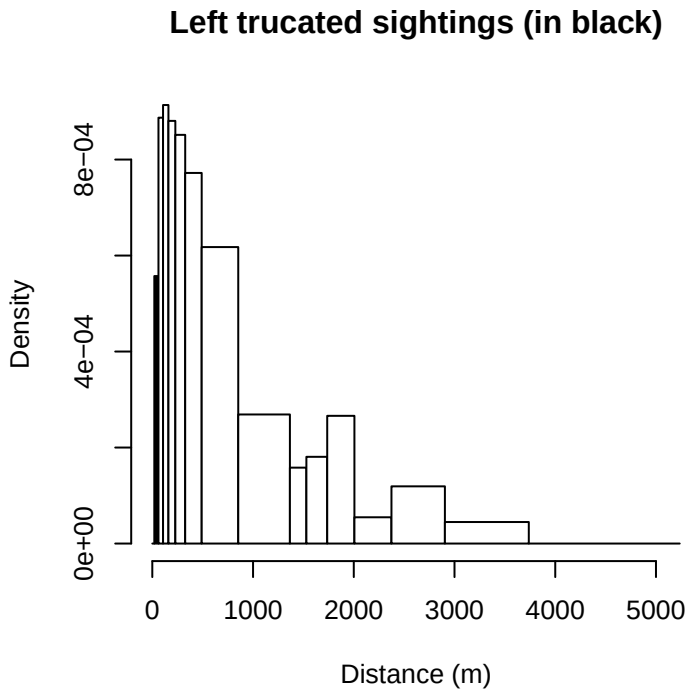

Figure 38: Density of sightings by perpendicular distance for NARWSS Twin Otters. Black bars on the left show sightings that were left truncated.

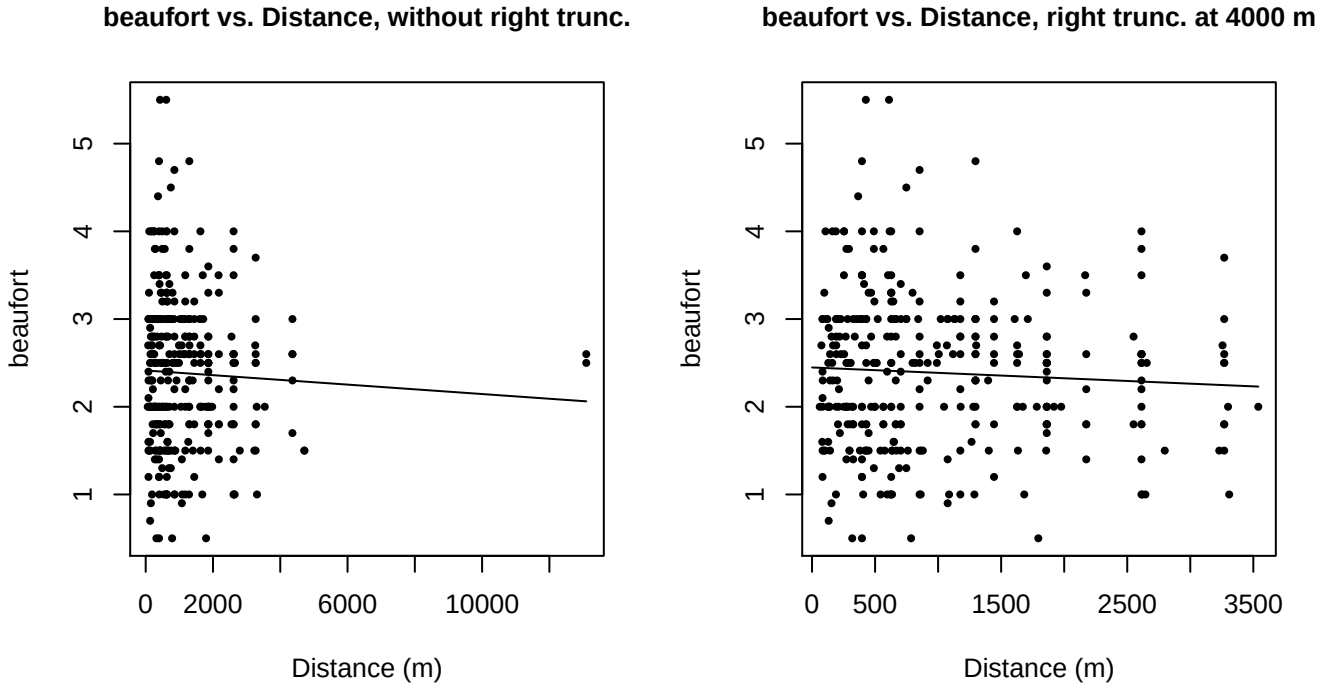

Figure 39: Scatterplots showing the relationship between Beaufort sea state and perpendicular sighting distance, for all sightings (left) and only those not right truncated (right). The line is a simple linear regression.

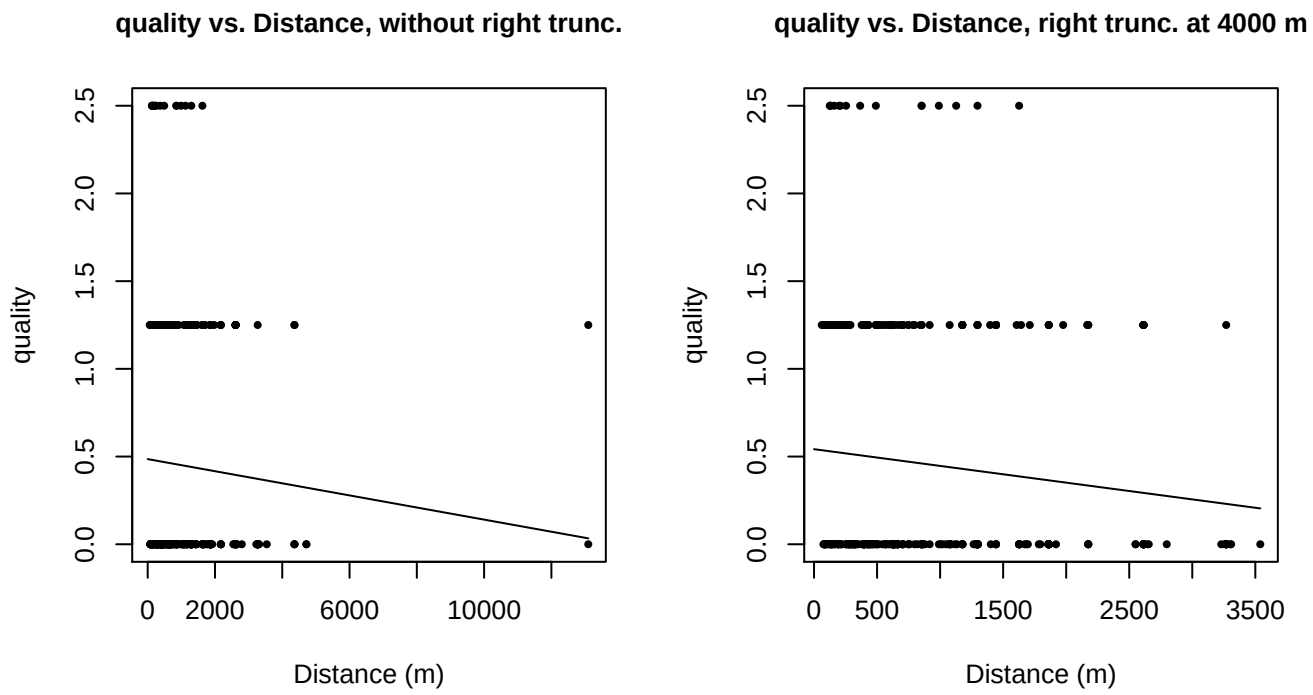

Figure 40: Scatterplots showing the relationship between the survey-specific index of the quality of observation conditions and perpendicular sighting distance, for all sightings (left) and only those not right truncated (right). Low values of the quality index correspond to better observation conditions. The line is a simple linear regression.

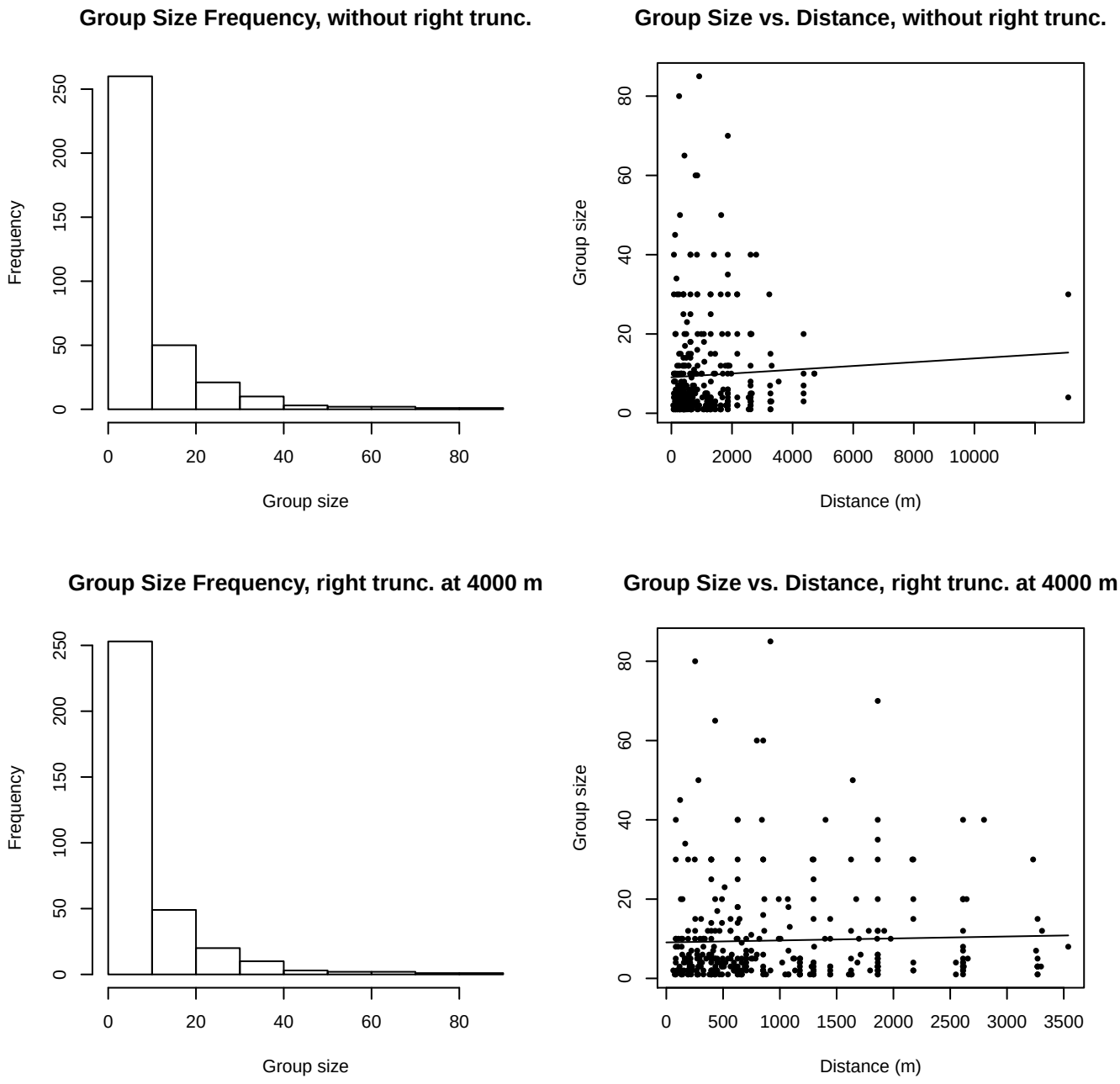

Figure 41: Histograms showing group size frequency and scatterplots showing the relationship between group size and perpendicular sighting distance, for all sightings (top row) and only those not right truncated (bottom row). In the scatterplot, the line is a simple linear regression.

g(0) Estimates

Platform	Surveys	Group Size	*g(0)*	Biases Addressed	Source
Shipboard	All	Any	0.585	Perception	Palka (2006)
Shipboard	NEFSC Abel-J Binocular Surveys	Any	0.50	Perception	Palka (2006)
Shipboard	NEFSC Endeavor	Any	0.67	Perception	Palka (2006)
Aerial	All	Any	0.607	Availability	Various

Table 21: Estimates of *g(0)* used in this density model.

Palka (2006) provided survey-specific g(0) estimates for two NOAA NEFSC shipboard surveys that used bigeye binoculars: the Abel-J 1998 survey (0.50) and the Endeavor 2004 survey (0.67). We used the estimates for the lower team, which was the primary team and the one for which we had sightings. These estimates accounted for perception bias but not availability bias.

For other binocular surveys, we used the simple mean (0.585) of Palka's two estimates. We also considered Barlow (2006), which estimated g(0)=0.76 for groups of 1-20 animals and g(0)=1.00 for groups larger than 20 animals. Although Palka's estimate does not consider group size, and pilot whales can occur in large groups, we used Palka's estimate because it was made in our study area, it incorporated more sightings, and it is specific to pilot whales (Barlow's estimate pooled pilot whales with many delphinds and estimated g(0) for the group). Finally, Palka (2006) did not provide an estimate for g(0) for pilot whales observed on the 1999 Abel-J naked eye survey, so we applied the same estimate we used for binocular surveys.

We did not find in the literature a g(0) estimate for pilot whales observed by aircraft. Pilot whales exhibit variable diving behavior that often includes long periods near the surface punctuated by occasional deep dives. Rather than base g(0) on availability bias estimated by from surface and dive intervals (following Carretta, 2000) as we did with other whales, we based it on percent- time-at-surface data reported from monitoring studies. Six short-finned pilot whales tracked with time-depth recorders near Madeira Island averaged 76.3% of the monitored period between 0-10m depth (Alves et al. 2013). Two pilot whales tracked with satellite tags near Florida spent 31% of the monitored period between 0-2m depth (Wells et al. 2013). One pilot whale tracked with a DTAG (species and location not given) spent 67% of the monitored period between 0-10m depth (Hooker et al. 2012). 14 long-finned pilot whales tracked with DTAGs in the Alboran Sea spent 57.49% of the monitored period at the surface (Canadas, 2011). Three long-finned pilot whales tracked with time-depth recorders near the Faroe Islands averaged 60.0% of the monitored period between 0-7m depth (Heide- Jorgensen et al. 2002). One large group of short-finned pilot whales tracked visually near the Gulf of California spent 66.6% of the monitored period visible at the surface (Barlow et al. 1997). We used the mean percent-time-at-surface (60.7%) for these 27 groups as the availability bias component of g(0). We did not incorporate an estimate of perception bias, thus our g(0) estimate is likely to be biased high.

Density Models

The two extant species of pilot whale, the long-finned pilot whale (Globicephala melas) and the short-finned pilot whale (Globicephala macrorhynchus) are very difficult for observers to distinguish at sea. Because the size, shape, and color pattern distinctions between the two species are so variable (including the length of the pectoral flippers), the shape of the skull is the most definitive characteristic for identifying the species (Olson 2008). Both species occur in the western North Atlantic; their ranges overlap in our east coast study area. Short-finned pilot whales, the warmer-water species, occur mainly in the southern part of the study area but range north to the southern flank of Georges Bank (Waring et al. 2014). Long-finned pilot whales, the colder-water species, occur mainly in the northern part of the study area, but range south along the shelf break as far south as New Jersey, with occasional strandings as far south as South Carolina (Waring et al. 2014).

The large majority of sightings reported by the surveys included in our study reported "unidentified pilot whale" as the taxonomic identification. According to NOAA, "the ability to separately assess the 2 species in U.S. Atlantic waters is complex and requires additional information on seasonal spatial distribution" (Waring et al. 2014). For its 2011 abundance estimates, NOAA fitted a logistic regression model to pilot whale biopsy samples collected between 1998 and 2007 from South Carolina to the southern flank of Georges Bank, using sea surface temperature and seafloor depth to classify the samples into one species or the other. NOAA then applied this model to their 2011 line-transect surveys to classify the visual sightings and produce species-specific abundance estimates.

Neither the biopsy data, the 2011 regression model, nor the 2011 line transect surveys were available for our use, so we could not build upon what NOAA had done. We investigated producing our own habitat-based classification model (as we had done with fin and sei whales, for example) but nearly all of the sightings reported on the surveys available to us were of "unidentified pilot whale", and we lacked sufficient fully-identified sightings to attempt a classification. Therefore, as NOAA has historically done, we modeled both species together as a guild.

None of the surveys used in our analysis reported sightings of pilot whales on the shelf south of about 40 N. The northern on-shelf sightings are most likely long-finned pilot whales, according to NOAA's description of their classification model's findings (Waring et al. 2014). We split our study area at the shelf break (defined as the 125 m isobath) to model these presumed long-finned pilot whales separately from mixed-species sightings present over the slope and abyss.

Payne and Heinemann (1993) described possible seasonal movements of pilot whales from 1033 sightings collected on surveys conducted between 1978-1988 (not used in our analysis). The authors linked some of these movements to seasonal distributions of prey species, such as squid and mackerel, but did not present evidence that pilot whales were undertaking large migrations, such as those made by baleen whales moving to and from feeding and calving grounds. Therefore, although seasonal movements were reported, there was no evidence of large-scale migratory behavior that would indicate seasonal changes in species-environment relationships large enough to warrant splitting the data into seasons and modeling them separately, as we did with several baleen whale species. Accordingly, we fitted year-round models to the two geographic sub-regions. (This is not to say that static models would necessarily result; if shifts in density correlated with the dynamic environmental predictors utilized in the models, the models could reproduce those shifts.)

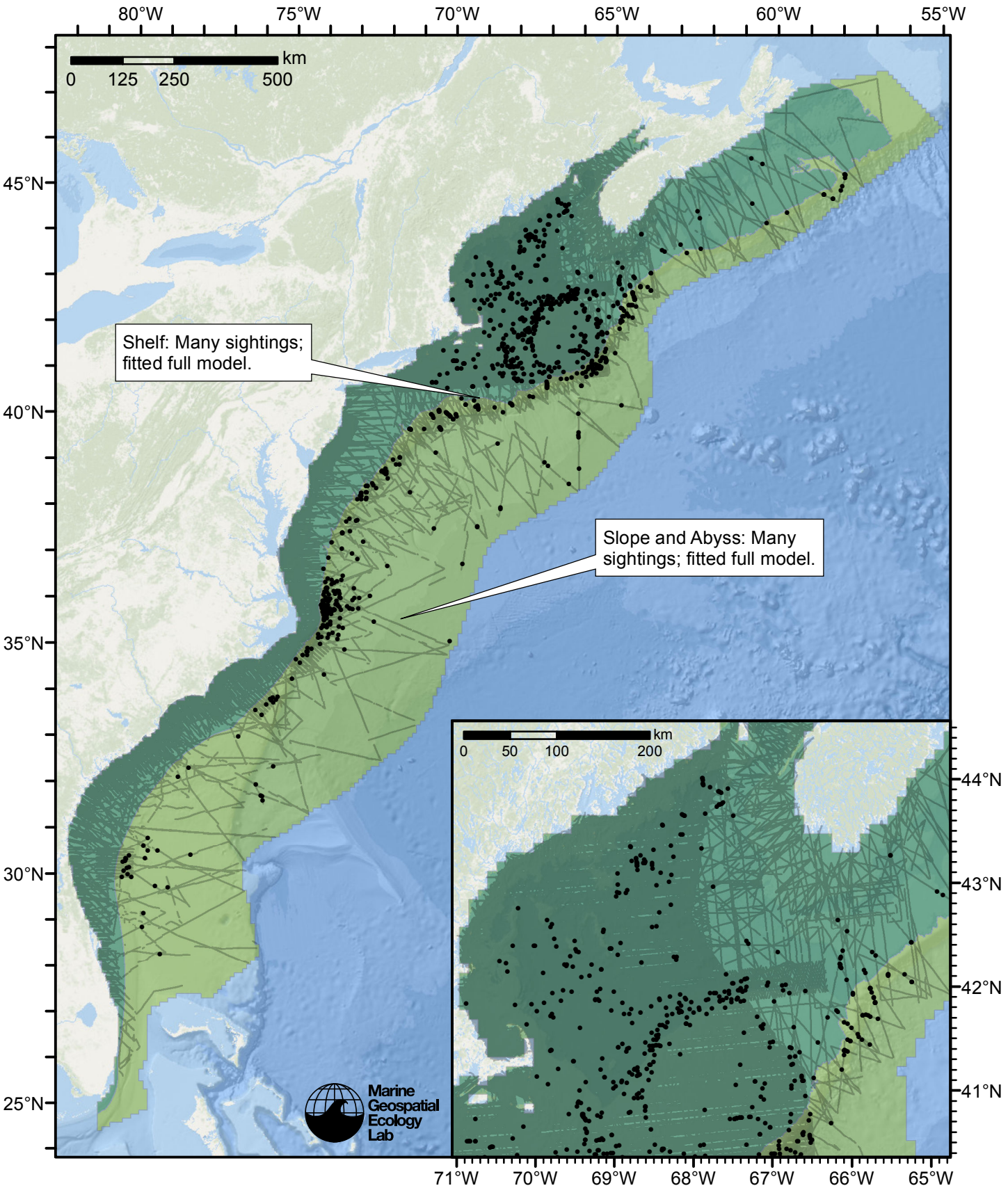

Figure 42: Pilot whales density model schematic. All on-effort sightings are shown, including those that were truncated when detection functions were fitted.

Climatological Model

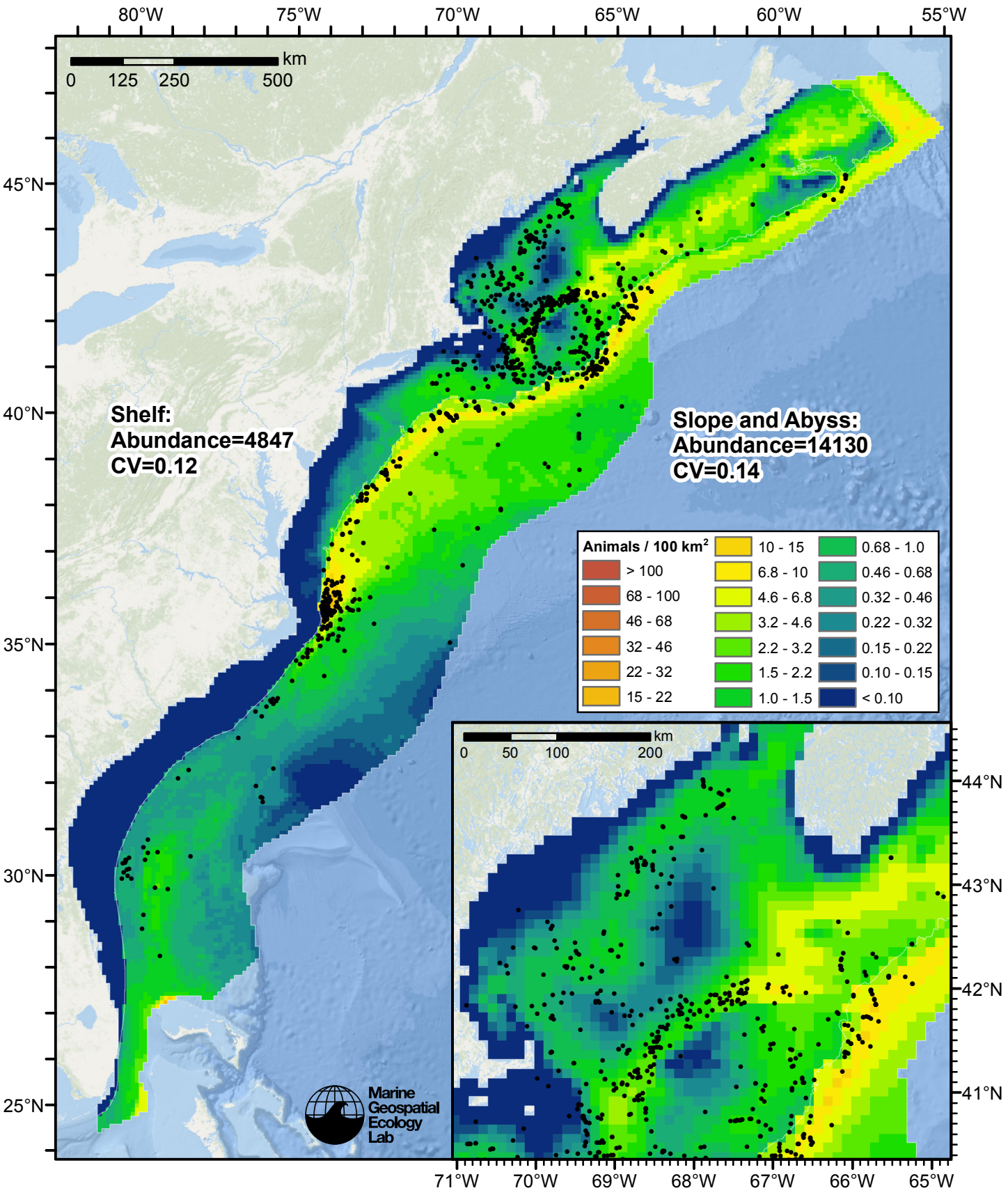

Figure 43: Pilot whales density predicted by the climatological model that explained the most deviance. Pixels are 10x10 km. The legend gives the estimated individuals per pixel; breaks are logarithmic. Abundance for each region was computed by summing the density cells occuring in that region.

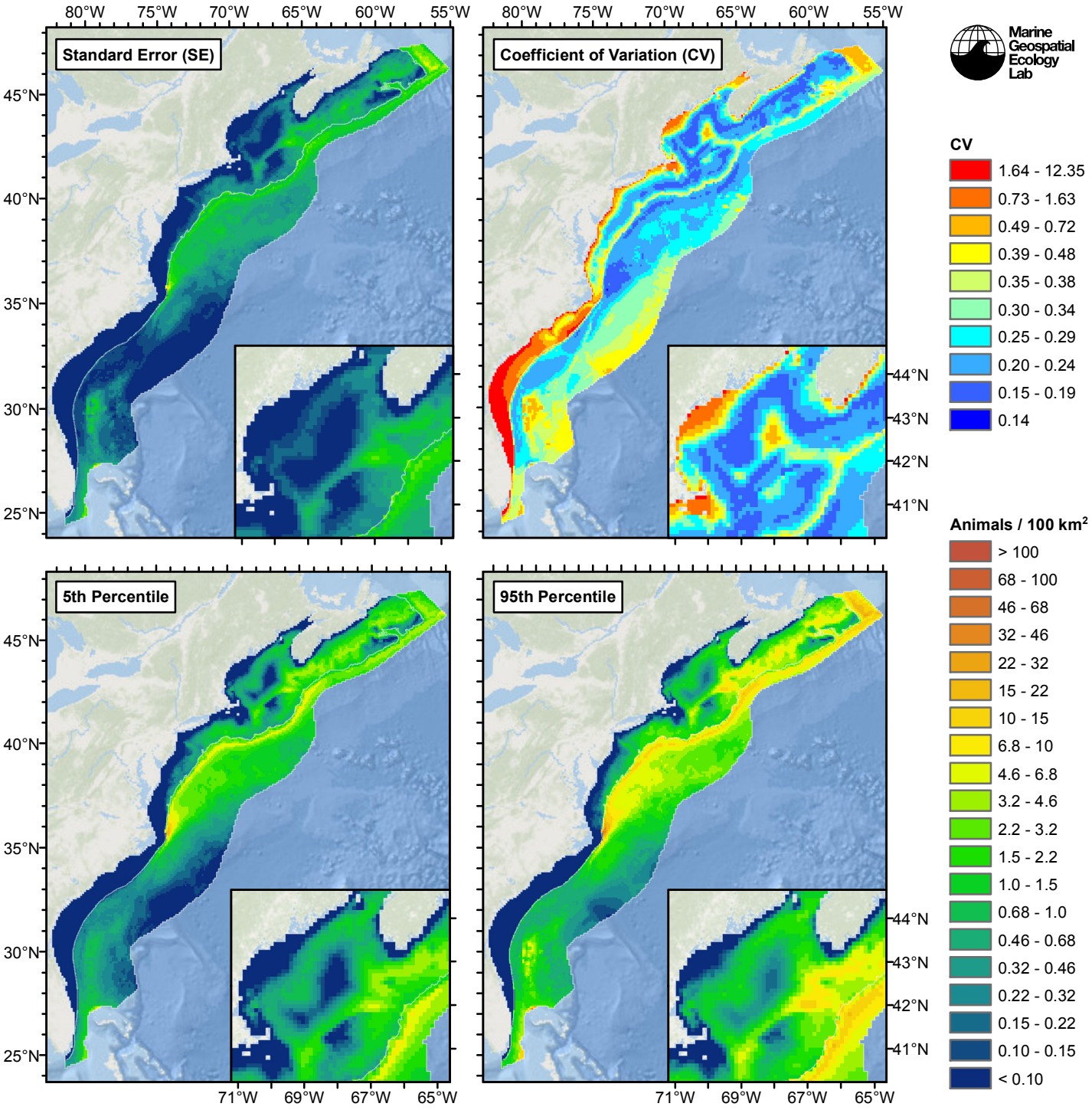

Figure 44: Estimated uncertainty for the climatological model that explained the most deviance. These estimates only incorporate the statistical uncertainty estimated for the spatial model (by the R mgcv package). They do not incorporate uncertainty in the detection functions, g(0) estimates, predictor variables, and so on.

Slope and Abyss

Statistical output

```
Rscript.exe: This is mgcv 1.8-2. For overview type 'help("mgcv-package")'.


Family: Tweedie(p=1.401)
```

```
Link function: log

Formula:
abundance ~ offset(log(area_km2)) + s(log10(Depth), bs = "ts",
    k = 5) + s(log10(Slope), bs = "ts", k = 5) + s(I(DistToCanyon/1000),
    bs = "ts", k = 5) + s(ClimSST, bs = "ts", k = 5) + s(I(ClimDistToFront1^(1/3)),
    bs = "ts", k = 5) + s(I(ClimDistToAEddy9/1000), bs = "ts",
    k = 5) + s(I(ClimCumVGPM90^(1/3)), bs = "ts", k = 5)

Parametric coefficients:
            Estimate Std. Error t value Pr(>|t|)
(Intercept)   -4.595      0.120   -38.3   <2e-16 ***
---
Signif. codes:  0 '***' 0.001 '**' 0.01 '*' 0.05 '.' 0.1 ' ' 1

Approximate significance of smooth terms:
                                edf Ref.df      F  p-value
s(log10(Depth))              2.5287      4  4.236 8.90e-05 ***
s(log10(Slope))              1.9676      4  1.883 0.009635 **
s(I(DistToCanyon/1000))      1.0289      4  4.585 5.54e-06 ***
s(ClimSST)                   3.5346      4 14.281 2.67e-13 ***
s(I(ClimDistToFront1^(1/3))) 1.0321      4  3.087 0.000188 ***
s(I(ClimDistToAEddy9/1000))  0.9537      4  1.973 0.002619 **
s(I(ClimCumVGPM90^(1/3)))    1.5744      4 16.420  < 2e-16 ***
---
Signif. codes:  0 '***' 0.001 '**' 0.01 '*' 0.05 '.' 0.1 ' ' 1

R-sq.(adj) =  0.039   Deviance explained = 36.3%
-REML = 2981.3  Scale est. = 84.533    n = 17371

All predictors were significant. This is the final model.
Creating term plots.
Diagnostic output from gam.check():

Method: REML   Optimizer: outer newton
full convergence after 12 iterations.
Gradient range [-8.914007e-05,0.0001240885]
(score 2981.253 & scale 84.53251).
Hessian positive definite, eigenvalue range [0.2165148,780.6817].
Model rank =  29 / 29

Basis dimension (k) checking results. Low p-value (k-index<1) may
indicate that k is too low, especially if edf is close to k'.

                                k'   edf k-index p-value
s(log10(Depth))              4.000 2.529   0.673    0.00
s(log10(Slope))              4.000 1.968   0.686    0.05
s(I(DistToCanyon/1000))      4.000 1.029   0.665    0.00
s(ClimSST)                   4.000 3.535   0.709    0.45
s(I(ClimDistToFront1^(1/3))) 4.000 1.032   0.698    0.13
s(I(ClimDistToAEddy9/1000))  4.000 0.954   0.668    0.01
s(I(ClimCumVGPM90^(1/3)))    4.000 1.574   0.652    0.00

Predictors retained during the model selection procedure: Depth, Slope, DistToCanyon, ClimSST,
ClimDistToFront1, ClimDistToAEddy9, ClimCumVGPM90

Predictors dropped during the model selection procedure: DistTo300m, ClimTKE, ClimDistToCEddy9
```

Model term plots

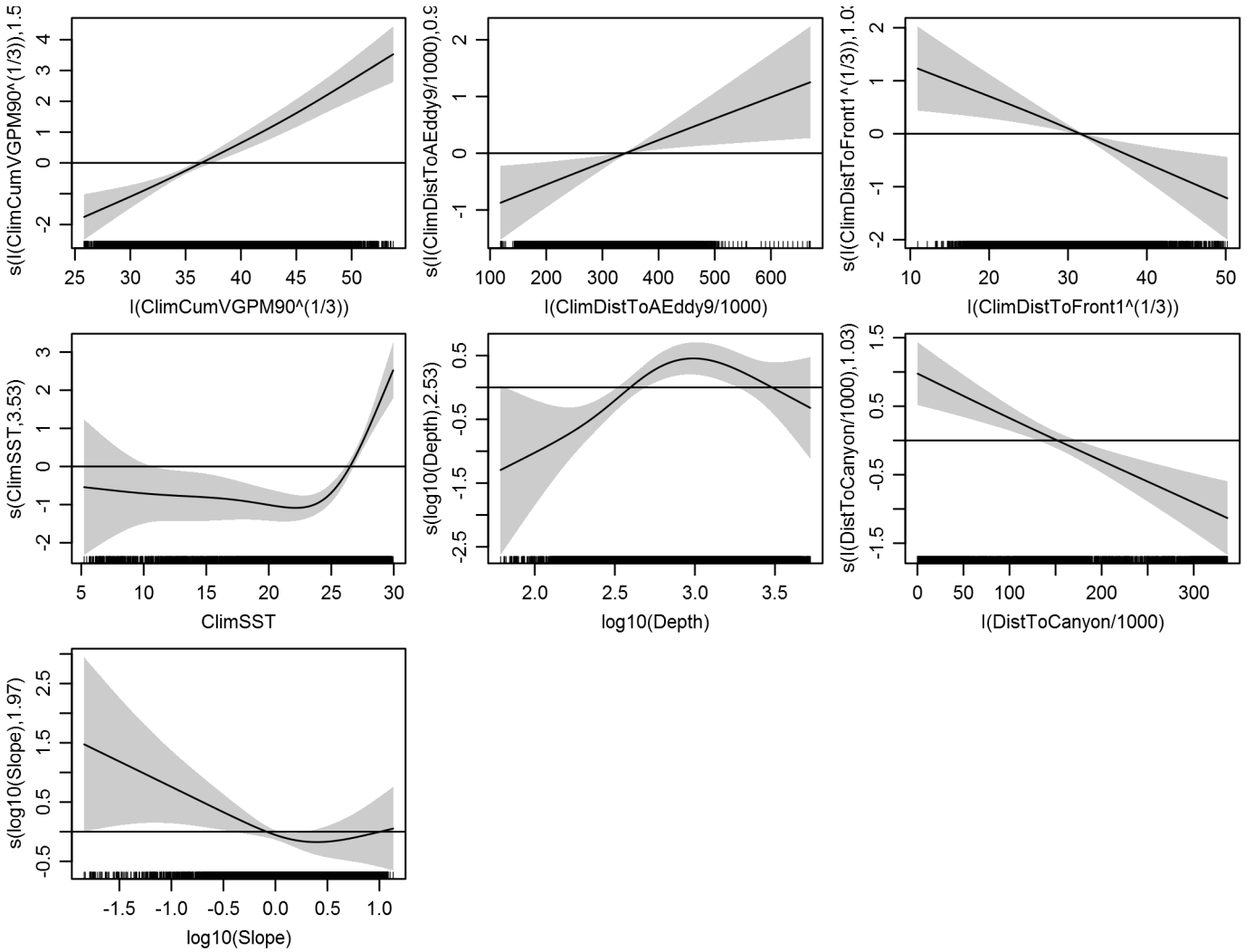

Diagnostic plots

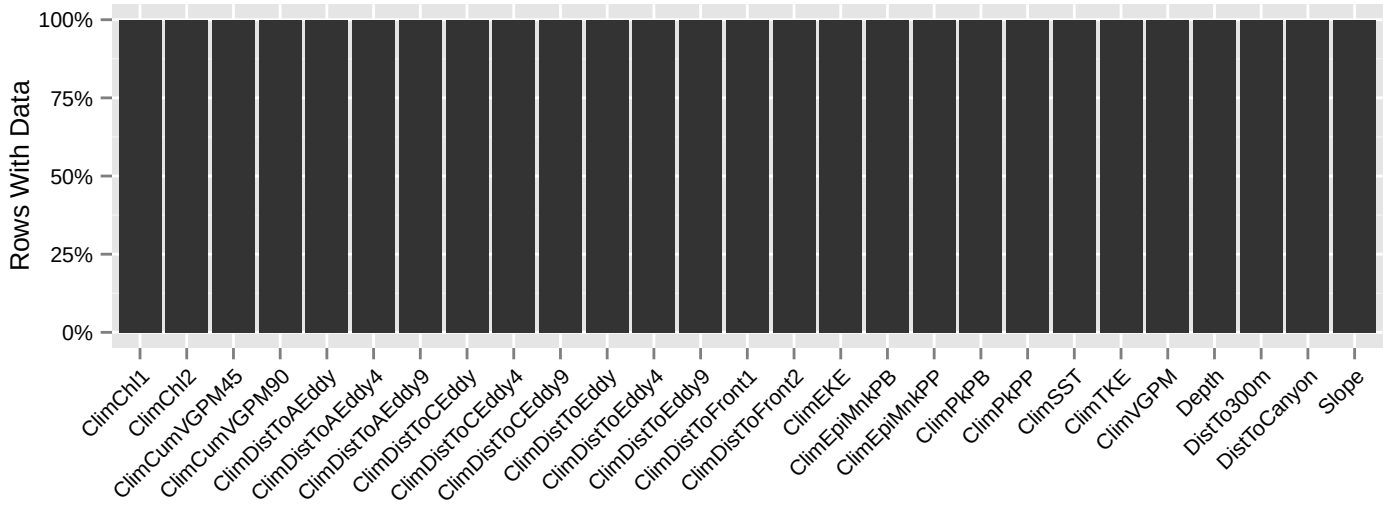

Figure 45: Segments with predictor values for the Pilot whales Climatological model, Slope and Abyss. This plot is used to assess how many segments would be lost by including a given predictor in a model.

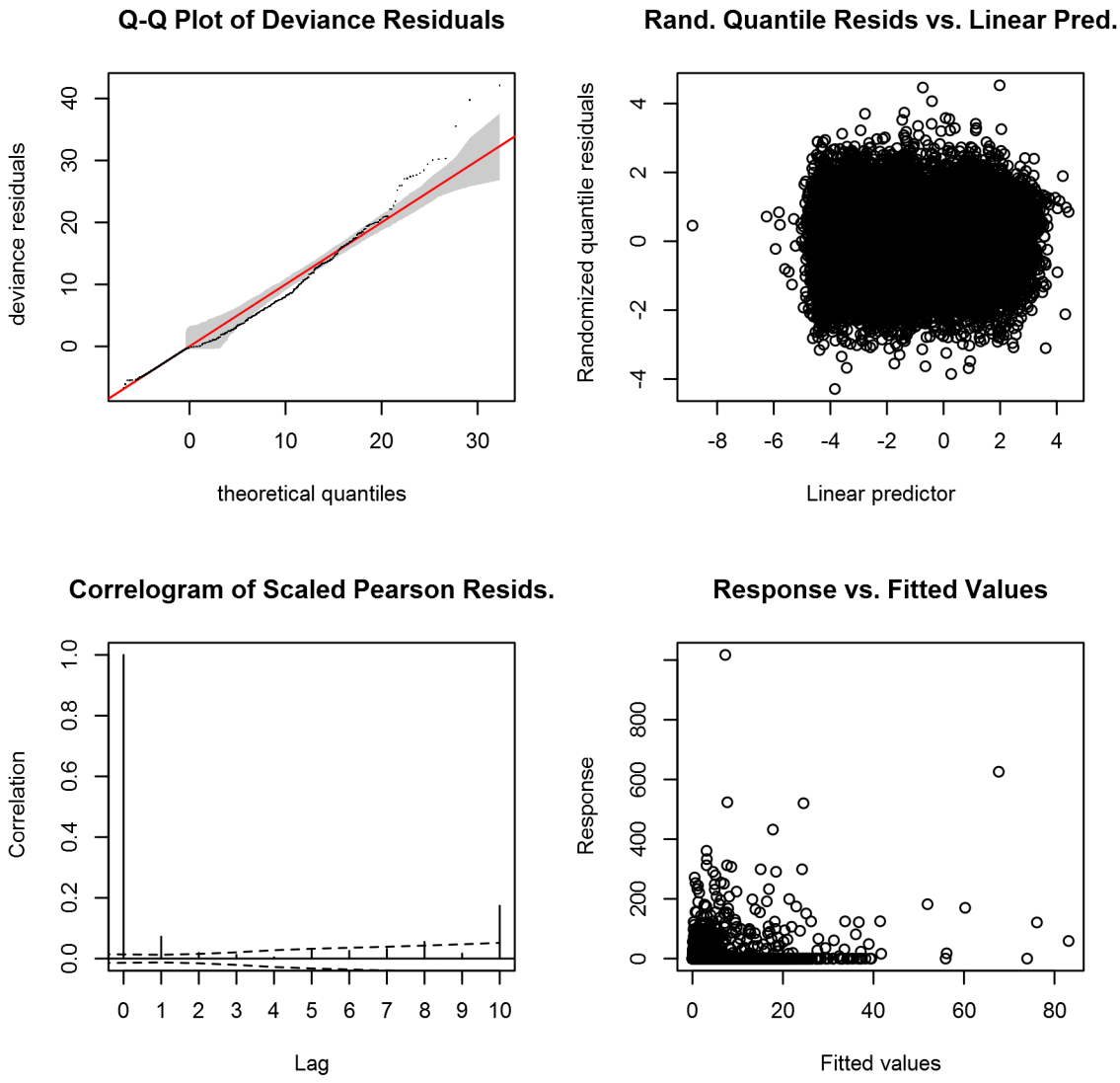

Figure 46: Statistical diagnostic plots for the Pilot whales Climatological model, Slope and Abyss.

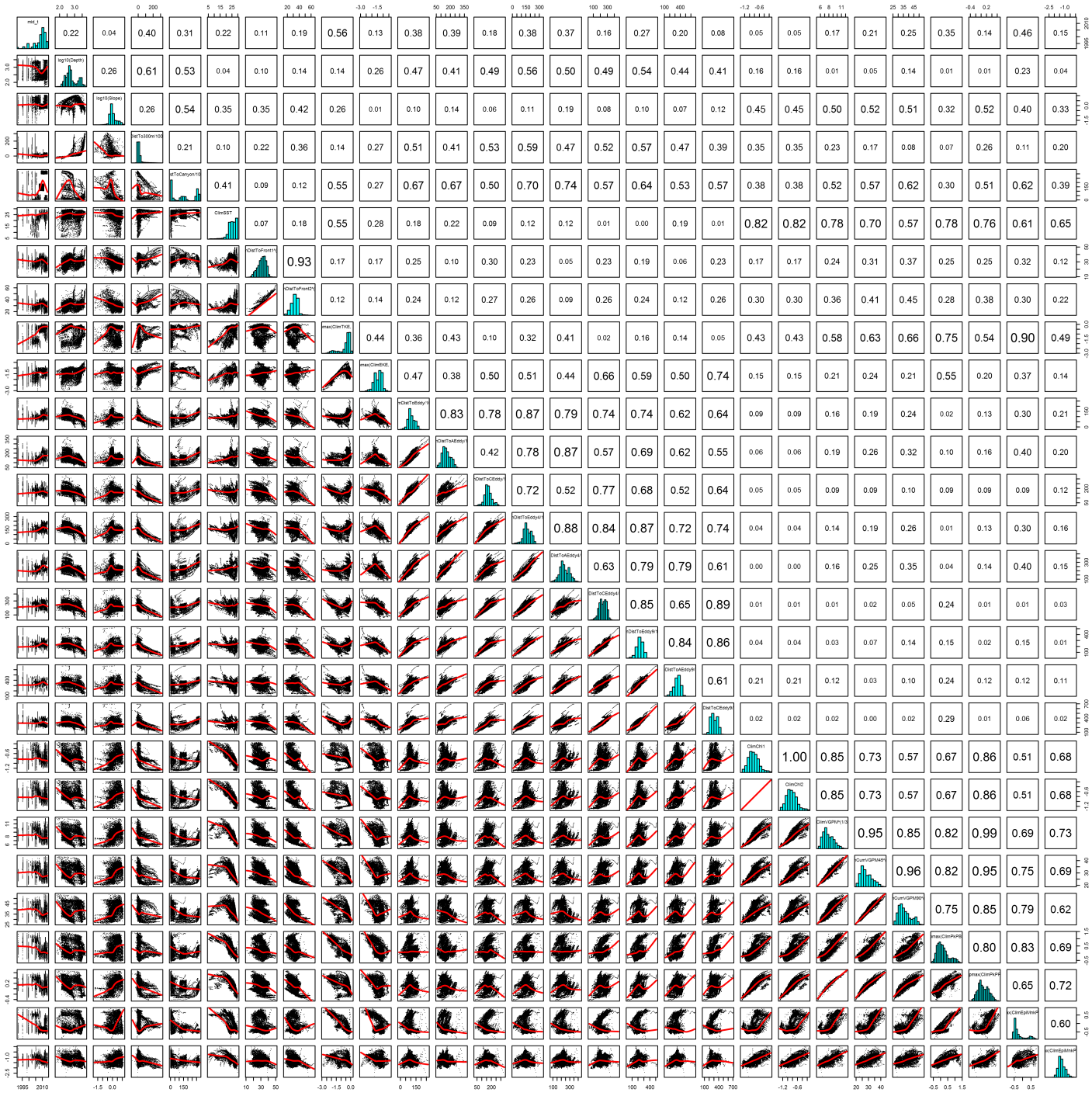

Figure 47: Scatterplot matrix for the Pilot whales Climatological model, Slope and Abyss. This plot is used to inspect the distribution of predictors (via histograms along the diagonal), simple correlation between predictors (via pairwise Pearson coefficients above the diagonal), and linearity of predictor correlations (via scatterplots below the diagonal). This plot is best viewed at high magnification.

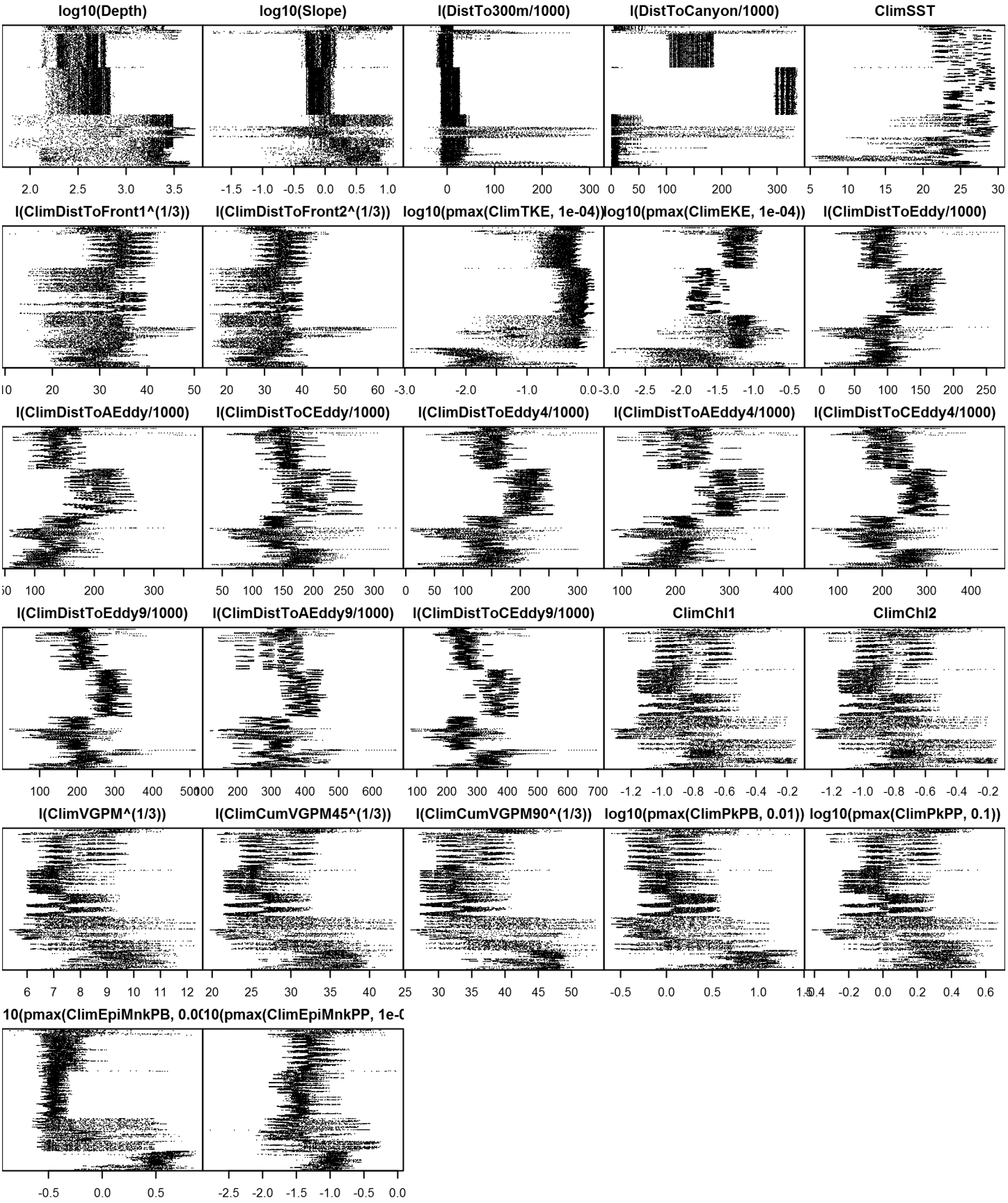

Figure 48: Dotplot for the Pilot whales Climatological model, Slope and Abyss. This plot is used to check for suspicious patterns and outliers in the data. Points are ordered vertically by transect ID, sequentially in time.

Shelf

Statistical output

```
Rscript.exe: This is mgcv 1.8-2. For overview type 'help("mgcv-package")'.


Family: Tweedie(p=1.492)
Link function: log

Formula:
abundance ~ offset(log(area_km2)) + s(log10(Depth), bs = "ts",
    k = 5) + s(I(DistTo125m/1000), bs = "ts", k = 5) + s(I(DistToCanyon/1000),
    bs = "ts", k = 5) + s(ClimSST, bs = "ts", k = 5) + s(log10(pmax(ClimPkPB,
    0.01)), bs = "ts", k = 5)

Parametric coefficients:
            Estimate Std. Error t value Pr(>|t|)
(Intercept) -10.0573     0.7844  -12.82   <2e-16 ***
---
Signif. codes:  0 '***' 0.001 '**' 0.01 '*' 0.05 '.' 0.1 ' ' 1

Approximate significance of smooth terms:
                                edf Ref.df      F  p-value
s(log10(Depth))               2.668      4 22.654  < 2e-16 ***
s(I(DistTo125m/1000))         2.591      4  4.872 2.97e-05 ***
s(I(DistToCanyon/1000))       3.824      4 21.920  < 2e-16 ***
s(ClimSST)                    3.031      4 10.034 2.40e-09 ***
s(log10(pmax(ClimPkPB, 0.01))) 2.165      4  5.794 3.31e-06 ***
---
Signif. codes:  0 '***' 0.001 '**' 0.01 '*' 0.05 '.' 0.1 ' ' 1

R-sq.(adj) =  0.000971   Deviance explained = 34.1%
-REML = 3879.6  Scale est. = 198.51    n = 86865

All predictors were significant. This is the final model.
Creating term plots.
Diagnostic output from gam.check():

Method: REML   Optimizer: outer newton
full convergence after 15 iterations.
Gradient range [-0.0003840434,0.001415365]
(score 3879.581 & scale 198.5065).
Hessian positive definite, eigenvalue range [0.2757569,1052.45].
Model rank =  21 / 21

Basis dimension (k) checking results. Low p-value (k-index<1) may
indicate that k is too low, especially if edf is close to k'.

                                k'   edf k-index p-value
s(log10(Depth))               4.000 2.668   0.587       0
s(I(DistTo125m/1000))         4.000 2.591   0.618       0
s(I(DistToCanyon/1000))       4.000 3.824   0.632       0
s(ClimSST)                    4.000 3.031   0.595       0
s(log10(pmax(ClimPkPB, 0.01))) 4.000 2.165   0.576       0

Predictors retained during the model selection procedure: Depth, DistTo125m, DistToCanyon, ClimSST,
ClimPkPB
```

```
Predictors dropped during the model selection procedure: Slope, ClimDistToFront1, ClimEKE
```

Model term plots

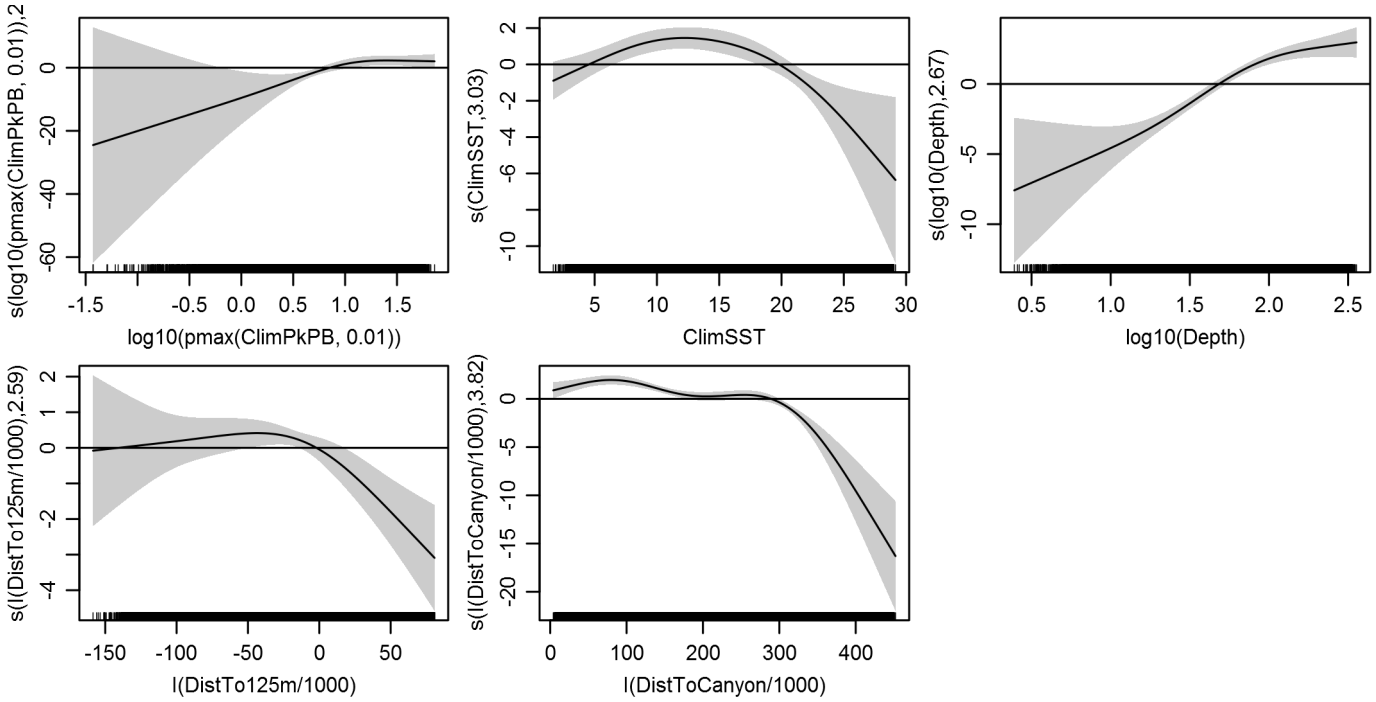

Diagnostic plots

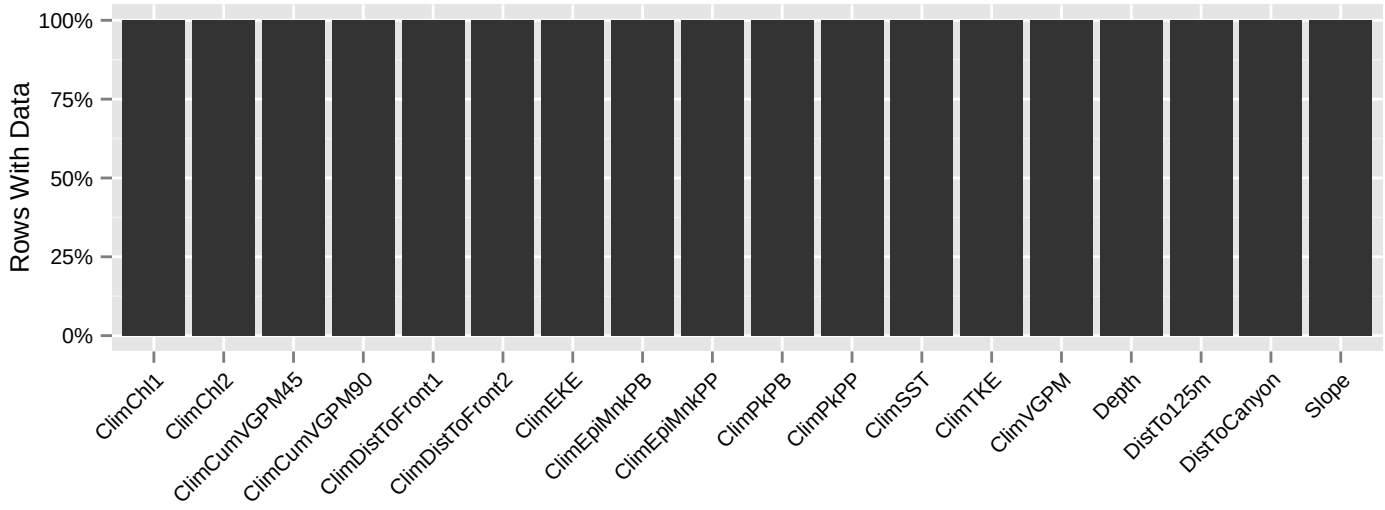

Figure 49: Segments with predictor values for the Pilot whales Climatological model, Shelf. This plot is used to assess how many segments would be lost by including a given predictor in a model.

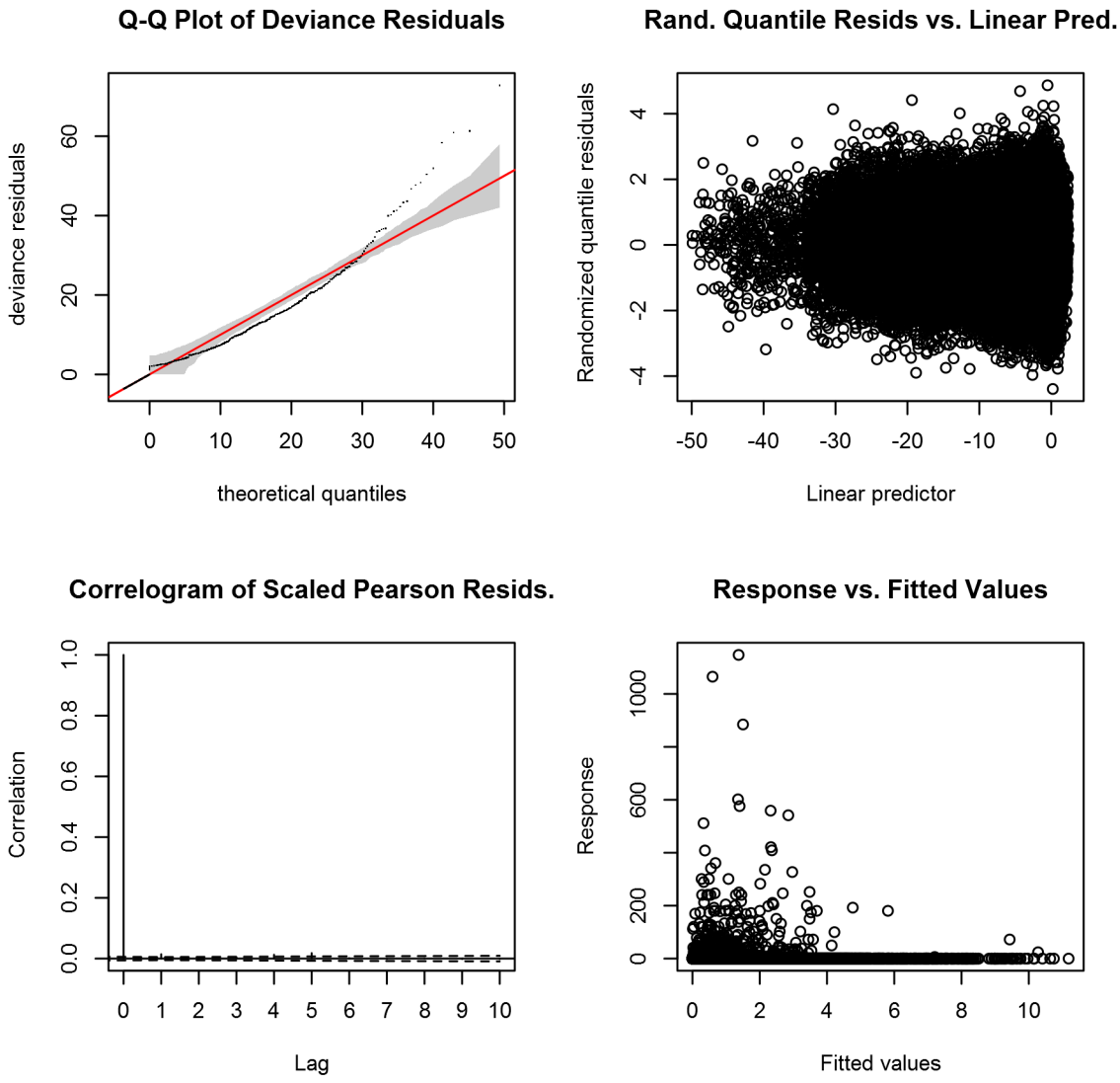

Figure 50: Statistical diagnostic plots for the Pilot whales Climatological model, Shelf.

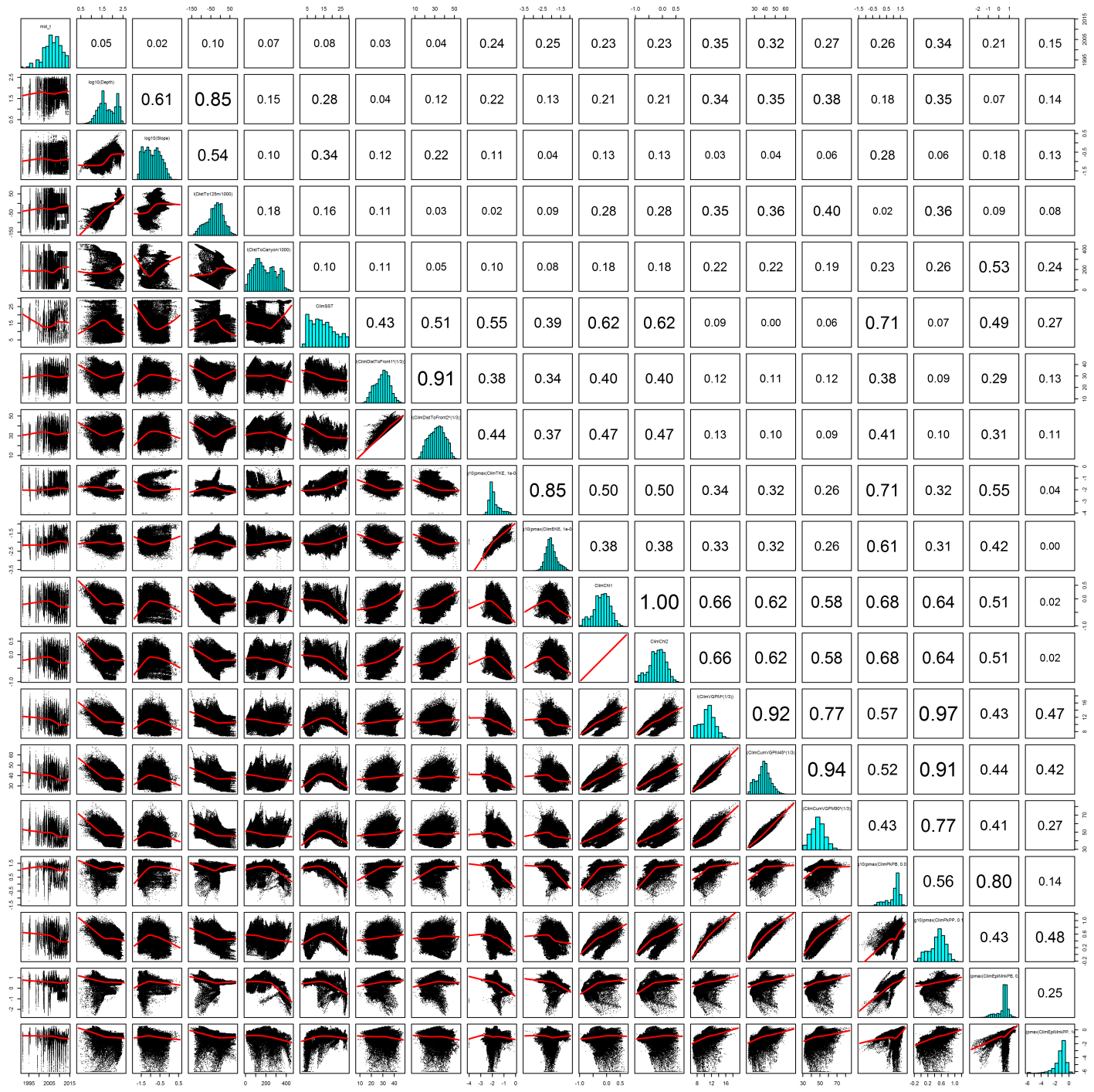

Figure 51: Scatterplot matrix for the Pilot whales Climatological model, Shelf. This plot is used to inspect the distribution of predictors (via histograms along the diagonal), simple correlation between predictors (via pairwise Pearson coefficients above the diagonal), and linearity of predictor correlations (via scatterplots below the diagonal). This plot is best viewed at high magnification.

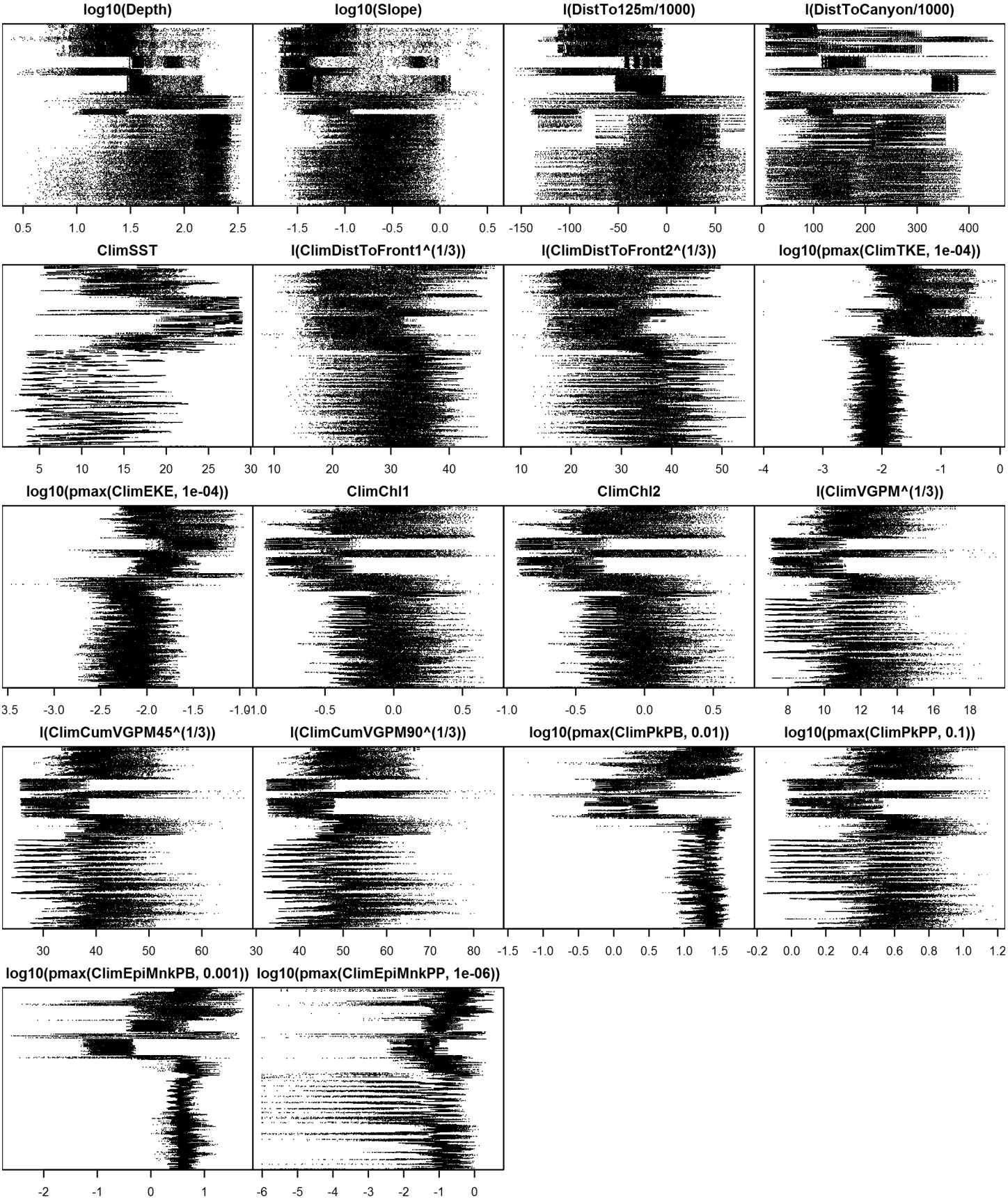

Figure 52: Dotplot for the Pilot whales Climatological model, Shelf. This plot is used to check for suspicious patterns and outliers in the data. Points are ordered vertically by transect ID, sequentially in time.

Contemporaneous Model

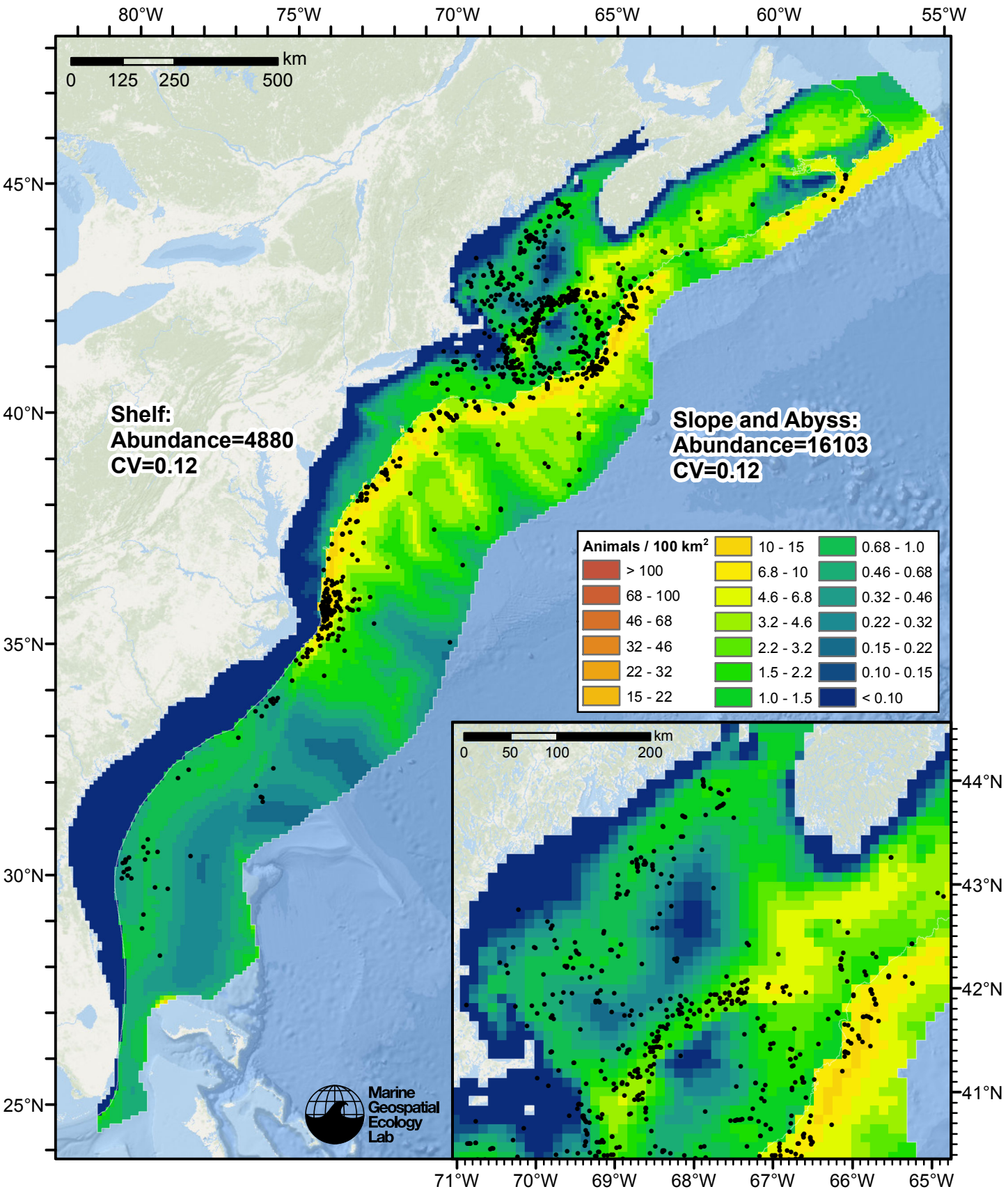

Figure 53: Pilot whales density predicted by the contemporaneous model that explained the most deviance. Pixels are 10x10 km. The legend gives the estimated individuals per pixel; breaks are logarithmic. Abundance for each region was computed by summing the density cells occuring in that region.

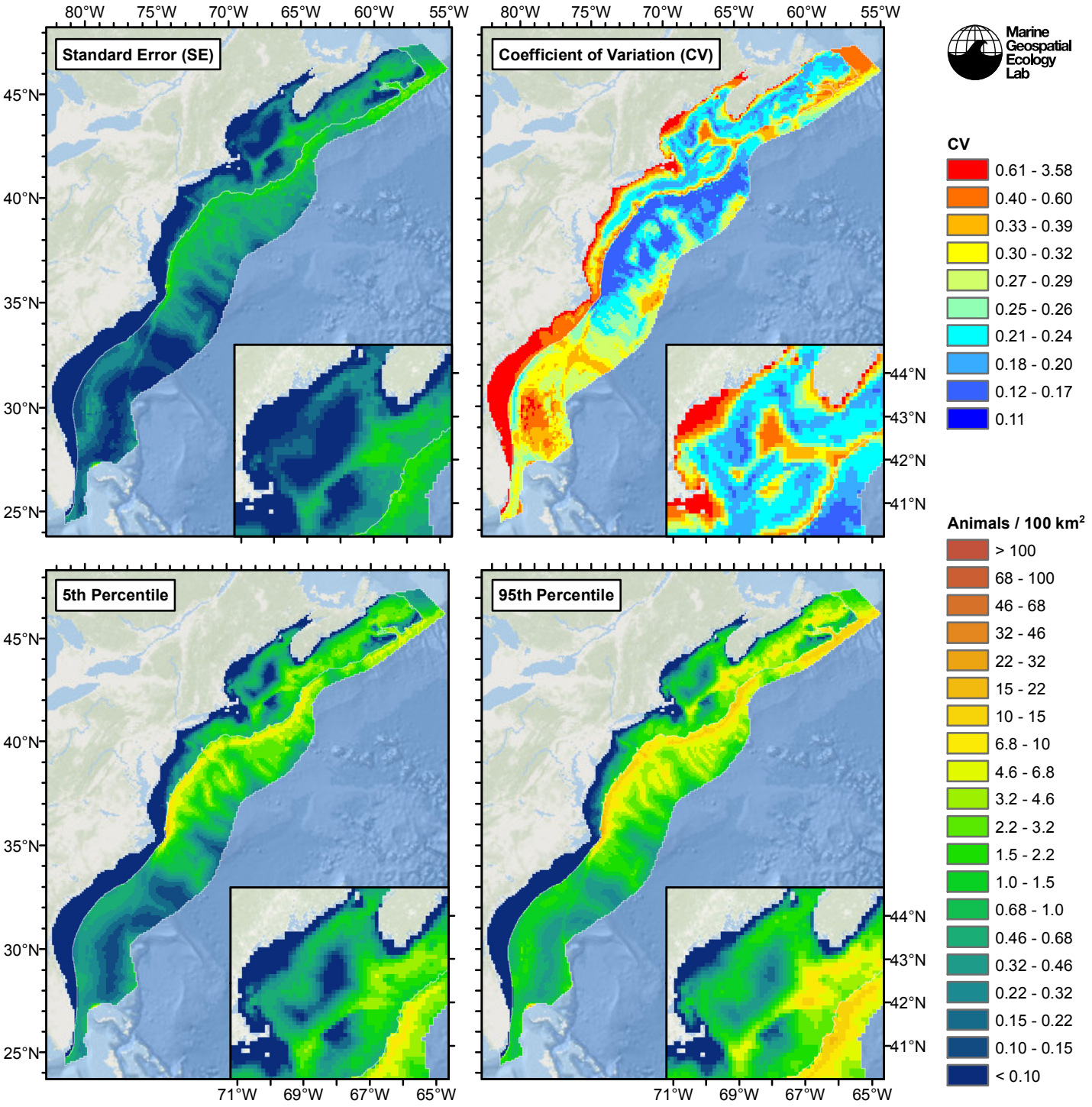

Figure 54: Estimated uncertainty for the contemporaneous model that explained the most deviance. These estimates only incorporate the statistical uncertainty estimated for the spatial model (by the R mgcv package). They do not incorporate uncertainty in the detection functions, g(0) estimates, predictor variables, and so on.

Slope and Abyss

Statistical output

```
Rscript.exe: This is mgcv 1.8-2. For overview type 'help("mgcv-package")'.


Family: Tweedie(p=1.405)
```

```
Link function: log

Formula:
abundance ~ offset(log(area_km2)) + s(log10(Slope), bs = "ts",
    k = 5) + s(I(DistToCanyon/1000), bs = "ts", k = 5) + s(SST,
    bs = "ts", k = 5) + s(I(CumVGPM90^(1/3)), bs = "ts", k = 5)

Parametric coefficients:
            Estimate Std. Error t value Pr(>|t|)
(Intercept)  -4.5969     0.1248  -36.83   <2e-16 ***
---
Signif. codes:  0 '***' 0.001 '**' 0.01 '*' 0.05 '.' 0.1 ' ' 1

Approximate significance of smooth terms:
                          edf Ref.df      F  p-value
s(log10(Slope))         1.813      4  2.508  0.00246 **
s(I(DistToCanyon/1000)) 3.201      4 10.874 2.84e-10 ***
s(SST)                  3.774      4 19.456  < 2e-16 ***
s(I(CumVGPM90^(1/3)))   1.363      4 16.795  < 2e-16 ***
---
Signif. codes:  0 '***' 0.001 '**' 0.01 '*' 0.05 '.' 0.1 ' ' 1

R-sq.(adj) =  0.0449   Deviance explained = 36.5%
-REML =   2820  Scale est. = 84.912    n = 16693

All predictors were significant. This is the final model.
Creating term plots.
Diagnostic output from gam.check():

Method: REML   Optimizer: outer newton
full convergence after 10 iterations.
Gradient range [-0.003261749,0.0002361061]
(score 2820.01 & scale 84.91154).
Hessian positive definite, eigenvalue range [0.2339766,737.9823].
Model rank =  17 / 17

Basis dimension (k) checking results. Low p-value (k-index<1) may
indicate that k is too low, especially if edf is close to k'.

                           k'   edf k-index p-value
s(log10(Slope))         4.000 1.813   0.716    0.00
s(I(DistToCanyon/1000)) 4.000 3.201   0.702    0.00
s(SST)                  4.000 3.774   0.743    0.32
s(I(CumVGPM90^(1/3)))   4.000 1.363   0.714    0.01

Predictors retained during the model selection procedure: Slope, DistToCanyon, SST, CumVGPM90

Predictors dropped during the model selection procedure: Depth, DistTo300m, DistToFront1, TKE,
DistToAEddy4, DistToCEddy4
```

Model term plots

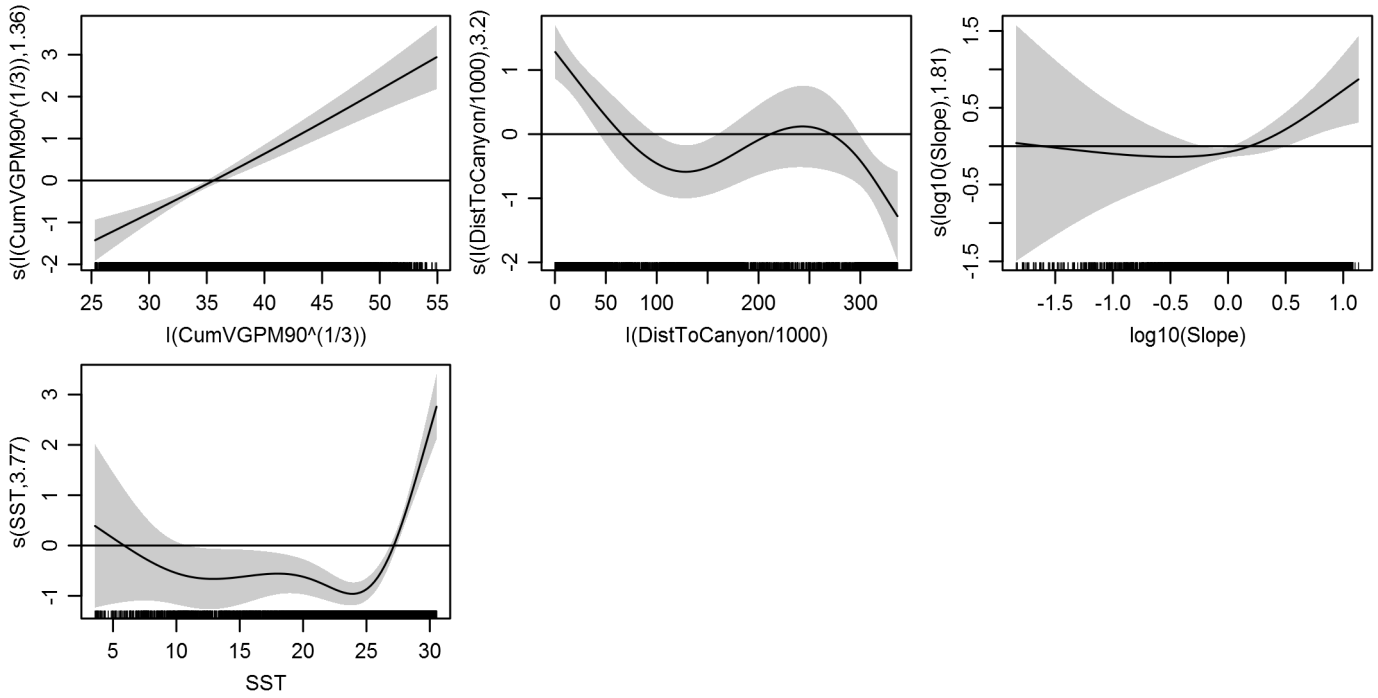

Diagnostic plots

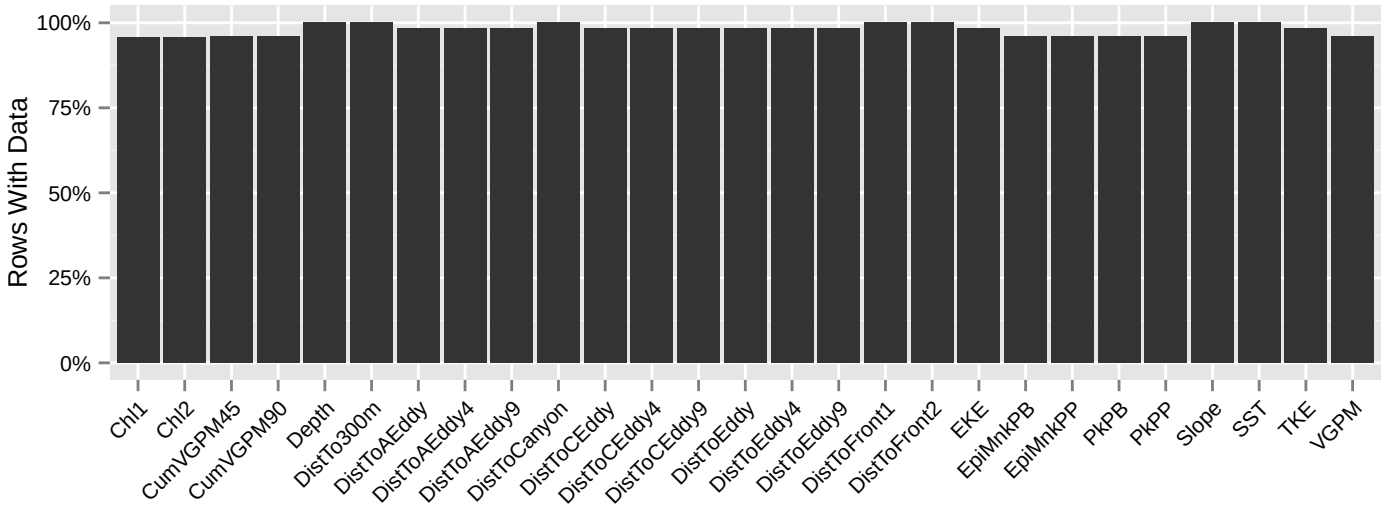

Figure 55: Segments with predictor values for the Pilot whales Contemporaneous model, Slope and Abyss. This plot is used to assess how many segments would be lost by including a given predictor in a model.

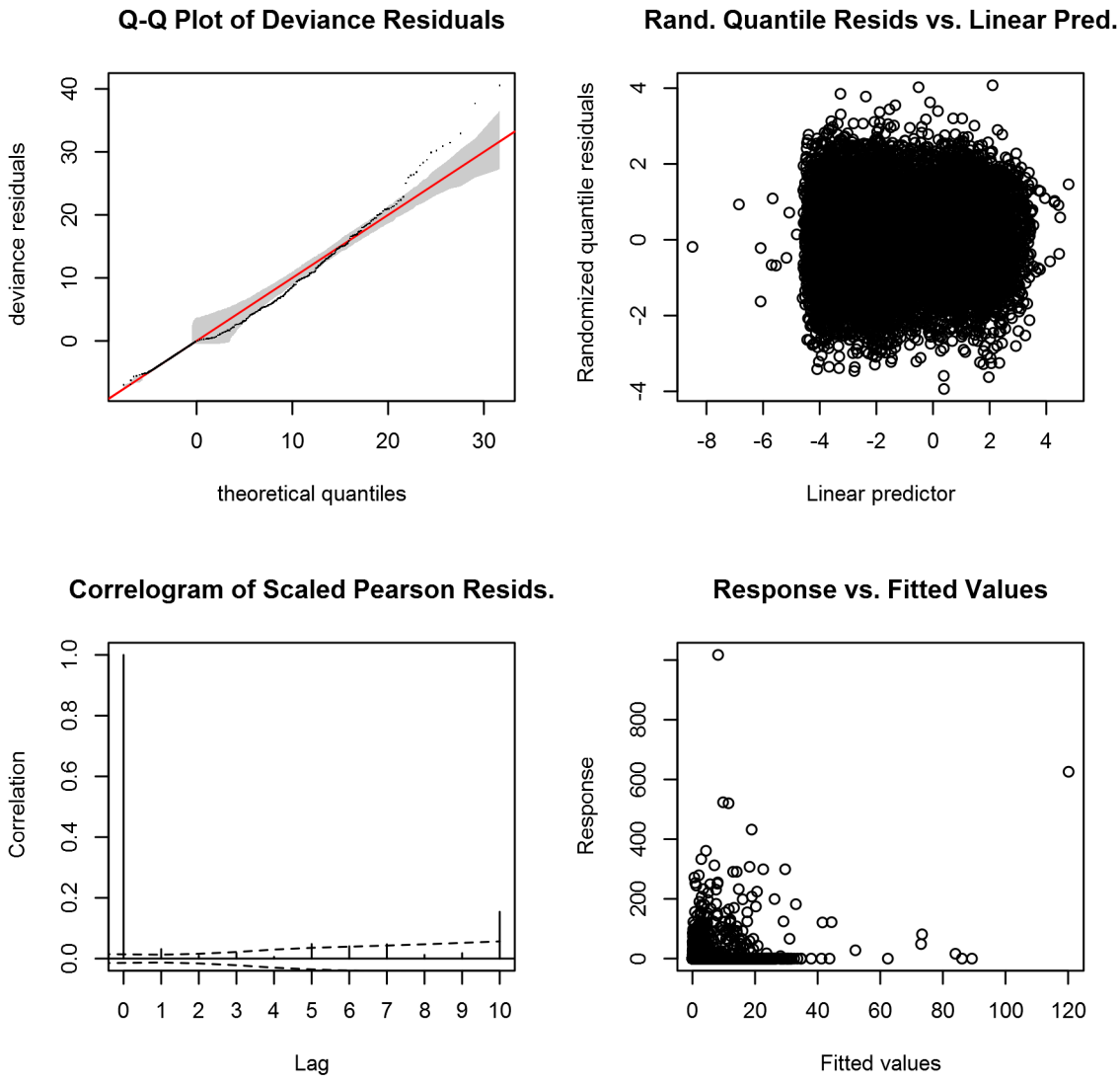

Figure 56: Statistical diagnostic plots for the Pilot whales Contemporaneous model, Slope and Abyss.

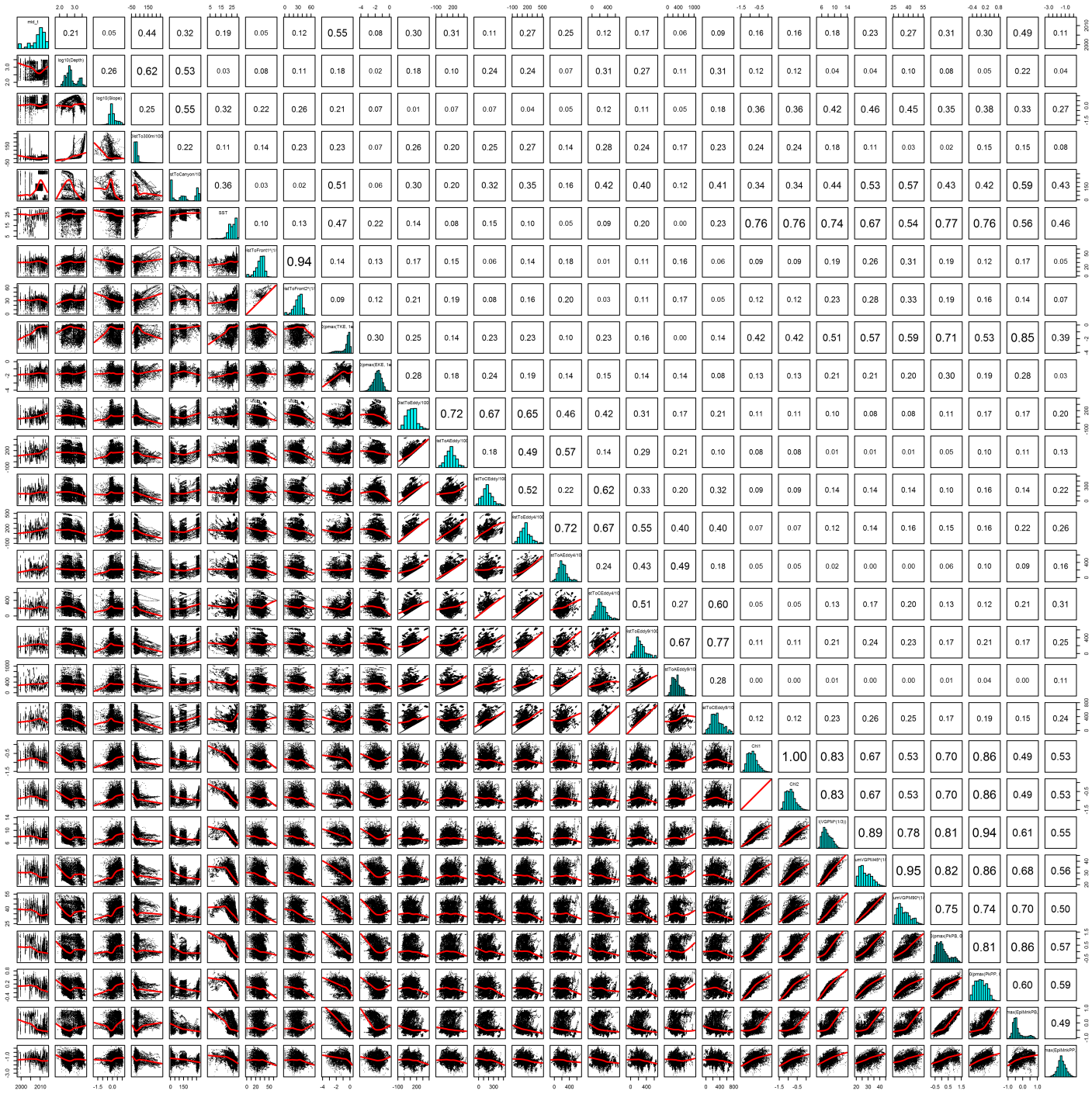

Figure 57: Scatterplot matrix for the Pilot whales Contemporaneous model, Slope and Abyss. This plot is used to inspect the distribution of predictors (via histograms along the diagonal), simple correlation between predictors (via pairwise Pearson coefficients above the diagonal), and linearity of predictor correlations (via scatterplots below the diagonal). This plot is best viewed at high magnification.

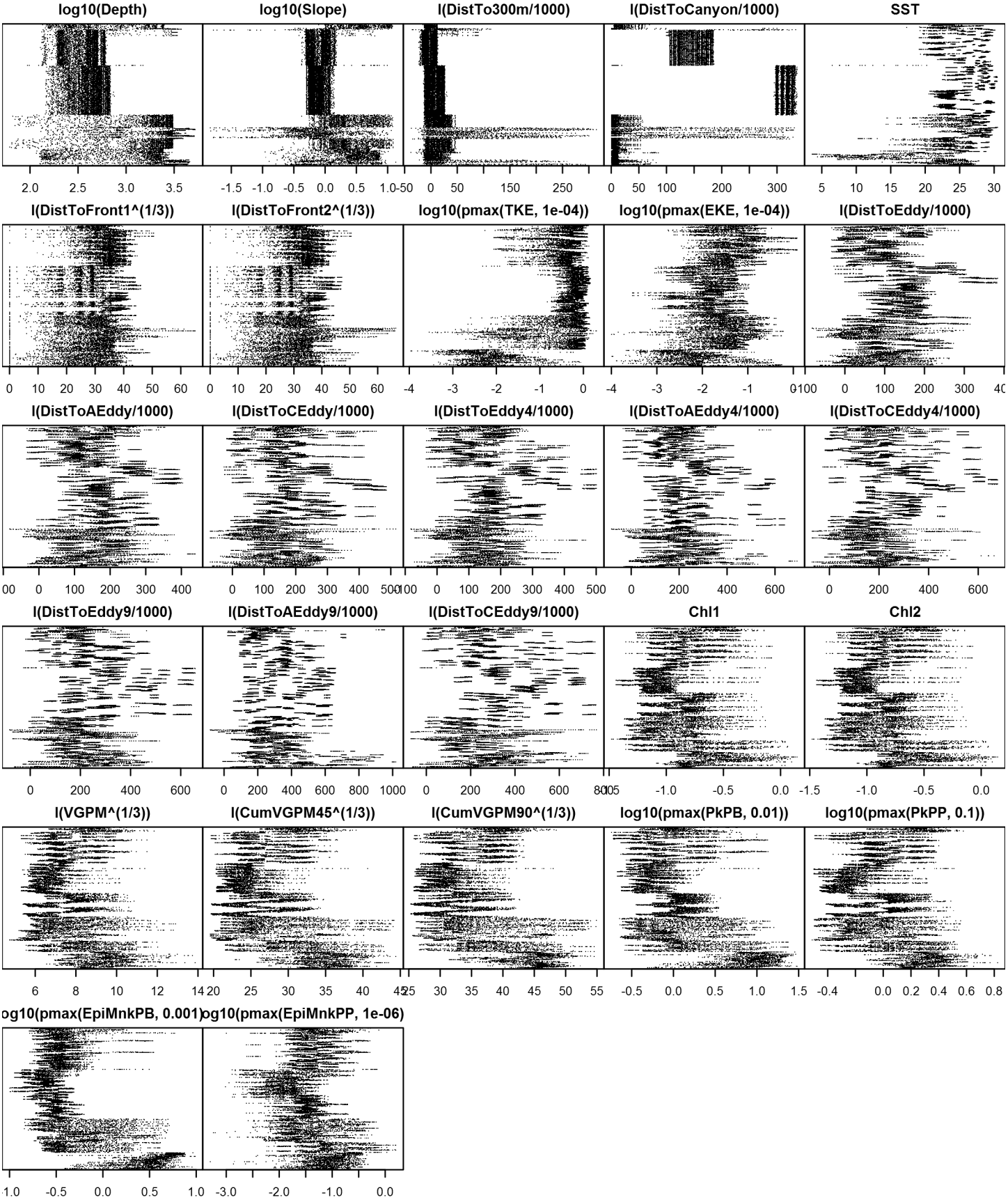

Figure 58: Dotplot for the Pilot whales Contemporaneous model, Slope and Abyss. This plot is used to check for suspicious patterns and outliers in the data. Points are ordered vertically by transect ID, sequentially in time.

Shelf

Statistical output

```
Rscript.exe: This is mgcv 1.8-2. For overview type 'help("mgcv-package")'.


Family: Tweedie(p=1.493)
Link function: log

Formula:
abundance ~ offset(log(area_km2)) + s(log10(Depth), bs = "ts",
    k = 5) + s(I(DistTo125m/1000), bs = "ts", k = 5) + s(I(DistToCanyon/1000),
    bs = "ts", k = 5) + s(SST, bs = "ts", k = 5) + s(I(DistToFront1^(1/3)),
    bs = "ts", k = 5) + s(log10(pmax(PkPB, 0.01)), bs = "ts",
    k = 5)

Parametric coefficients:
            Estimate Std. Error t value Pr(>|t|)
(Intercept)  -9.1373     0.5249  -17.41   <2e-16 ***
---
Signif. codes:  0 '***' 0.001 '**' 0.01 '*' 0.05 '.' 0.1 ' ' 1

Approximate significance of smooth terms:
                              edf Ref.df      F  p-value
s(log10(Depth))            2.7789      4 22.866  < 2e-16 ***
s(I(DistTo125m/1000))      2.4921      4  3.976  0.00020 ***
s(I(DistToCanyon/1000))    3.8147      4 23.278  < 2e-16 ***
s(SST)                     3.1454      4 10.548 8.43e-10 ***
s(I(DistToFront1^(1/3)))   0.9478      4  1.524  0.00885 **
s(log10(pmax(PkPB, 0.01))) 2.2598      4  5.716 4.41e-06 ***
---
Signif. codes:  0 '***' 0.001 '**' 0.01 '*' 0.05 '.' 0.1 ' ' 1

R-sq.(adj) =  0.000219   Deviance explained = 33.3%
-REML = 3845.5  Scale est. = 198.72    n = 83244

All predictors were significant. This is the final model.
Creating term plots.
Diagnostic output from gam.check():

Method: REML   Optimizer: outer newton
full convergence after 16 iterations.
Gradient range [-1.798009e-05,3.14284e-05]
(score 3845.513 & scale 198.7187).
Hessian positive definite, eigenvalue range [0.2051677,1038.617].
Model rank =  25 / 25

Basis dimension (k) checking results. Low p-value (k-index<1) may
indicate that k is too low, especially if edf is close to k'.

                              k'   edf k-index p-value
s(log10(Depth))            4.000 2.779   0.536    0.00
s(I(DistTo125m/1000))      4.000 2.492   0.548    0.00
s(I(DistToCanyon/1000))    4.000 3.815   0.560    0.00
s(SST)                     4.000 3.145   0.541    0.00
s(I(DistToFront1^(1/3)))   4.000 0.948   0.619    0.18
s(log10(pmax(PkPB, 0.01))) 4.000 2.260   0.485    0.00
```

Predictors retained during the model selection procedure: Depth, DistTo125m, DistToCanyon, SST, DistToFront1, PkPB

Predictors dropped during the model selection procedure: Slope, TKE

Model term plots

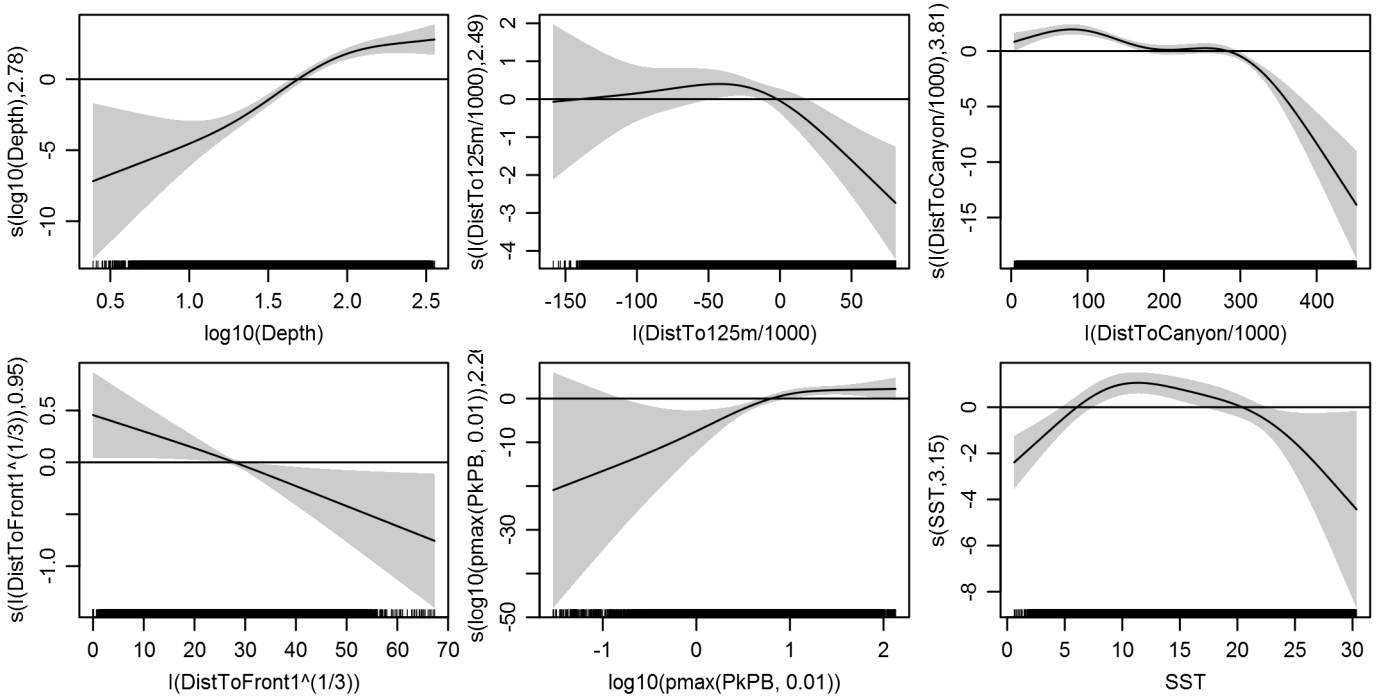

Diagnostic plots

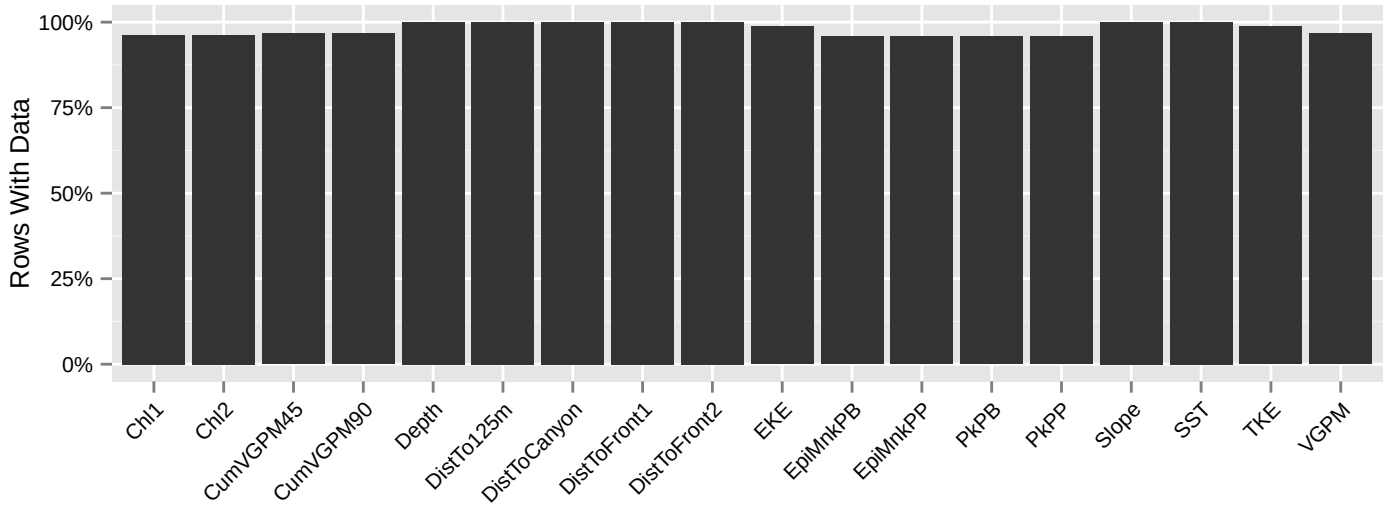

Figure 59: Segments with predictor values for the Pilot whales Contemporaneous model, Shelf. This plot is used to assess how many segments would be lost by including a given predictor in a model.

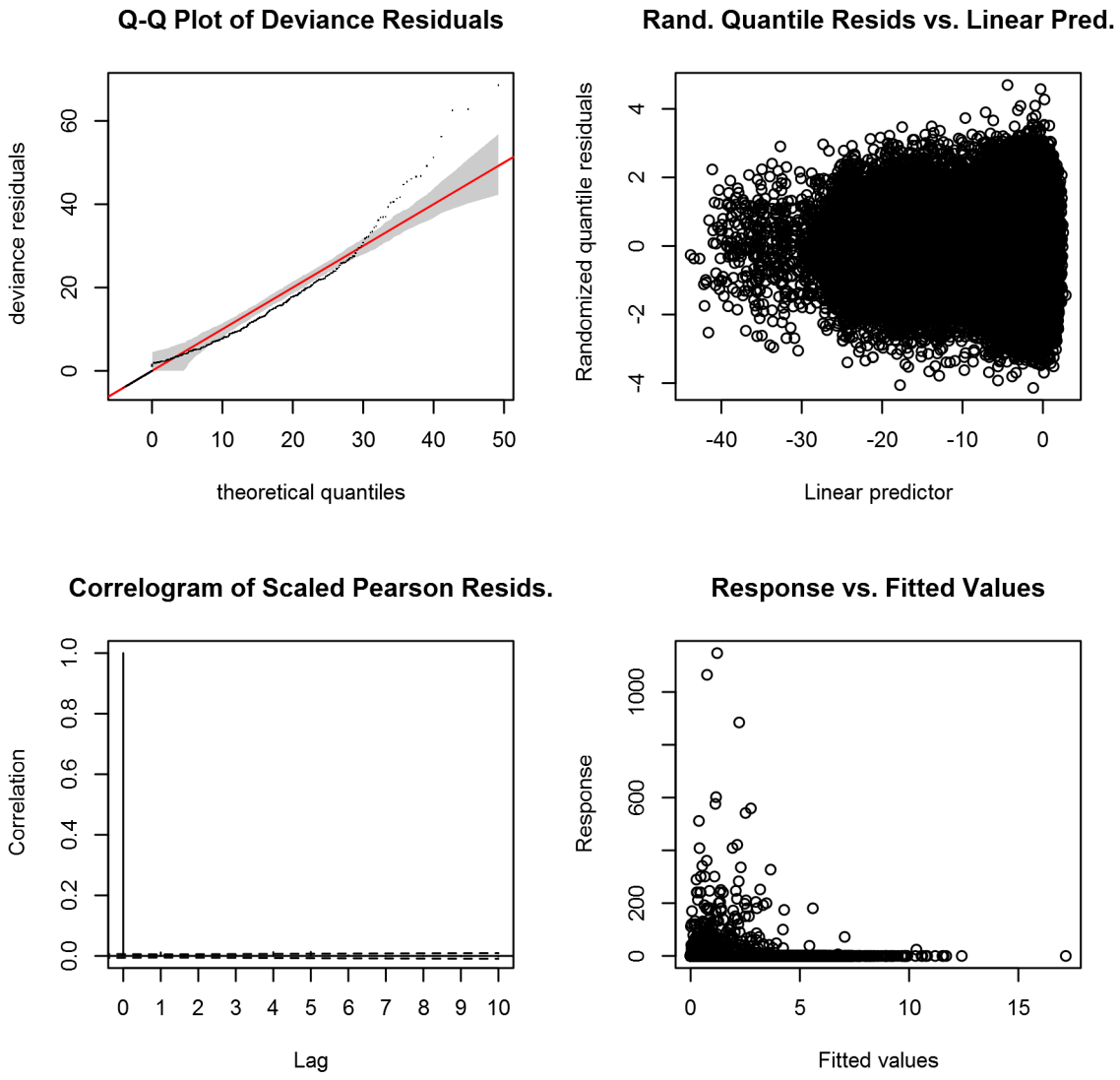

Figure 60: Statistical diagnostic plots for the Pilot whales Contemporaneous model, Shelf.

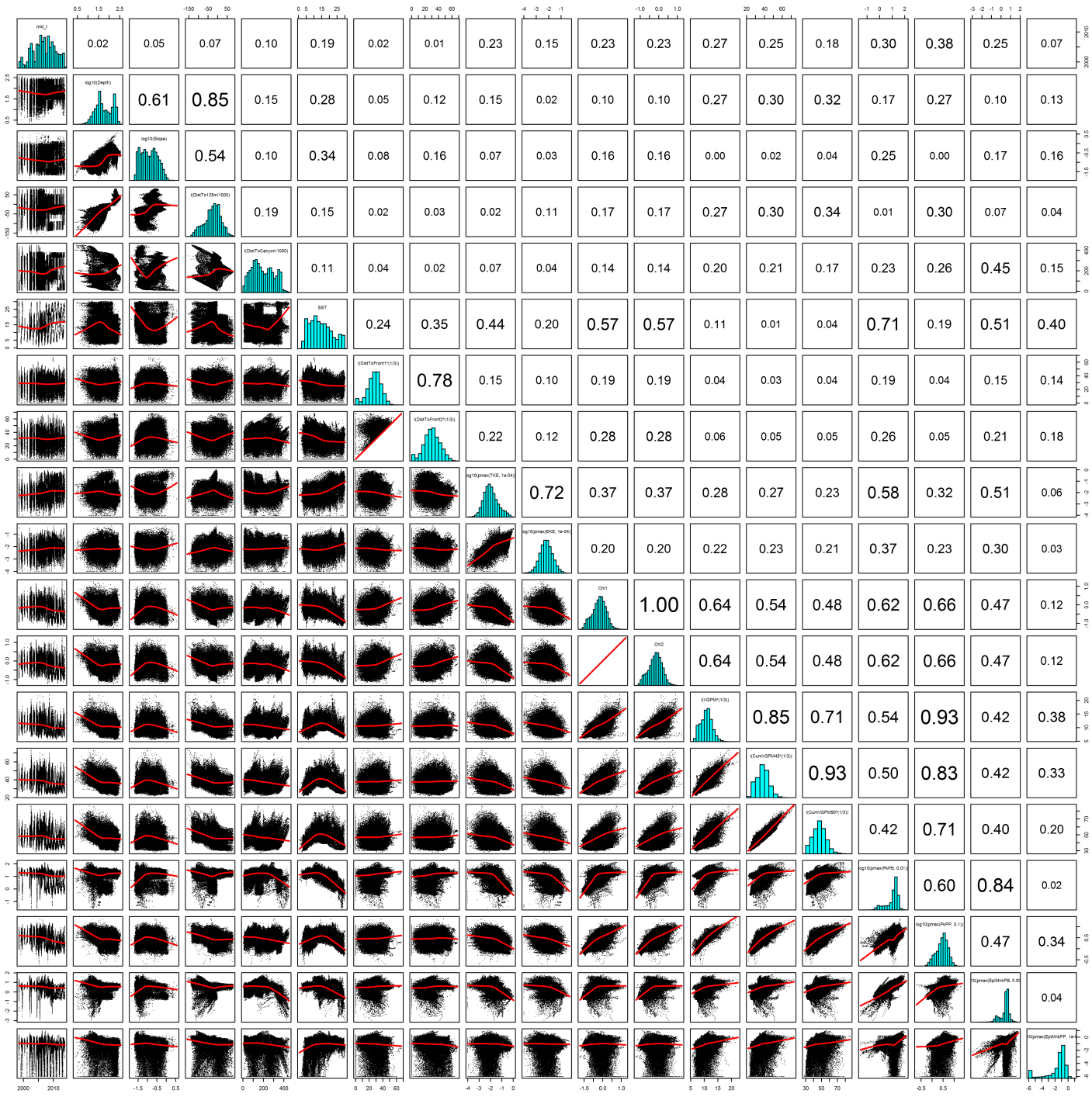

Figure 61: Scatterplot matrix for the Pilot whales Contemporaneous model, Shelf. This plot is used to inspect the distribution of predictors (via histograms along the diagonal), simple correlation between predictors (via pairwise Pearson coefficients above the diagonal), and linearity of predictor correlations (via scatterplots below the diagonal). This plot is best viewed at high magnification.

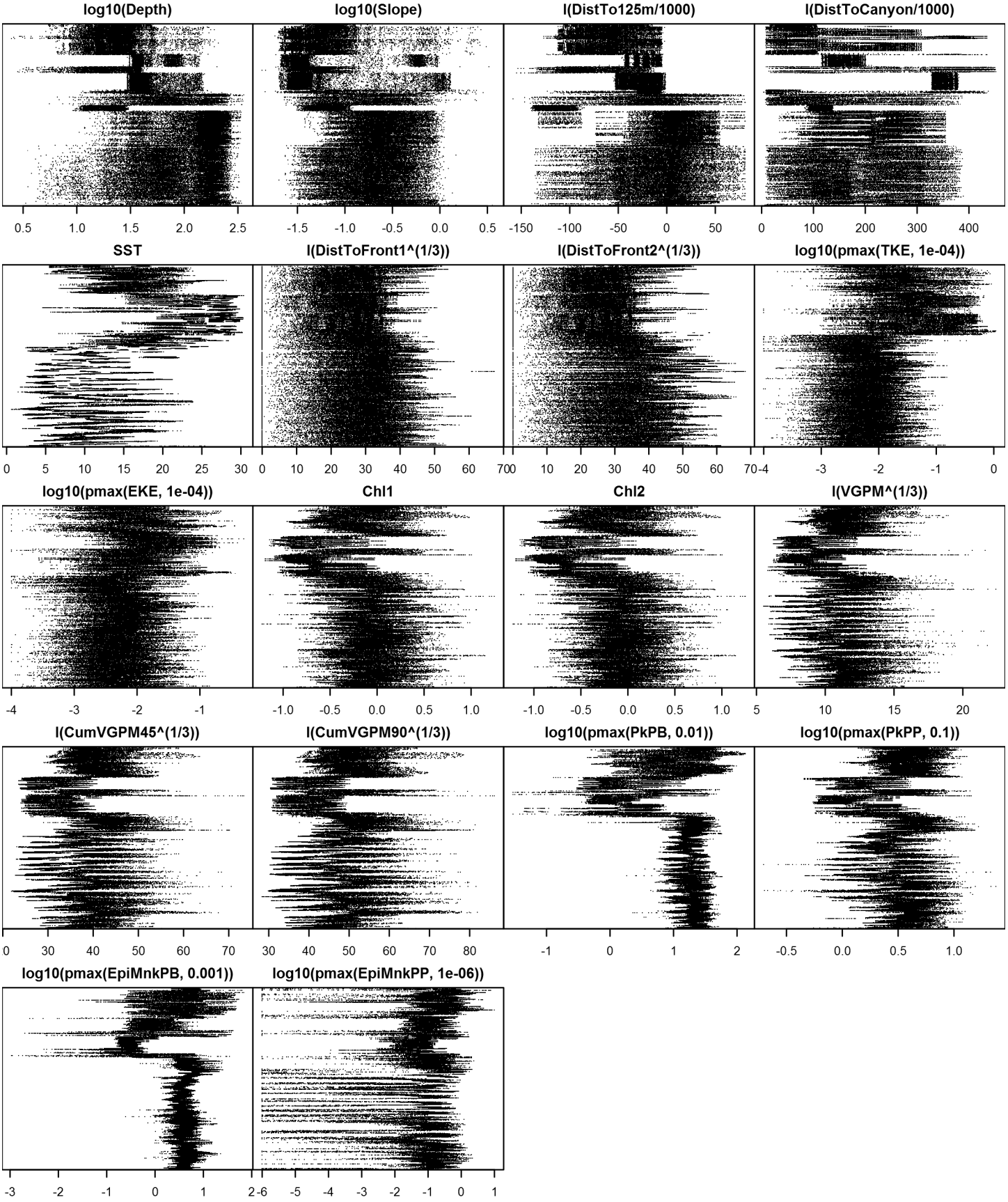

Figure 62: Dotplot for the Pilot whales Contemporaneous model, Shelf. This plot is used to check for suspicious patterns and outliers in the data. Points are ordered vertically by transect ID, sequentially in time.

Climatological Same Segments Model

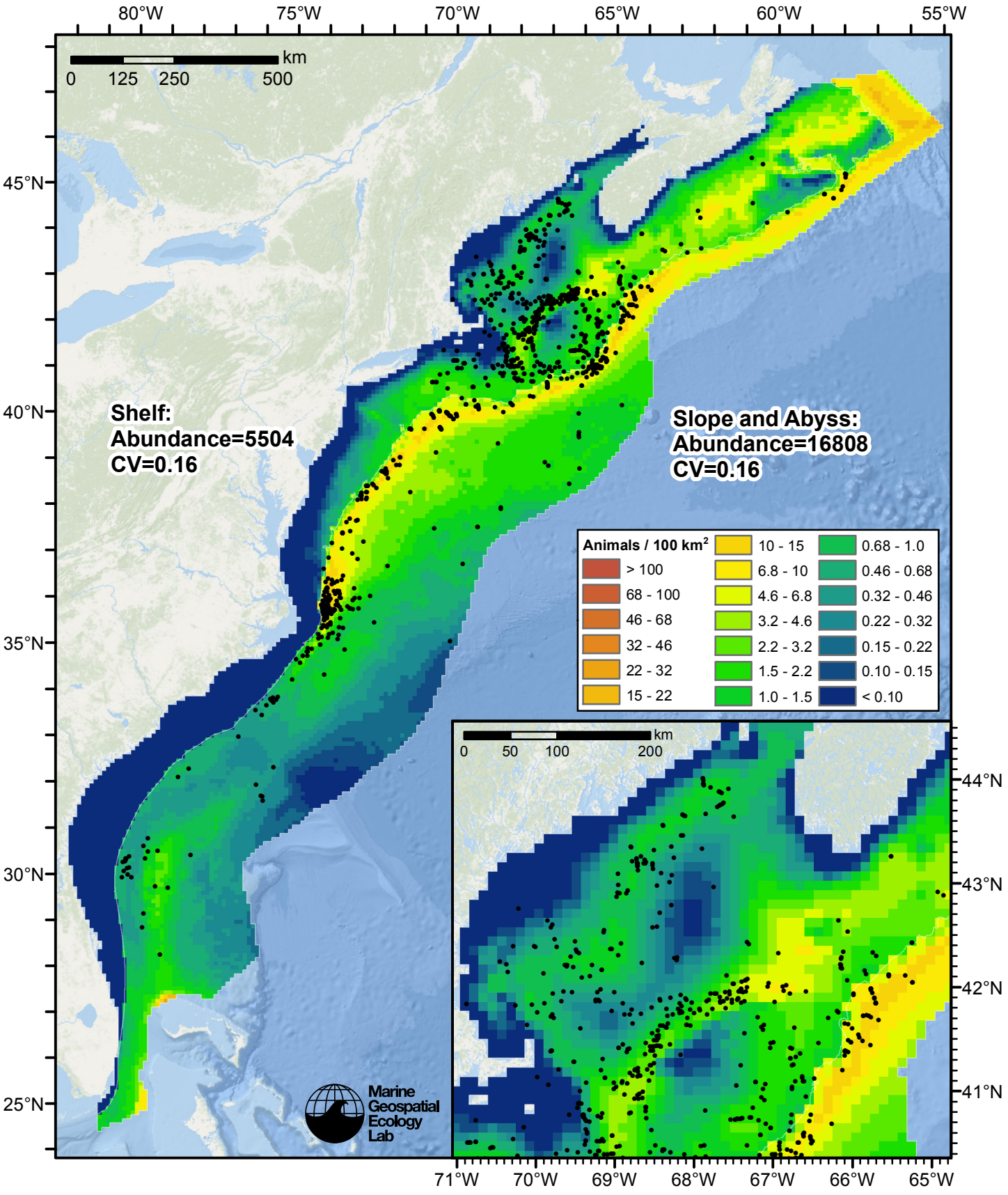

Figure 63: Pilot whales density predicted by the climatological same segments model that explained the most deviance. Pixels are 10x10 km. The legend gives the estimated individuals per pixel; breaks are logarithmic. Abundance for each region was computed by summing the density cells occuring in that region.

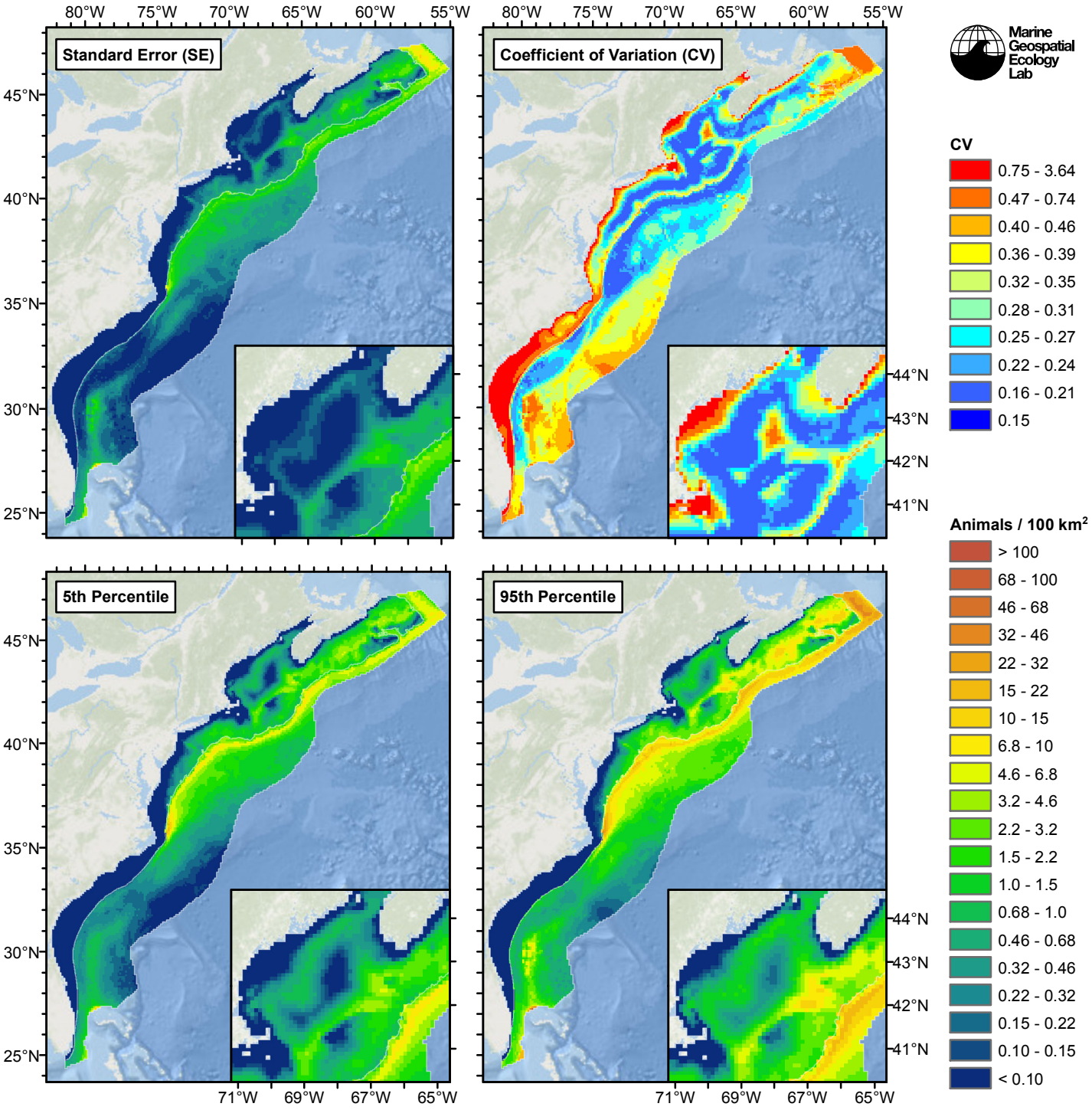

Figure 64: Estimated uncertainty for the climatological same segments model that explained the most deviance. These estimates only incorporate the statistical uncertainty estimated for the spatial model (by the R mgcv package). They do not incorporate uncertainty in the detection functions, g(0) estimates, predictor variables, and so on.

Slope and Abyss

Statistical output

```
Rscript.exe: This is mgcv 1.8-2. For overview type 'help("mgcv-package")'.


Family: Tweedie(p=1.401)
```

```
Link function: log

Formula:
abundance ~ offset(log(area_km2)) + s(log10(Depth), bs = "ts",
    k = 5) + s(log10(Slope), bs = "ts", k = 5) + s(I(DistToCanyon/1000),
    bs = "ts", k = 5) + s(ClimSST, bs = "ts", k = 5) + s(I(ClimDistToFront1^(1/3)),
    bs = "ts", k = 5) + s(log10(pmax(ClimTKE, 1e-04)), bs = "ts",
    k = 5) + s(I(ClimDistToAEddy9/1000), bs = "ts", k = 5) +
    s(I(ClimCumVGPM90^(1/3)), bs = "ts", k = 5)

Parametric coefficients:
            Estimate Std. Error t value Pr(>|t|)
(Intercept)  -4.7001     0.1301  -36.12   <2e-16 ***
---
Signif. codes:  0 '***' 0.001 '**' 0.01 '*' 0.05 '.' 0.1 ' ' 1

Approximate significance of smooth terms:
                                edf Ref.df      F  p-value
s(log10(Depth))               2.2547      4  3.752 0.000184 ***
s(log10(Slope))               2.0624      4  1.581 0.022406 *
s(I(DistToCanyon/1000))       0.9949      4  3.834 2.94e-05 ***
s(ClimSST)                    3.5333      4 16.568 1.23e-15 ***
s(I(ClimDistToFront1^(1/3)))  1.0143      4  2.522 0.000665 ***
s(log10(pmax(ClimTKE, 1e-04))) 0.9373     4  2.230 0.001192 **
s(I(ClimDistToAEddy9/1000))   1.0237      4  3.532 7.72e-05 ***
s(I(ClimCumVGPM90^(1/3)))     1.4479      4 10.862 9.95e-13 ***
---
Signif. codes:  0 '***' 0.001 '**' 0.01 '*' 0.05 '.' 0.1 ' ' 1

R-sq.(adj) =  0.0386   Deviance explained = 38.7%
-REML = 2803.9  Scale est. = 82.466    n = 16693

All predictors were significant. This is the final model.
Creating term plots.
Diagnostic output from gam.check():

Method: REML   Optimizer: outer newton
full convergence after 12 iterations.
Gradient range [-0.0004368538,0.001003732]
(score 2803.89 & scale 82.46597).
Hessian positive definite, eigenvalue range [0.2200033,737.2283].
Model rank =  33 / 33

Basis dimension (k) checking results. Low p-value (k-index<1) may
indicate that k is too low, especially if edf is close to k'.

                                k'   edf k-index p-value
s(log10(Depth))               4.000 2.255   0.687    0.00
s(log10(Slope))               4.000 2.062   0.690    0.00
s(I(DistToCanyon/1000))       4.000 0.995   0.698    0.01
s(ClimSST)                    4.000 3.533   0.708    0.04
s(I(ClimDistToFront1^(1/3)))  4.000 1.014   0.723    0.24
s(log10(pmax(ClimTKE, 1e-04))) 4.000 0.937   0.701    0.00
s(I(ClimDistToAEddy9/1000))   4.000 1.024   0.709    0.06
s(I(ClimCumVGPM90^(1/3)))     4.000 1.448   0.657    0.00

Predictors retained during the model selection procedure: Depth, Slope, DistToCanyon, ClimSST,
ClimDistToFront1, ClimTKE, ClimDistToAEddy9, ClimCumVGPM90
```

```
Predictors dropped during the model selection procedure: DistTo300m, ClimDistToCEddy9
```

Model term plots

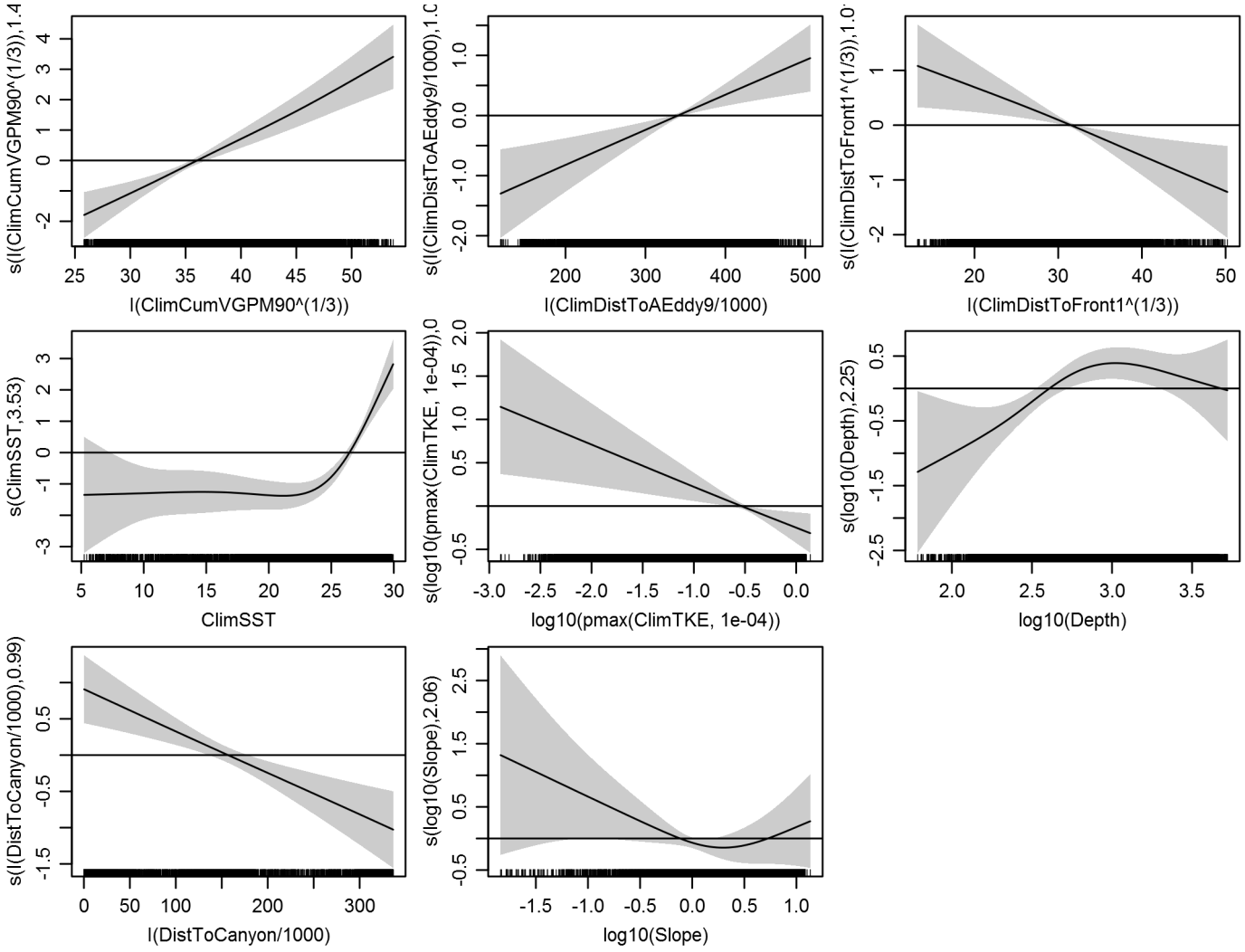

Diagnostic plots

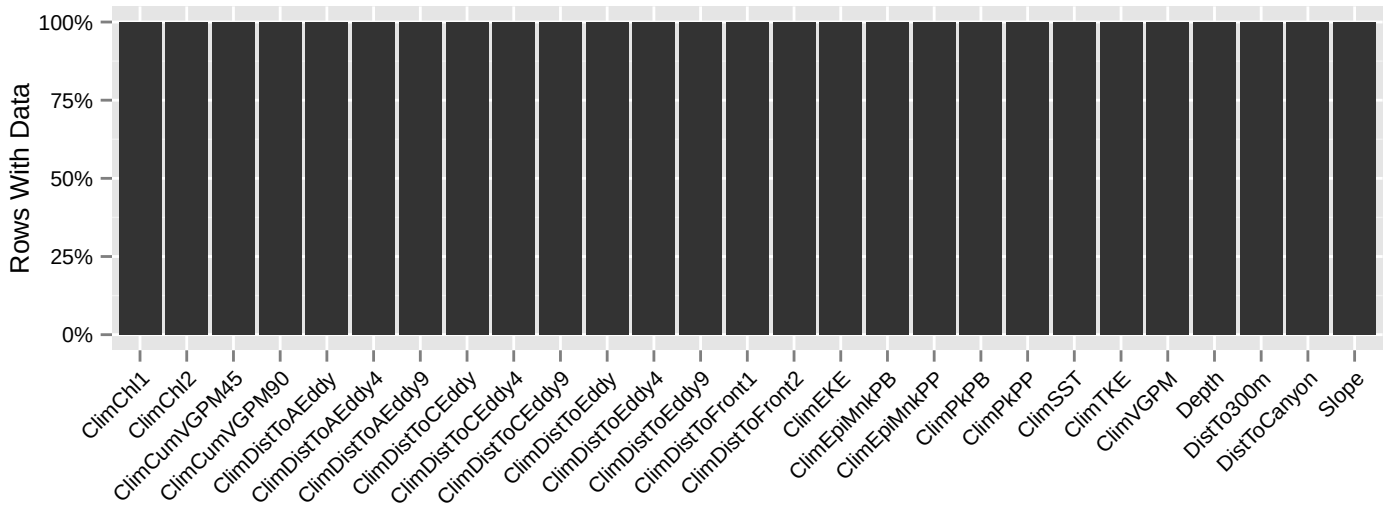

Figure 65: Segments with predictor values for the Pilot whales Climatological model, Slope and Abyss. This plot is used to assess how many segments would be lost by including a given predictor in a model.

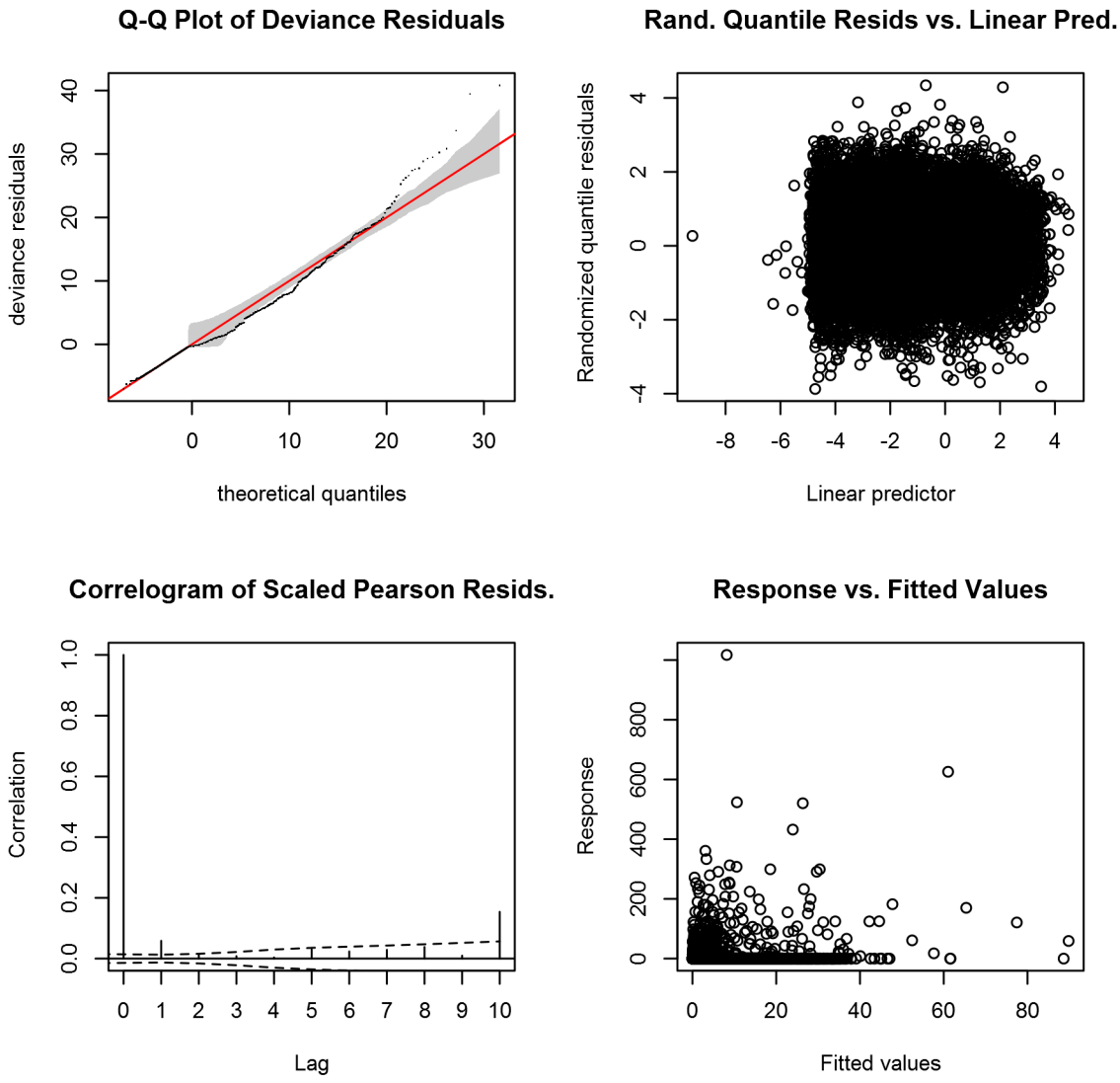

Figure 66: Statistical diagnostic plots for the Pilot whales Climatological model, Slope and Abyss.

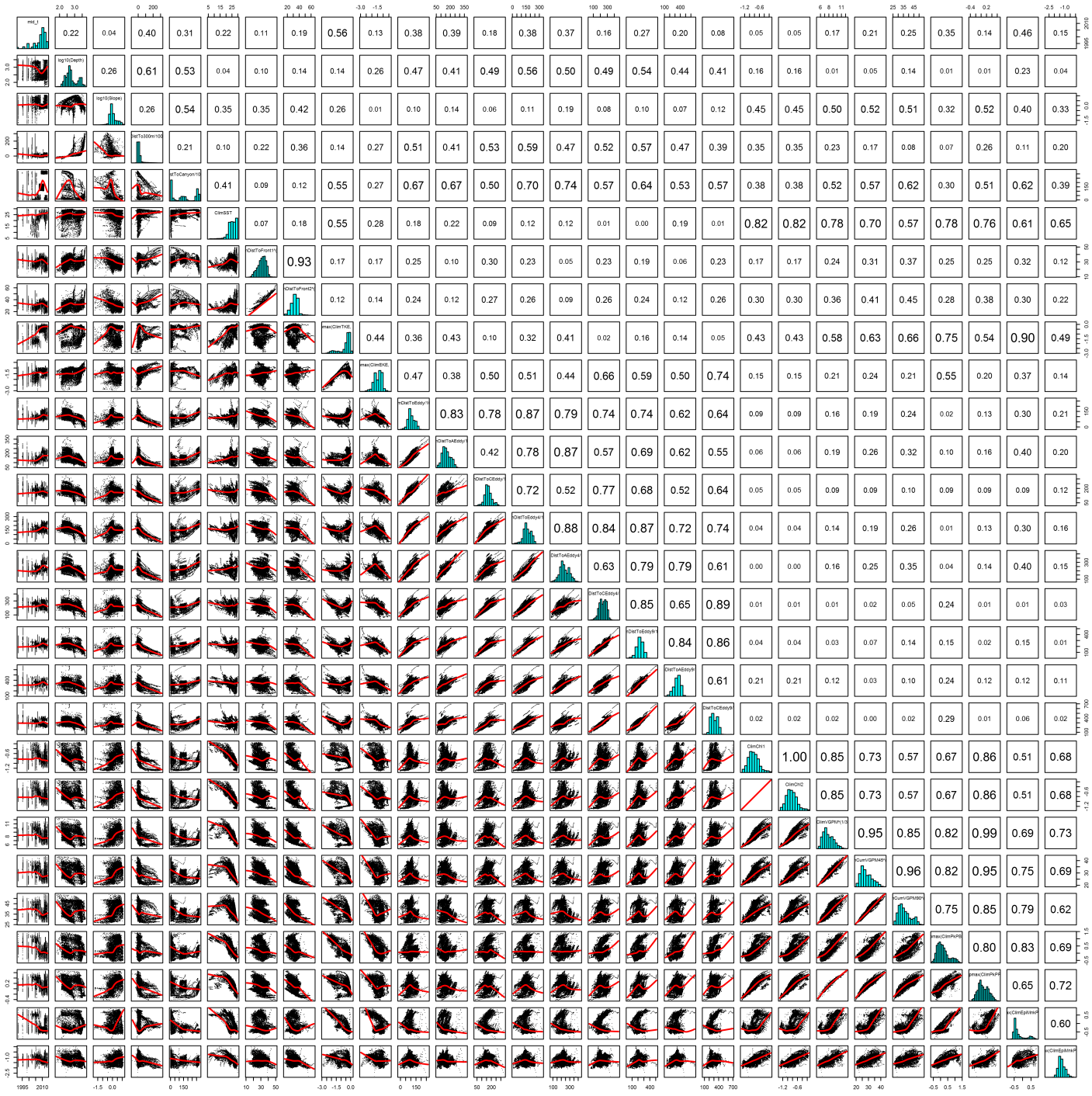

Figure 67: Scatterplot matrix for the Pilot whales Climatological model, Slope and Abyss. This plot is used to inspect the distribution of predictors (via histograms along the diagonal), simple correlation between predictors (via pairwise Pearson coefficients above the diagonal), and linearity of predictor correlations (via scatterplots below the diagonal). This plot is best viewed at high magnification.

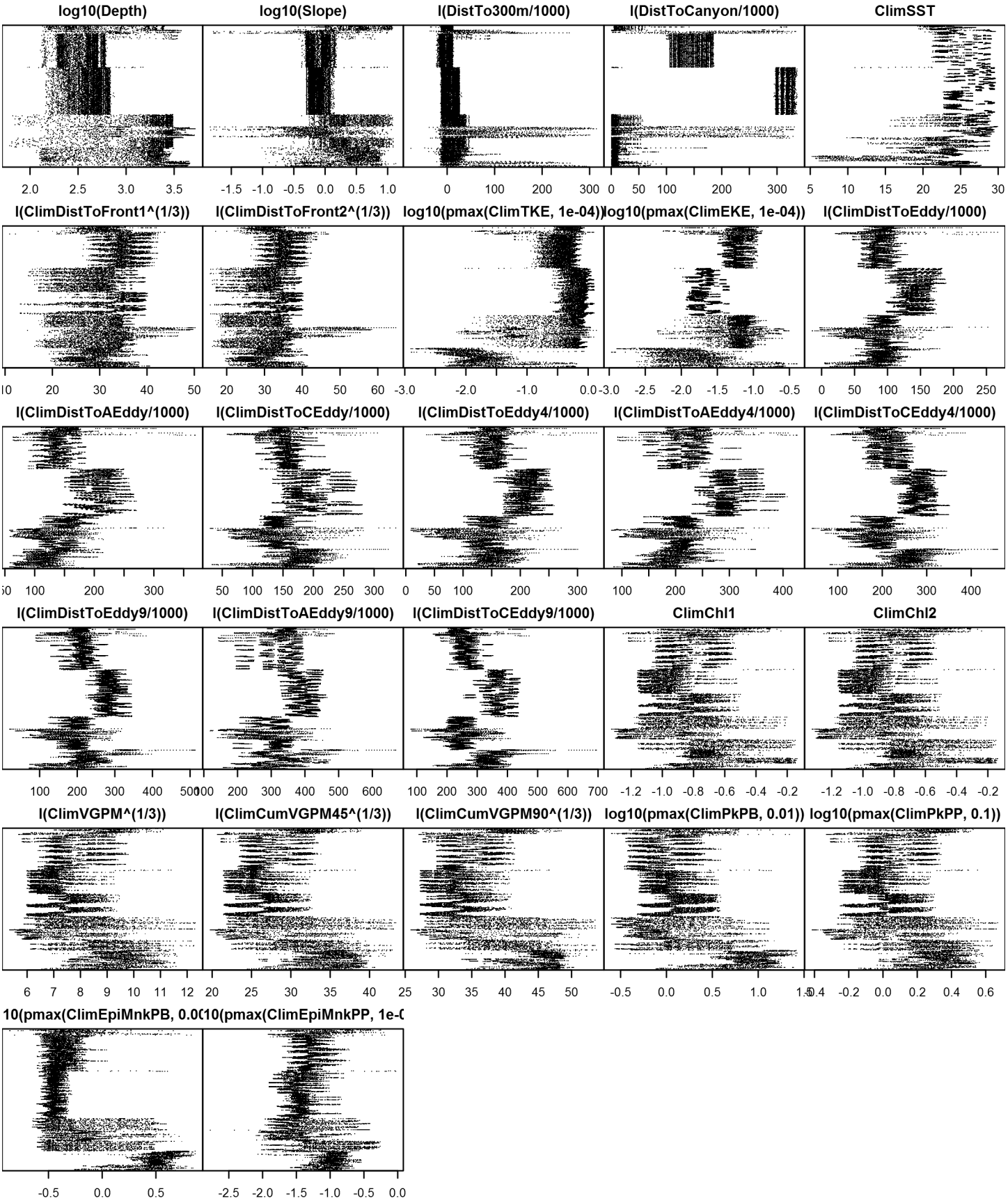

Figure 68: Dotplot for the Pilot whales Climatological model, Slope and Abyss. This plot is used to check for suspicious patterns and outliers in the data. Points are ordered vertically by transect ID, sequentially in time.

Shelf

Statistical output

```
Rscript.exe: This is mgcv 1.8-2. For overview type 'help("mgcv-package")'.


Family: Tweedie(p=1.488)
Link function: log

Formula:
abundance ~ offset(log(area_km2)) + s(log10(Depth), bs = "ts",
    k = 5) + s(I(DistTo125m/1000), bs = "ts", k = 5) + s(I(DistToCanyon/1000),
    bs = "ts", k = 5) + s(ClimSST, bs = "ts", k = 5) + s(I(ClimDistToFront1^(1/3)),
    bs = "ts", k = 5) + s(log10(pmax(ClimEKE, 1e-04)), bs = "ts",
    k = 5)

Parametric coefficients:
            Estimate Std. Error t value Pr(>|t|)
(Intercept) -10.2207     0.6901  -14.81   <2e-16 ***
---
Signif. codes:  0 '***' 0.001 '**' 0.01 '*' 0.05 '.' 0.1 ' ' 1

Approximate significance of smooth terms:
                                edf Ref.df      F  p-value
s(log10(Depth))               2.6927      4 20.662  < 2e-16 ***
s(I(DistTo125m/1000))         2.2548      4  3.674 0.000265 ***
s(I(DistToCanyon/1000))       3.8360      4 15.657 7.19e-14 ***
s(ClimSST)                    3.7434      4 15.429 1.97e-13 ***
s(I(ClimDistToFront1^(1/3)))  0.8670      4  1.245 0.013849 *
s(log10(pmax(ClimEKE, 1e-04))) 0.9303      4  1.851 0.003426 **
---
Signif. codes:  0 '***' 0.001 '**' 0.01 '*' 0.05 '.' 0.1 ' ' 1

R-sq.(adj) =  0.00117   Deviance explained = 33.5%
-REML = 3881.8  Scale est. = 197.05    n = 85799

All predictors were significant. This is the final model.
Creating term plots.
Diagnostic output from gam.check():

Method: REML   Optimizer: outer newton
full convergence after 17 iterations.
Gradient range [-2.320714e-06,1.028617e-06]
(score 3881.838 & scale 197.0475).
Hessian positive definite, eigenvalue range [0.3218853,1063.432].
Model rank =  25 / 25

Basis dimension (k) checking results. Low p-value (k-index<1) may
indicate that k is too low, especially if edf is close to k'.

                                k'   edf k-index p-value
s(log10(Depth))               4.000 2.693   0.547    0.00
s(I(DistTo125m/1000))         4.000 2.255   0.556    0.00
s(I(DistToCanyon/1000))       4.000 3.836   0.580    0.00
s(ClimSST)                    4.000 3.743   0.551    0.00
s(I(ClimDistToFront1^(1/3)))  4.000 0.867   0.625    0.03
s(log10(pmax(ClimEKE, 1e-04))) 4.000 0.930   0.584    0.00
```

```
Predictors retained during the model selection procedure: Depth, DistTo125m, DistToCanyon, ClimSST,
ClimDistToFront1, ClimEKE

Predictors dropped during the model selection procedure: Slope
```

Model term plots

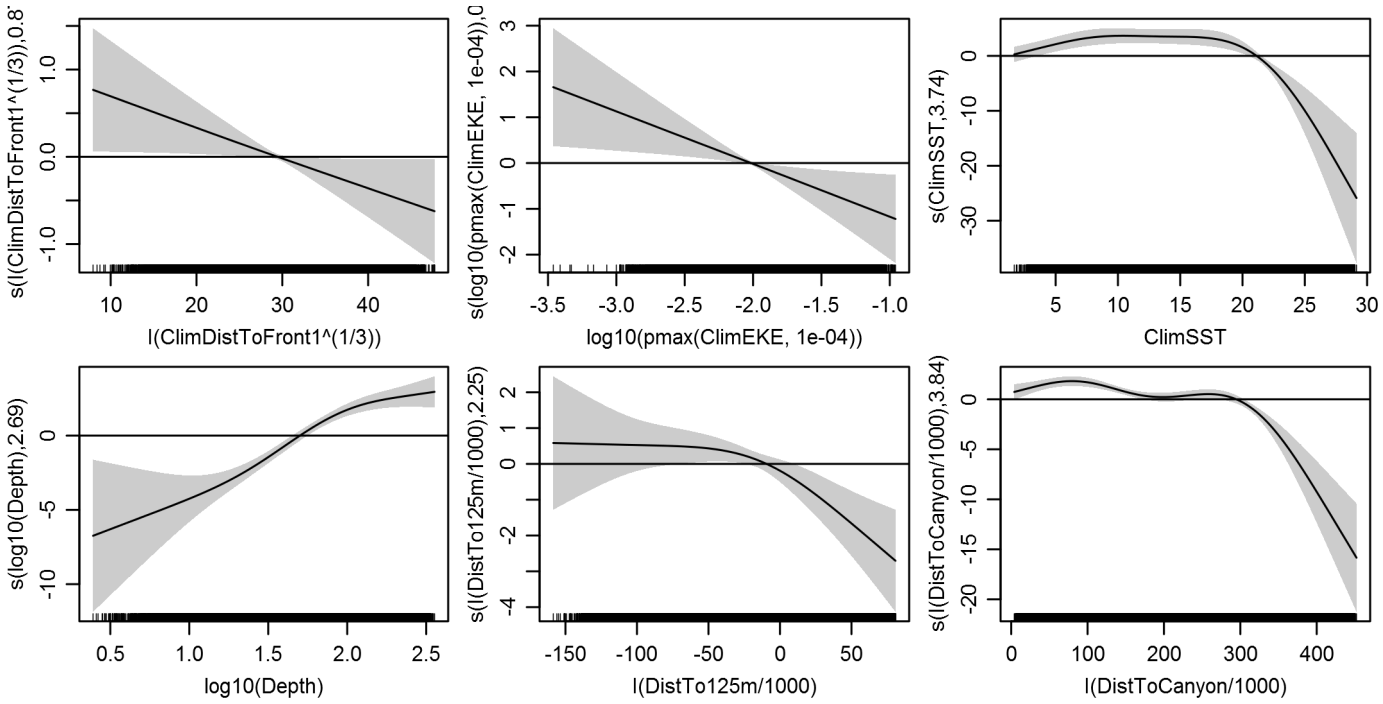

Diagnostic plots

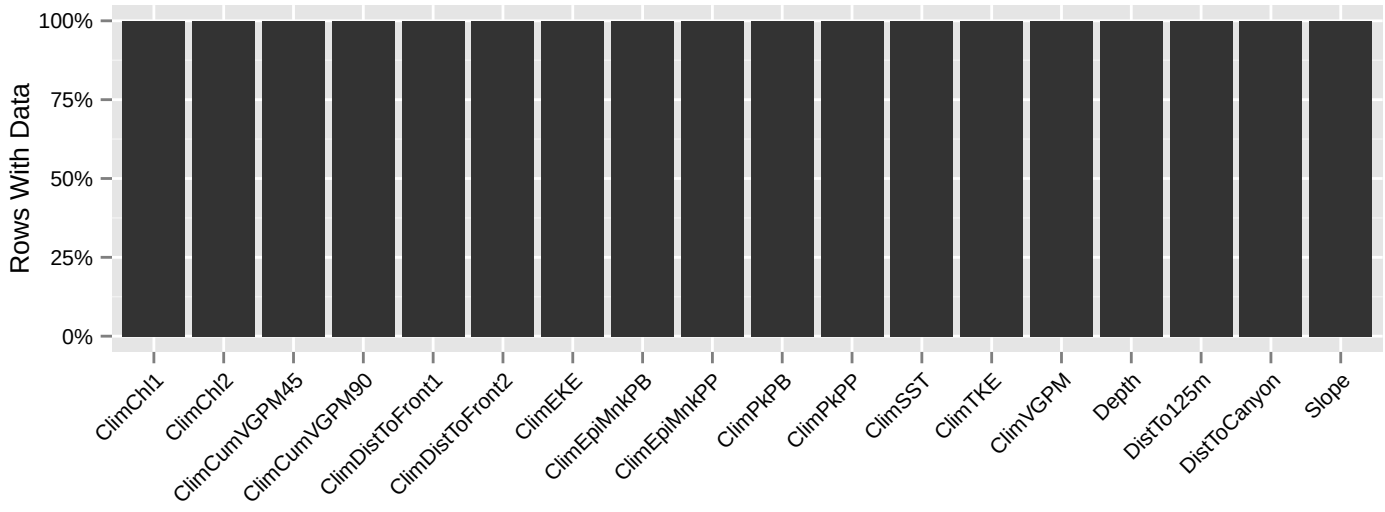

Figure 69: Segments with predictor values for the Pilot whales Climatological model, Shelf. This plot is used to assess how many segments would be lost by including a given predictor in a model.

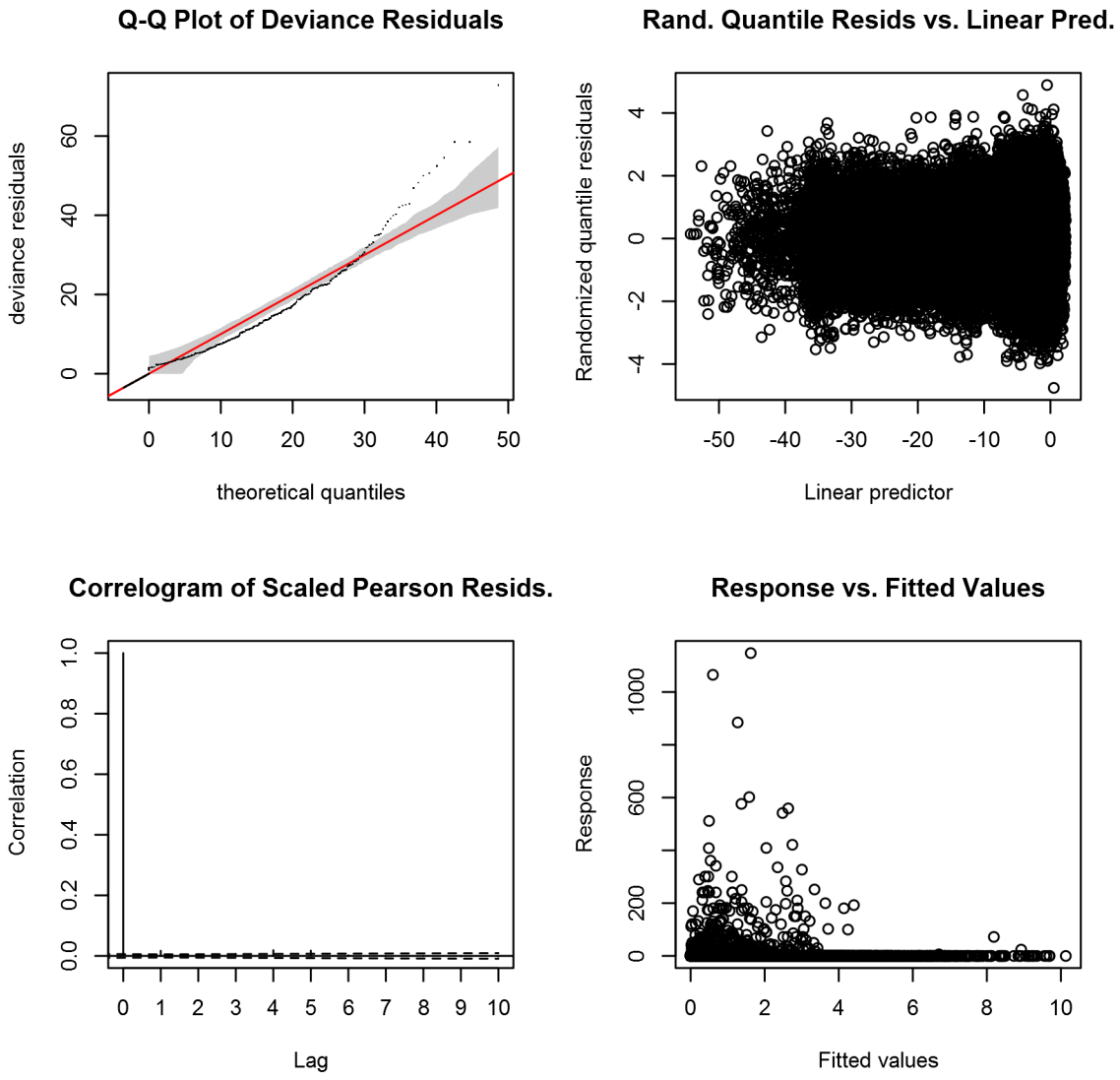

Figure 70: Statistical diagnostic plots for the Pilot whales Climatological model, Shelf.

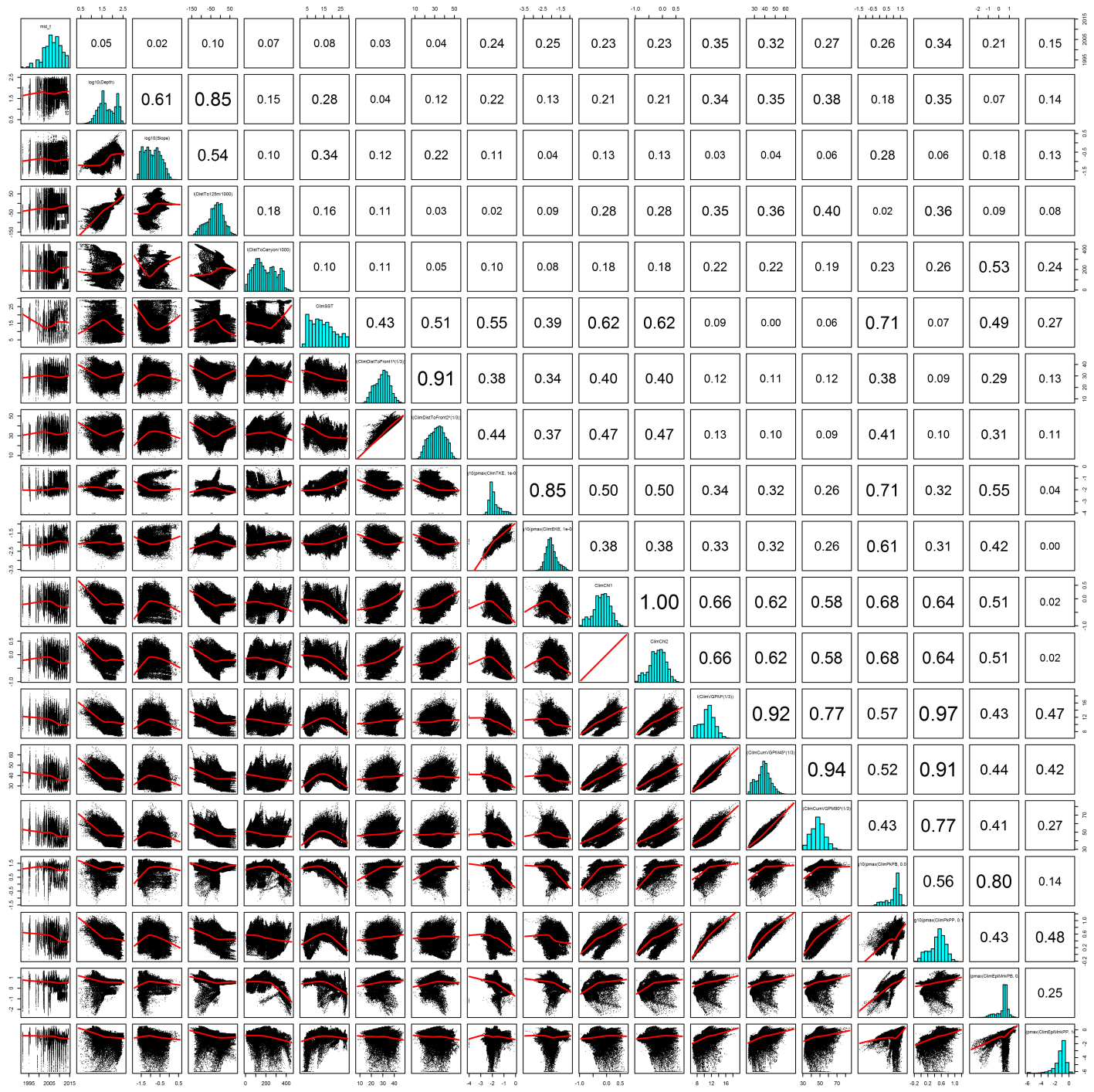

Figure 71: Scatterplot matrix for the Pilot whales Climatological model, Shelf. This plot is used to inspect the distribution of predictors (via histograms along the diagonal), simple correlation between predictors (via pairwise Pearson coefficients above the diagonal), and linearity of predictor correlations (via scatterplots below the diagonal). This plot is best viewed at high magnification.

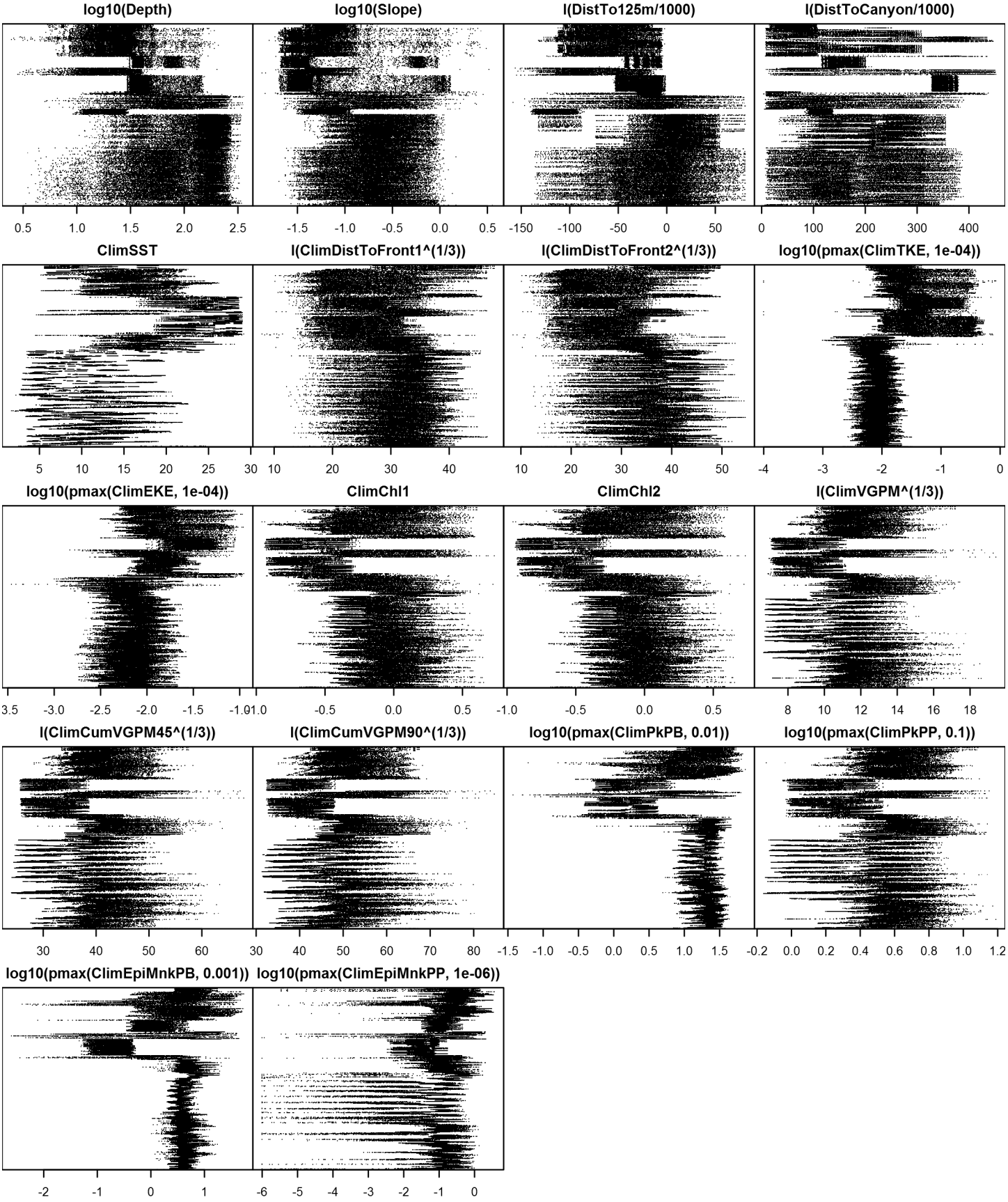

Figure 72: Dotplot for the Pilot whales Climatological model, Shelf. This plot is used to check for suspicious patterns and outliers in the data. Points are ordered vertically by transect ID, sequentially in time.

Model Comparison

Spatial Model Performance

The table below summarizes the performance of the candidate spatial models that were tested. For each subregion, the first model contained only physiographic predictors. Subsequent models added additional suites of predictors of based on when they became available via remote sensing.

For each model, three versions were fitted; the % Dev Expl columns give the % deviance explained by each one. The "climatological" models were fitted to 8-day climatologies of the environmental predictors. Because the environmental predictors were always available, no segments were lost, allowing these models to consider the maximal amount of survey data. The "contemporaneous" models were fitted to day-of-sighting images of the environmental predictors; these were smoothed to reduce data loss due to clouds, but some segments still failed to retrieve environmental values and were lost. Finally, the "climatological same segments" models fitted climatological predictors to the segments retained by the contemporaneous model, so that the explantory power of the two types of predictors could be directly compared. For each of the three models, predictors were selected independently via shrinkage smoothers; thus the three models did not necessarily utilize the same predictors.

Predictors derived from ocean currents first became available in January 1993 after the launch of the TOPEX/Poseidon satellite; productivity predictors first became available in September 1997 after the launch of the SeaWiFS sensor. Contemporaneous and climatological same segments models considering these predictors usually suffered data loss. Date Range shows the years spanned by the retained segments. The Segments column gives the number of segments retained; % Lost gives the percentage lost.

Predictors	Climatol % Dev Expl	Contemp % Dev Expl	Climatol Same Segs % Dev Expl	Segments	% Lost	Date Range
Slope and Abyss:						
Phys	30.0			17371		1992-2013
Phys+SST	32.8	32.7	32.8	17371	0.0	1992-2013
Phys+SST+Curr	35.2	33.0	35.2	17112	1.5	1995-2013
Phys+SST+Curr+Prod	36.3	36.5	38.7	16693	3.9	1998-2013
Shelf:						
Phys	27.6			86865		1992-2014
Phys+SST	33.2	33.3	33.2	86865	0.0	1992-2014
Phys+SST+Curr	33.8	33.2	33.5	85799	1.2	1995-2013
Phys+SST+Curr+Prod	34.1	33.3	33.0	83244	4.2	1998-2013

Table 22: Deviance explained by the candidate density models.

Abundance Estimates

The table below shows the estimated mean abundance (number of animals) within the study area, for the models that explained the most deviance for each model type. Mean abundance was calculated by first predicting density maps for a series of time steps, then computing the abundance for each map, and then averaging the abundances. For the climatological models, we used 8-day climatologies, resulting in 46 abundance maps. For the contemporaneous models, we used daily images, resulting in 365 predicted abundance maps per year that the prediction spanned. The Dates column gives the dates to which the estimates apply. For our models, these are the years for which both survey data and remote sensing data were available.

The Assumed g(0)=1 column specifies whether the abundance estimate assumed that detection was certain along the survey trackline. Studies that assumed this did not correct for availability or perception bias, and therefore underestimated abundance. The In our models column specifies whether the survey data from the study was also used in our models. If not, the study

provides a completely independent estimate of abundance.

Dates	Model or study	Estimated abundance	CV	Assumed g(0)=1	In our models
1992-2014	Climatological model*	18977	0.11	No	
1998-2013	Contemporaneous model	20983	0.09	No	
1992-2014	Climatological same segments model	22312	0.13	No	
Jun-Aug 2011	Central Florida to Central Virginia, short-finned only (Waring et al. 2014)	16946	0.43	No	No
Jun-Aug 2011	Central Virginia to lower Bay of Fundy, short-finned only	4569	0.67	No	No
Jun-Aug 2011	Central Florida to lower Bay of Fundy, short-finned only	21515	0.37	No	No
Jun-Aug 2011	Central Virginia to lower Bay of Fundy, long-finned only	5636	0.63	No	No
Jun-Aug 2011	Central Virginia to lower Bay of Fundy, both species combined	10205	0.43	No	No
Jun-Aug 2011	Central Florida to lower Bay of Fundy, both species combined	27151	0.31	No	No
August 2006	Southern Gulf of Maine to Bay of Fundy and Gulf of St. Lawrence, long-finned only (Waring 2011; Palka 2006)	26535	0.35	No	Yes
2006-2011	Central Florida to Bay of Fundy and Gulf of St. Lawrence, 2006 estimate for long-finned plus 2011 estimate for short-finned	48050		No	
Jun-Aug 2004	Florida to Bay of Fundy, both species combined (Waring 2011; Palka 2006)	36784	0.34	No	Yes

Table 23: Estimated mean abundance within the study area. We selected the model marked with * as our best estimate of the abundance and distribution of this taxon. For comparison, independent abundance estimates from NOAA technical reports and/or the scientific literature are shown. Please see the Discussion section below for our evaluation of our models compared to the other estimates. Note that our abundance estimates are averaged over the whole year, while the other studies may have estimated abundance for specific months or seasons. Our coefficients of variation (CVs) underestimate the true uncertainty in our estimates, as they only incorporated the uncertainty of the GAM stage of our models. Other sources of uncertainty include the detection functions and g(0) estimates. It was not possible to incorporate these into our CVs without undertaking a computationally-prohibitive bootstrap; we hope to attempt that in a future version of our models.

Density Maps

Climatological Model

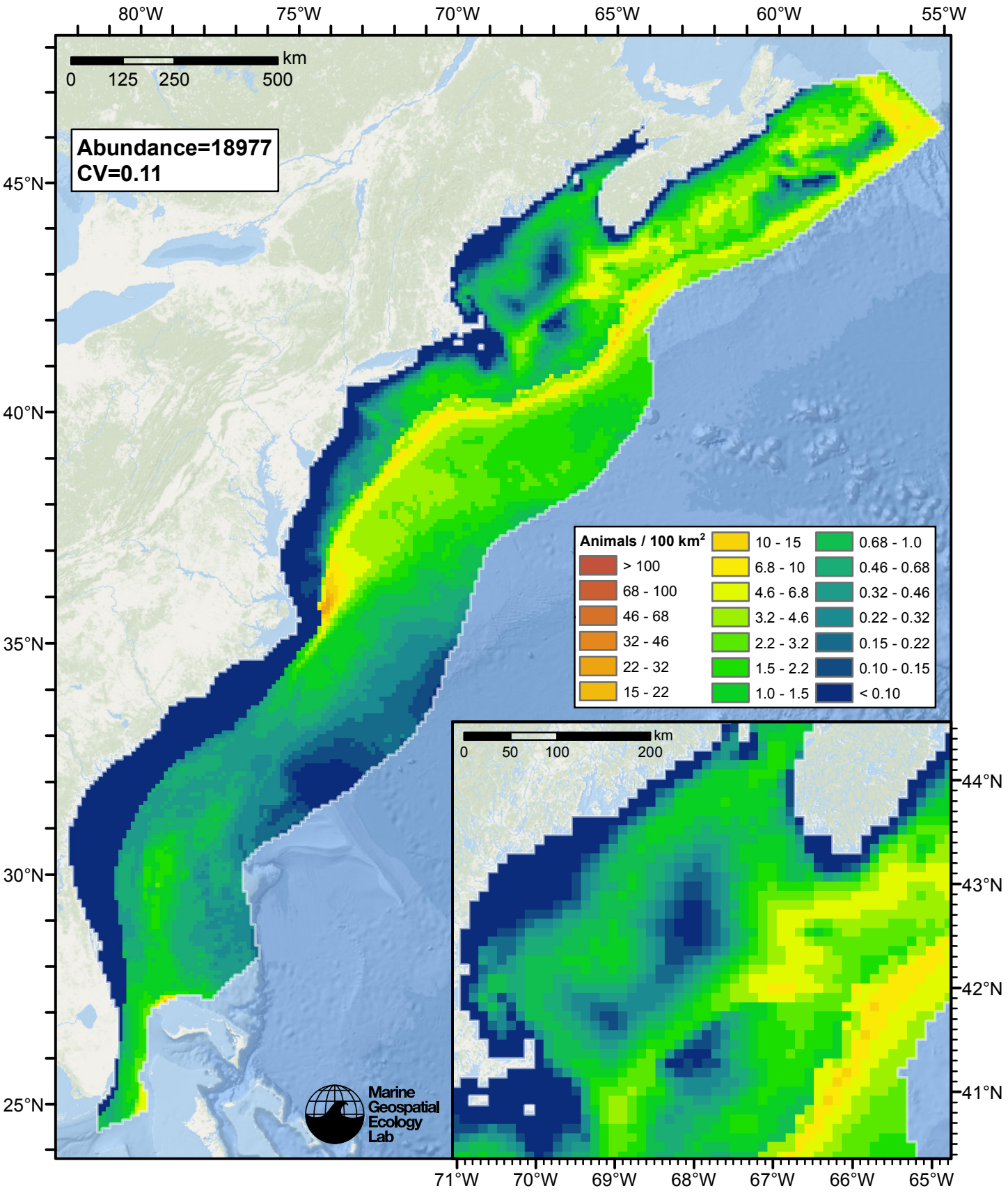

Figure 73: Pilot whales density and abundance predicted by the climatological model that explained the most deviance. Regions inside the study area (white line) where the background map is visible are areas we did not model (see text).

Contemporaneous Model

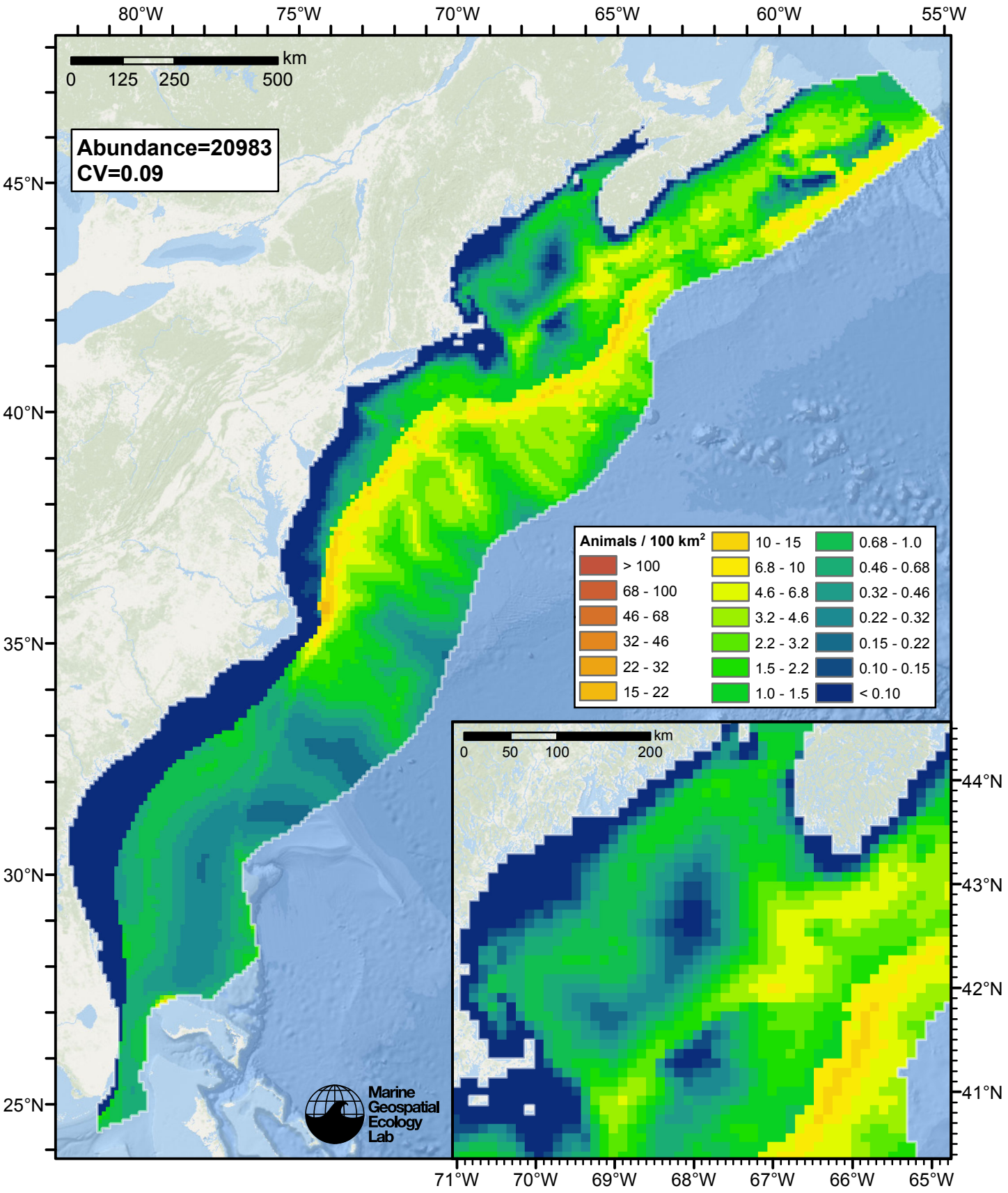

Figure 74: Pilot whales density and abundance predicted by the contemporaneous model that explained the most deviance. Regions inside the study area (white line) where the background map is visible are areas we did not model (see text).

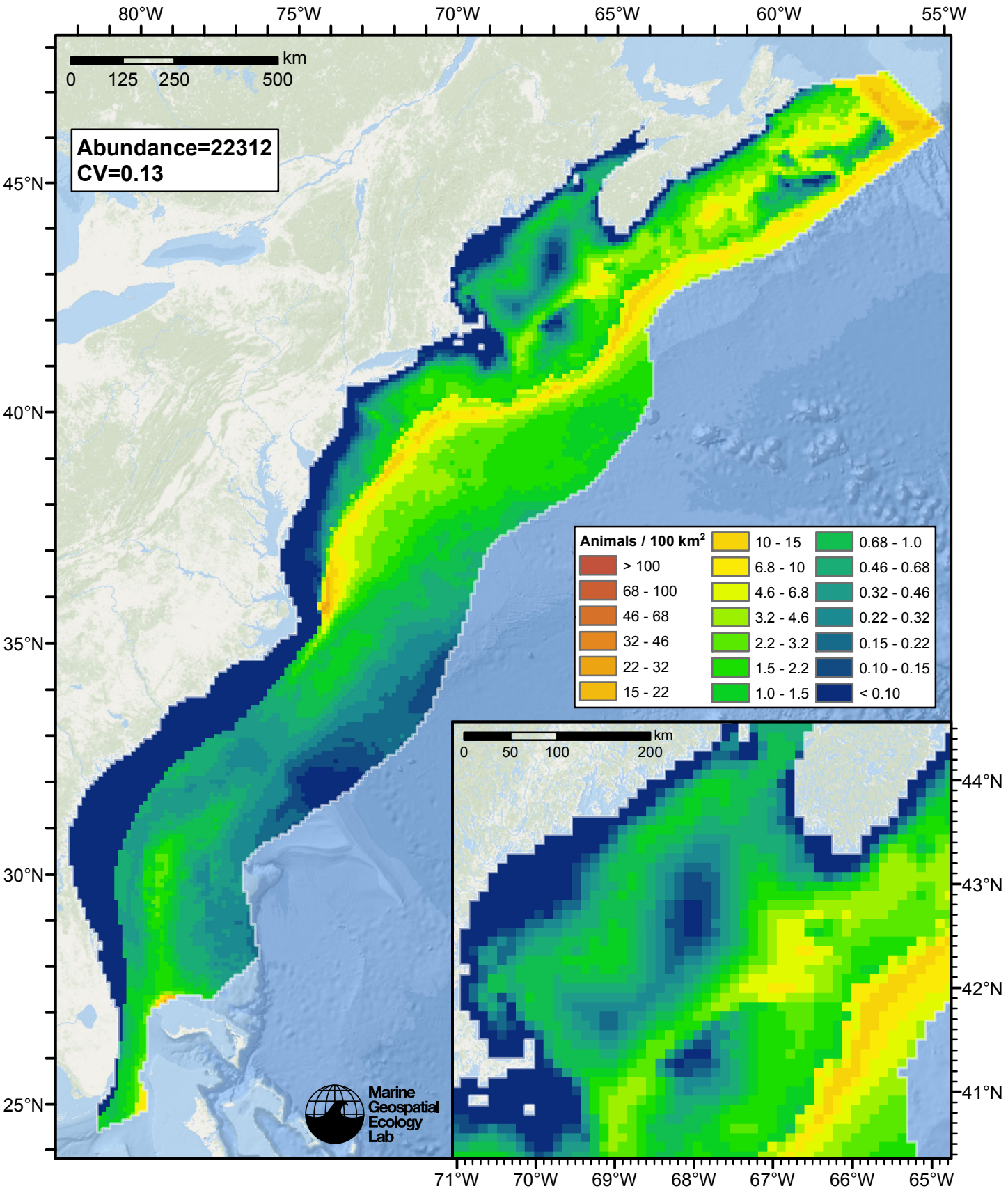

Figure 75: Pilot whales density and abundance predicted by the climatological same segments model that explained the most deviance. Regions inside the study area (white line) where the background map is visible are areas we did not model (see text).

Temporal Variability

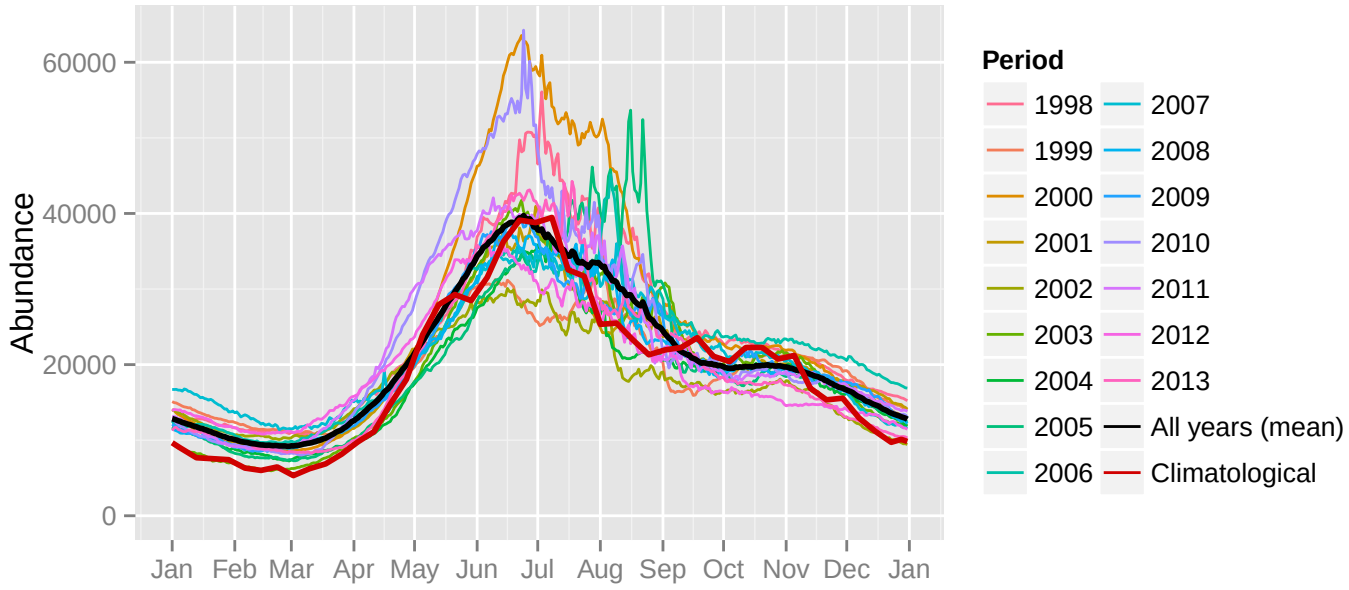

Figure 76: Comparison of Pilot whales abundance predicted at a daily time step for different time periods. Individual years were predicted using contemporaneous models. "All years (mean)" averages the individual years, giving the mean annual abundance of the contemporaneous model. "Climatological" was predicted using the climatological model. The results for the climatological same segments model are not shown.

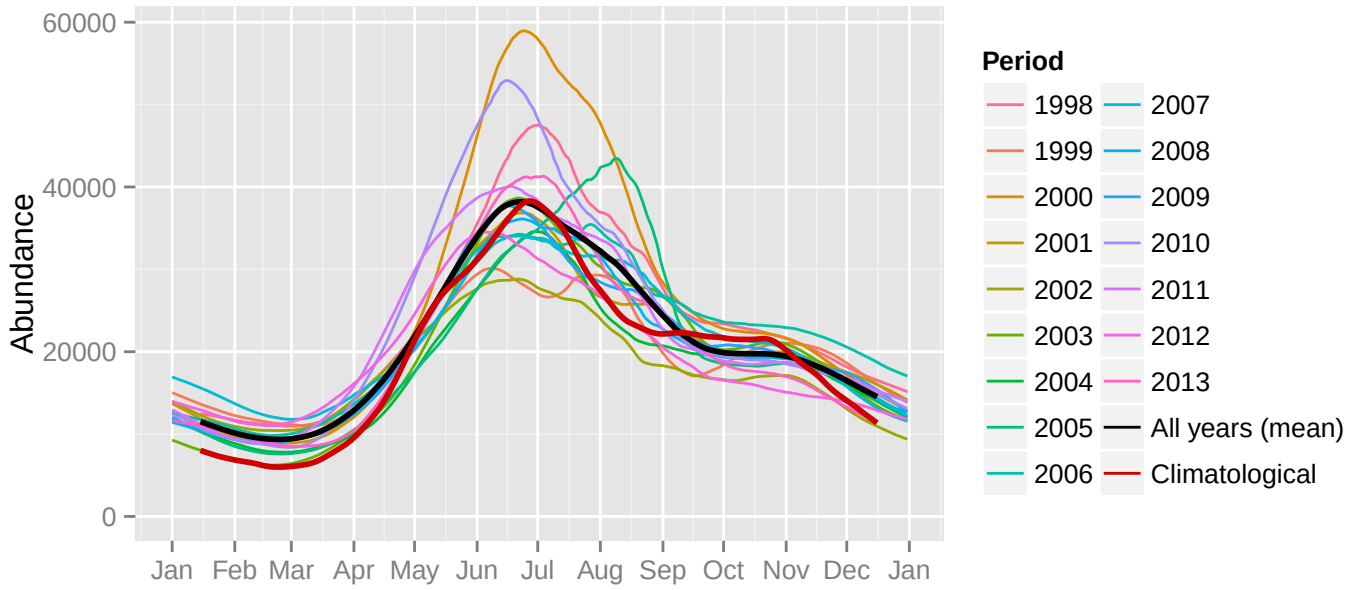

Figure 77: The same data as the preceding figure, but with a 30-day moving average applied.

Climatological Model

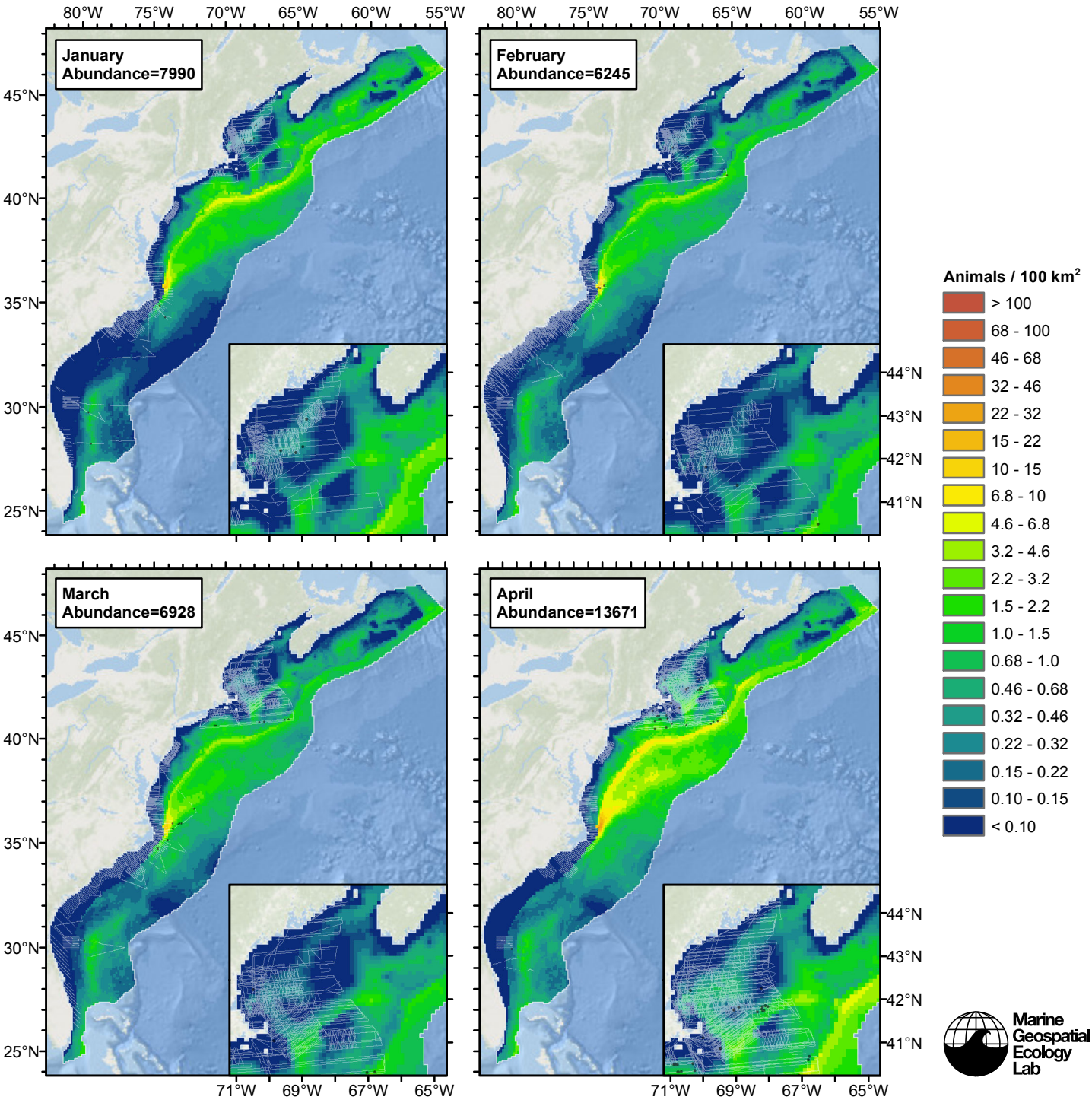

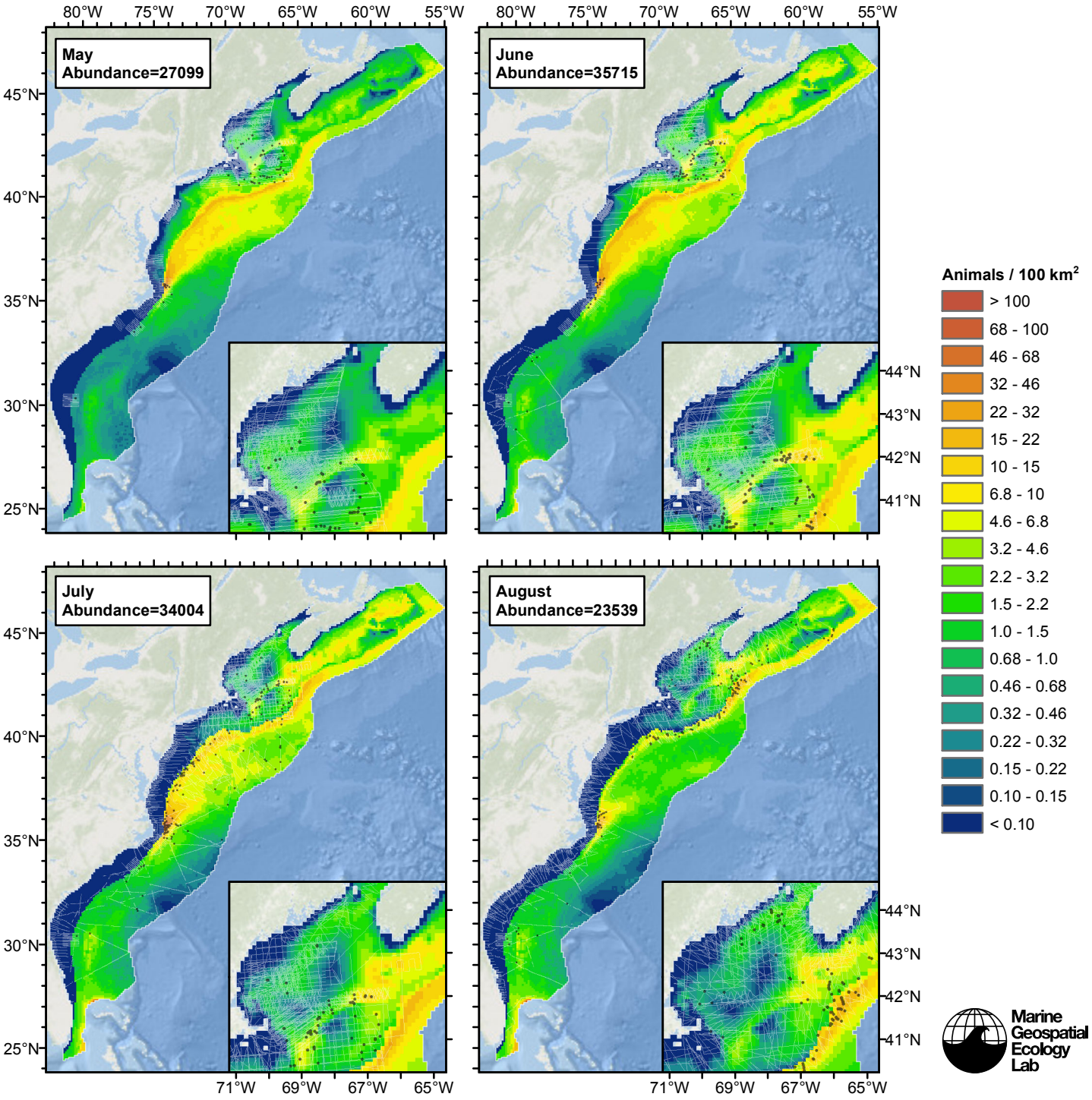
May
Abundance=27099
June
Abundance=35715
July
Abundance=34004
August
Abundance=23539
80°W
75°W
70°W
65°W
60°W
55°W
45°N
40°N
35°N
30°N
25°N
44°N
43°N
42°N
41°N
71°W
69°W
67°W
65°W
Animals / 100 km²
> 100
68 - 100
46 - 68
32 - 46
22 - 32
15 - 22
10 - 15
6.8 - 10
4.6 - 6.8
3.2 - 4.6
2.2 - 3.2
1.5 - 2.2
1.0 - 1.5
0.68 - 1.0
0.46 - 0.68
0.32 - 0.46
0.22 - 0.32
0.15 - 0.22
0.10 - 0.15
< 0.10
Marine
Geospatial
Ecology
Lab

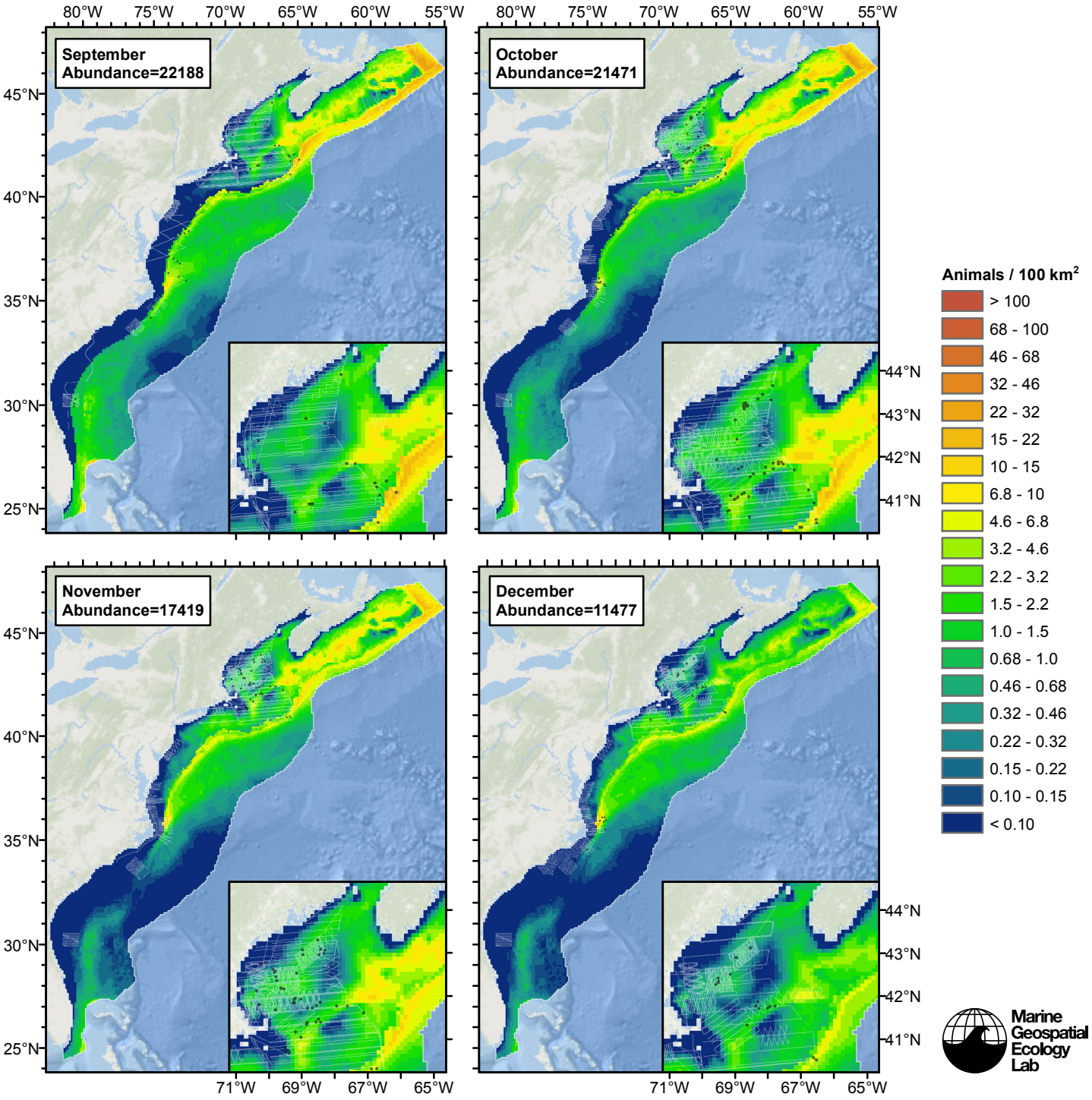
September
Abundance=22188
October
Abundance=21471
November
Abundance=17419
December
Abundance=11477
80°W
75°W
70°W
65°W
60°W
55°W
45°N
40°N
35°N
30°N
25°N
44°N
43°N
42°N
41°N
71°W
69°W
67°W
65°W
Animals / 100 km²
> 100
68 - 100
46 - 68
32 - 46
22 - 32
15 - 22
10 - 15
6.8 - 10
4.6 - 6.8
3.2 - 4.6
2.2 - 3.2
1.5 - 2.2
1.0 - 1.5
0.68 - 1.0
0.46 - 0.68
0.32 - 0.46
0.22 - 0.32
0.15 - 0.22
0.10 - 0.15
< 0.10
Marine
Geospatial
Ecology
Lab

Contemporaneous Model

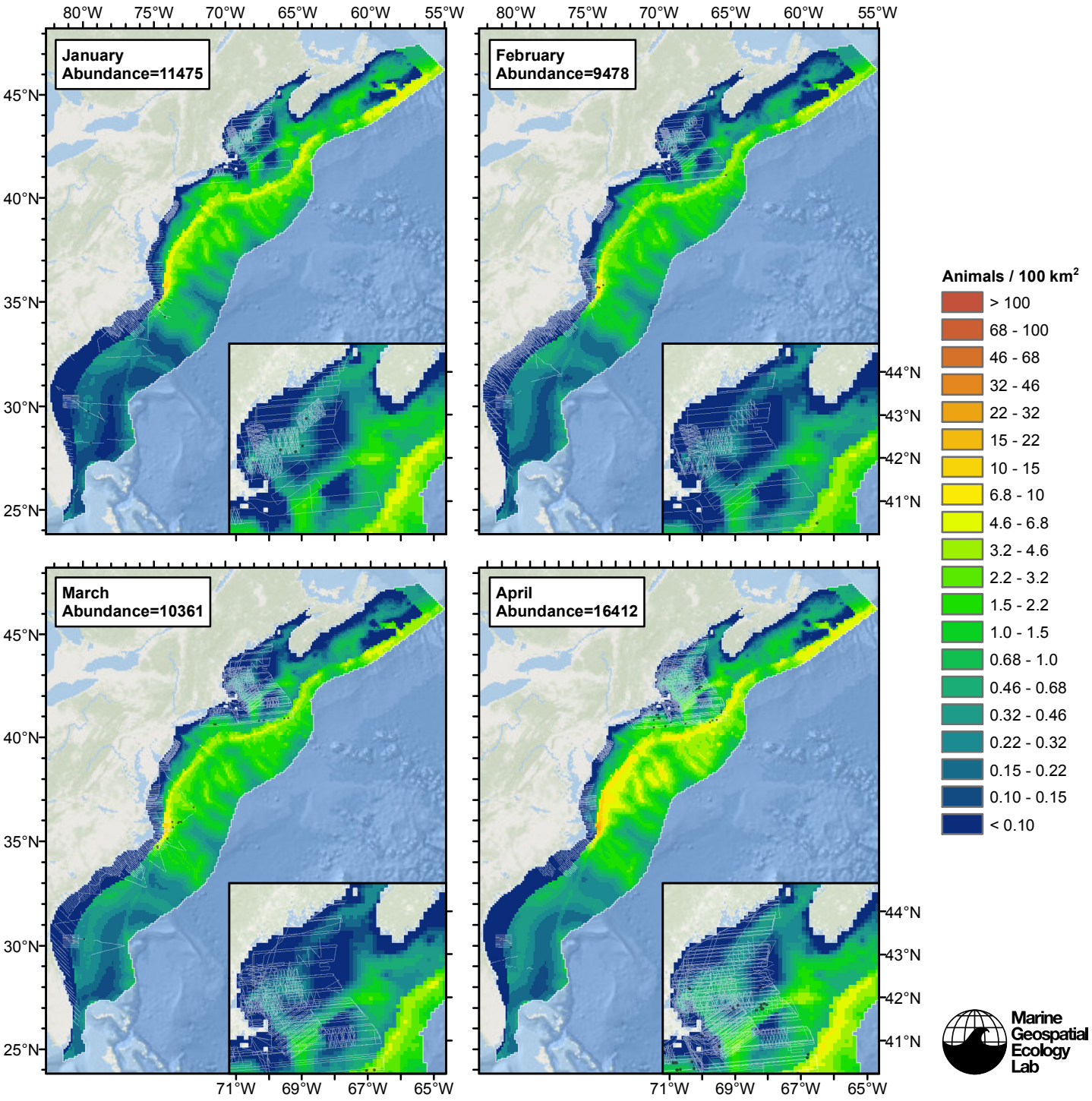

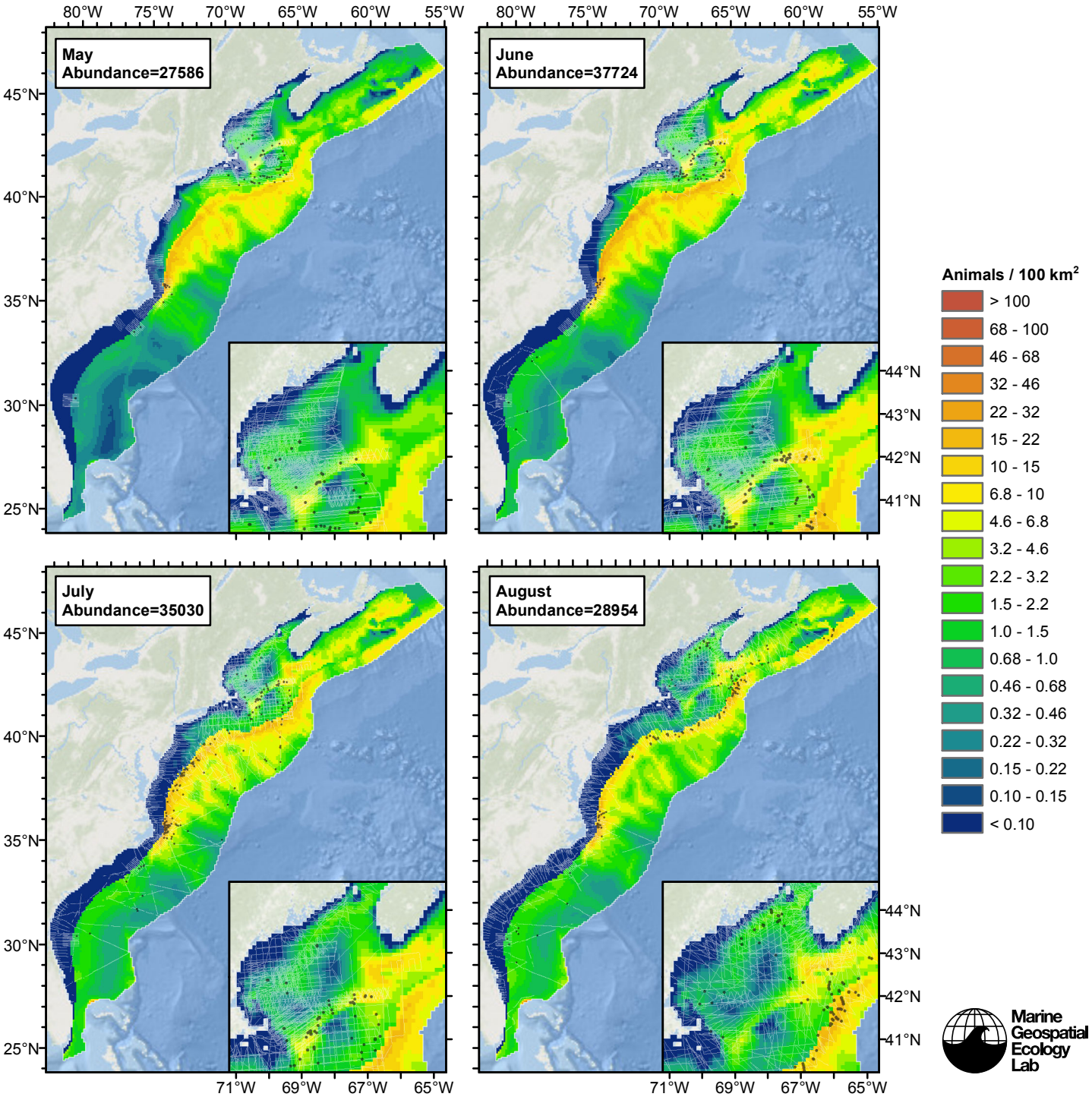
May
Abundance=27586
June
Abundance=37724
July
Abundance=35030
August
Abundance=28954
80°W
75°W
70°W
65°W
60°W
55°W
45°N
40°N
35°N
30°N
25°N
44°N
43°N
42°N
41°N
71°W
69°W
67°W
65°W
Animals / 100 km²
> 100
68 - 100
46 - 68
32 - 46
22 - 32
15 - 22
10 - 15
6.8 - 10
4.6 - 6.8
3.2 - 4.6
2.2 - 3.2
1.5 - 2.2
1.0 - 1.5
0.68 - 1.0
0.46 - 0.68
0.32 - 0.46
0.22 - 0.32
0.15 - 0.22
0.10 - 0.15
< 0.10
Marine
Geospatial
Ecology
Lab

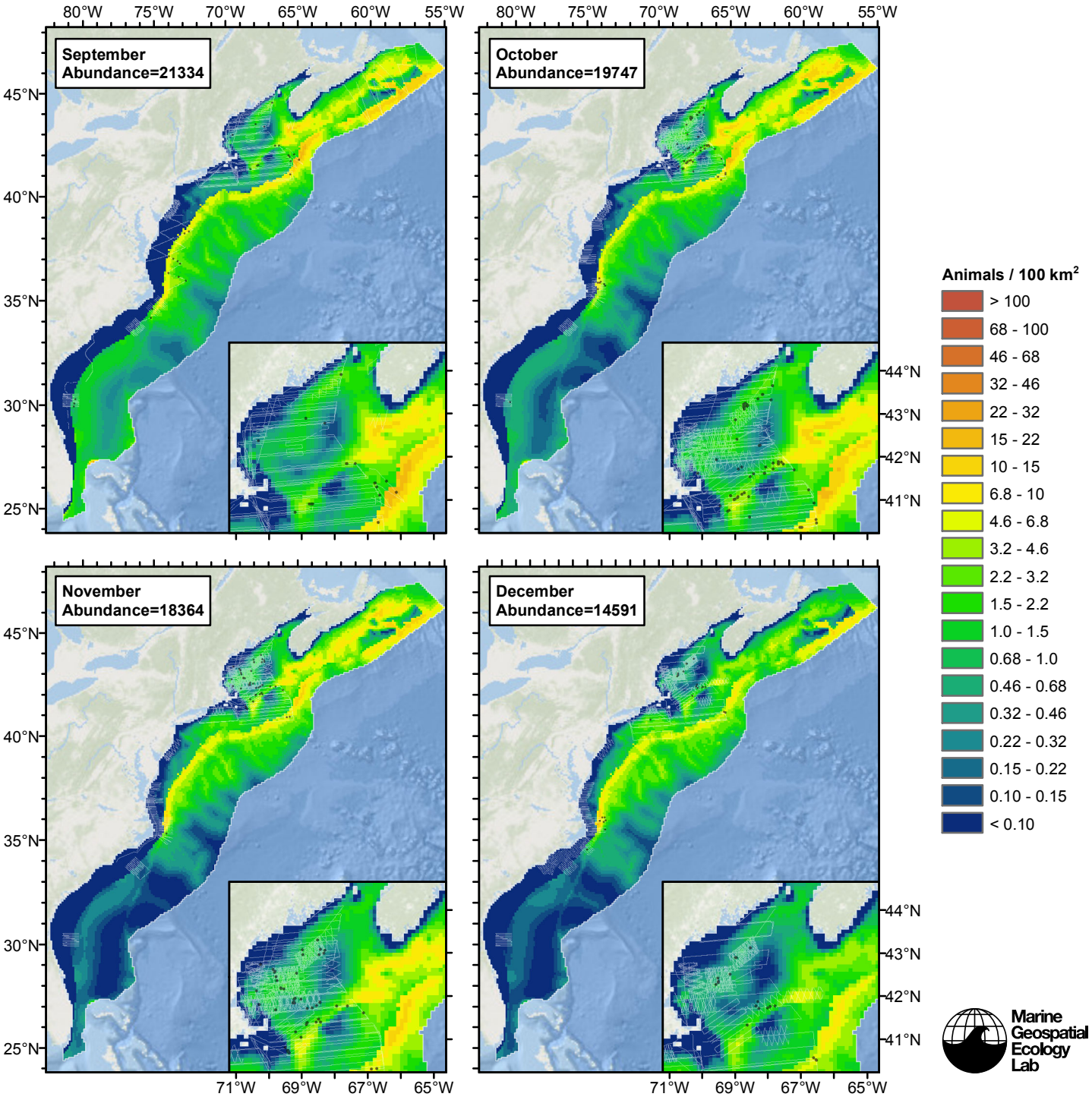
September
Abundance=21334
October
Abundance=19747
November
Abundance=18364
December
Abundance=14591
80°W
75°W
70°W
65°W
60°W
55°W
45°N
40°N
35°N
30°N
25°N
44°N
43°N
42°N
41°N
71°W
69°W
67°W
65°W
Animals / 100 km²
> 100
68 - 100
46 - 68
32 - 46
22 - 32
15 - 22
10 - 15
6.8 - 10
4.6 - 6.8
3.2 - 4.6
2.2 - 3.2
1.5 - 2.2
1.0 - 1.5
0.68 - 1.0
0.46 - 0.68
0.32 - 0.46
0.22 - 0.32
0.15 - 0.22
0.10 - 0.15
< 0.10
Marine
Geospatial
Ecology
Lab

Climatological Same Segments Model

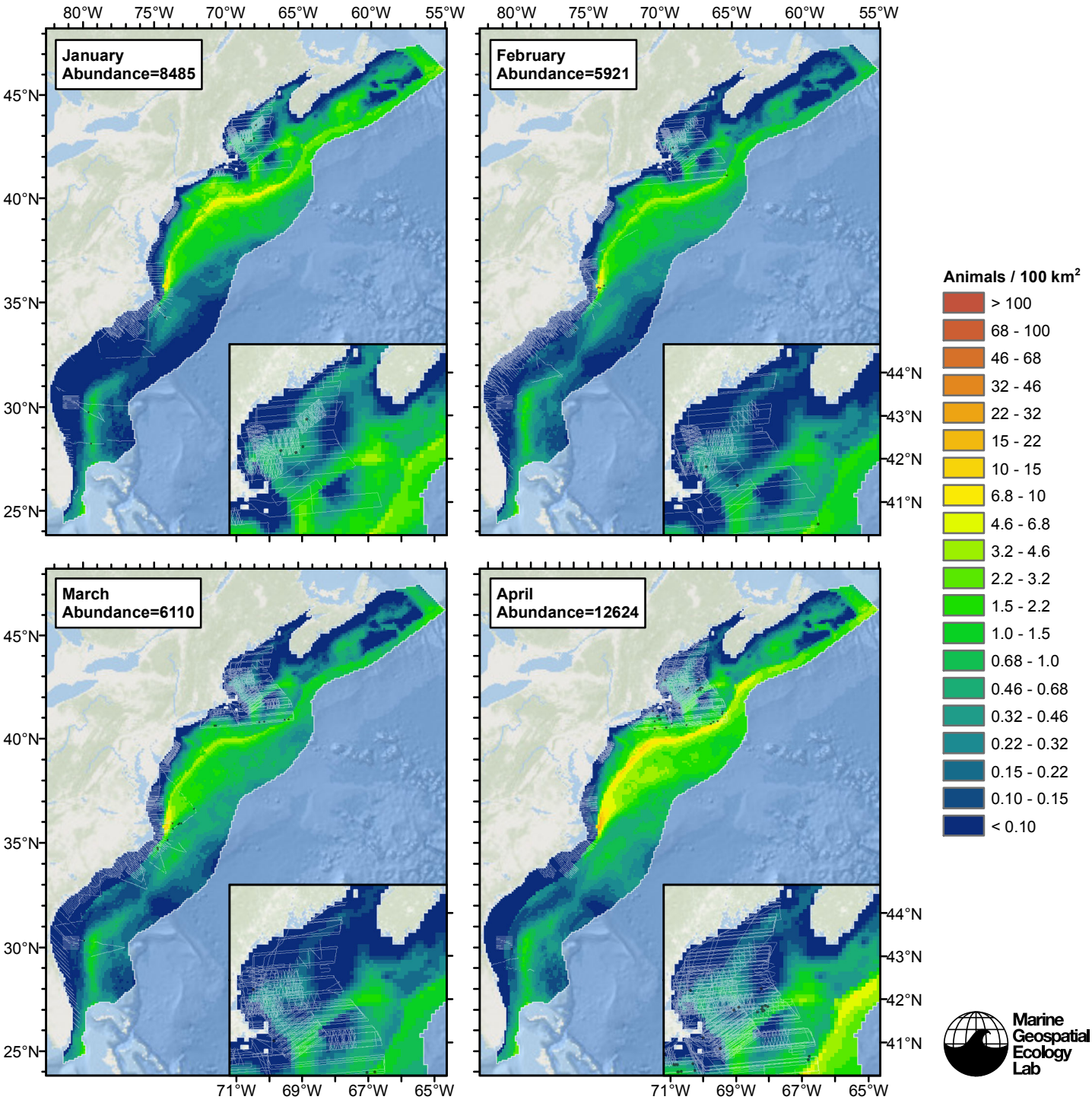

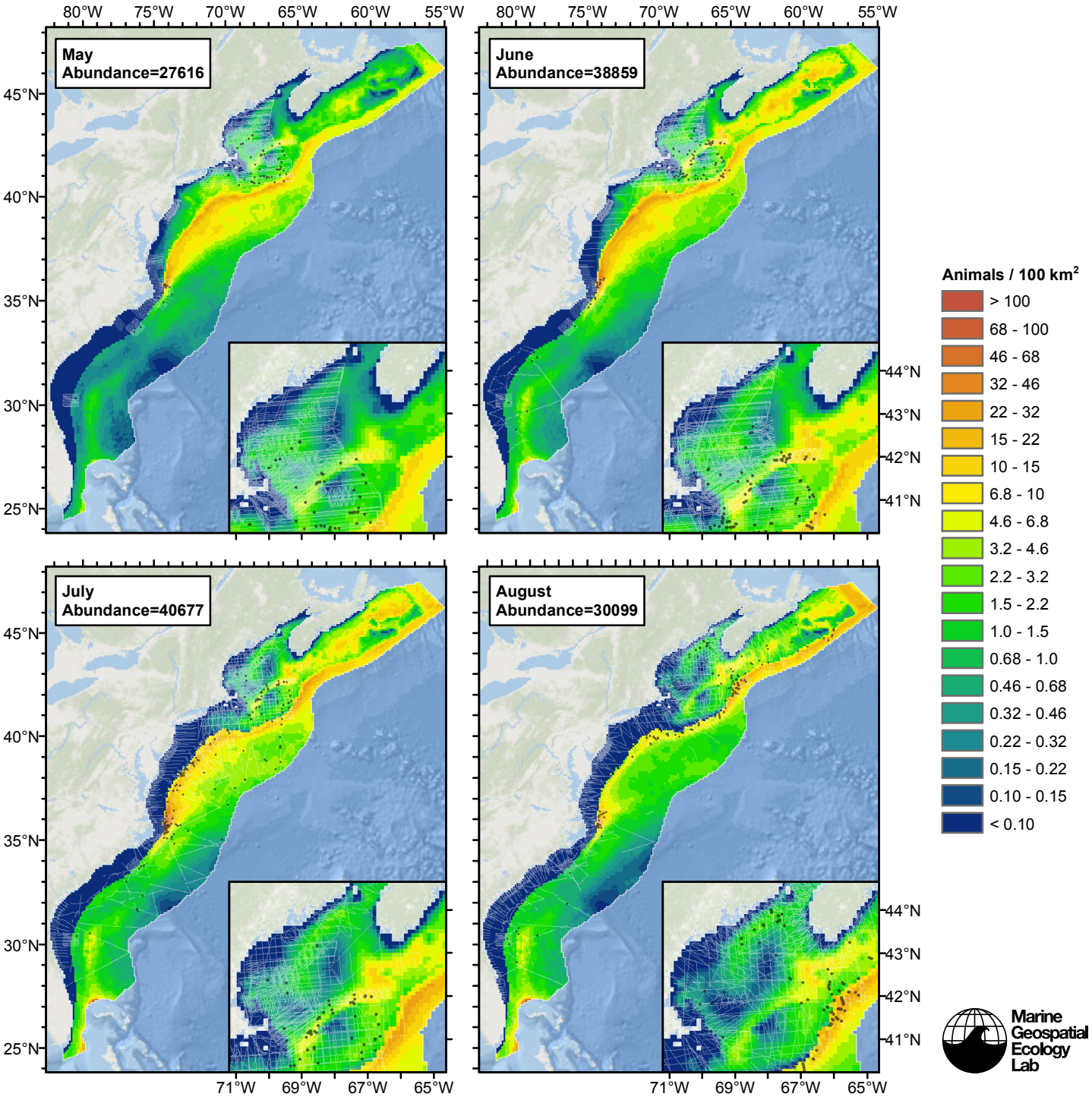
May
Abundance=27616
June
Abundance=38859
July
Abundance=40677
August
Abundance=30099
80°W
75°W
70°W
65°W
60°W
55°W
45°N
40°N
35°N
30°N
25°N
44°N
43°N
42°N
41°N
71°W
69°W
67°W
65°W
Animals / 100 km²
> 100
68 - 100
46 - 68
32 - 46
22 - 32
15 - 22
10 - 15
6.8 - 10
4.6 - 6.8
3.2 - 4.6
2.2 - 3.2
1.5 - 2.2
1.0 - 1.5
0.68 - 1.0
0.46 - 0.68
0.32 - 0.46
0.22 - 0.32
0.15 - 0.22
0.10 - 0.15
< 0.10
Marine
Geospatial
Ecology
Lab

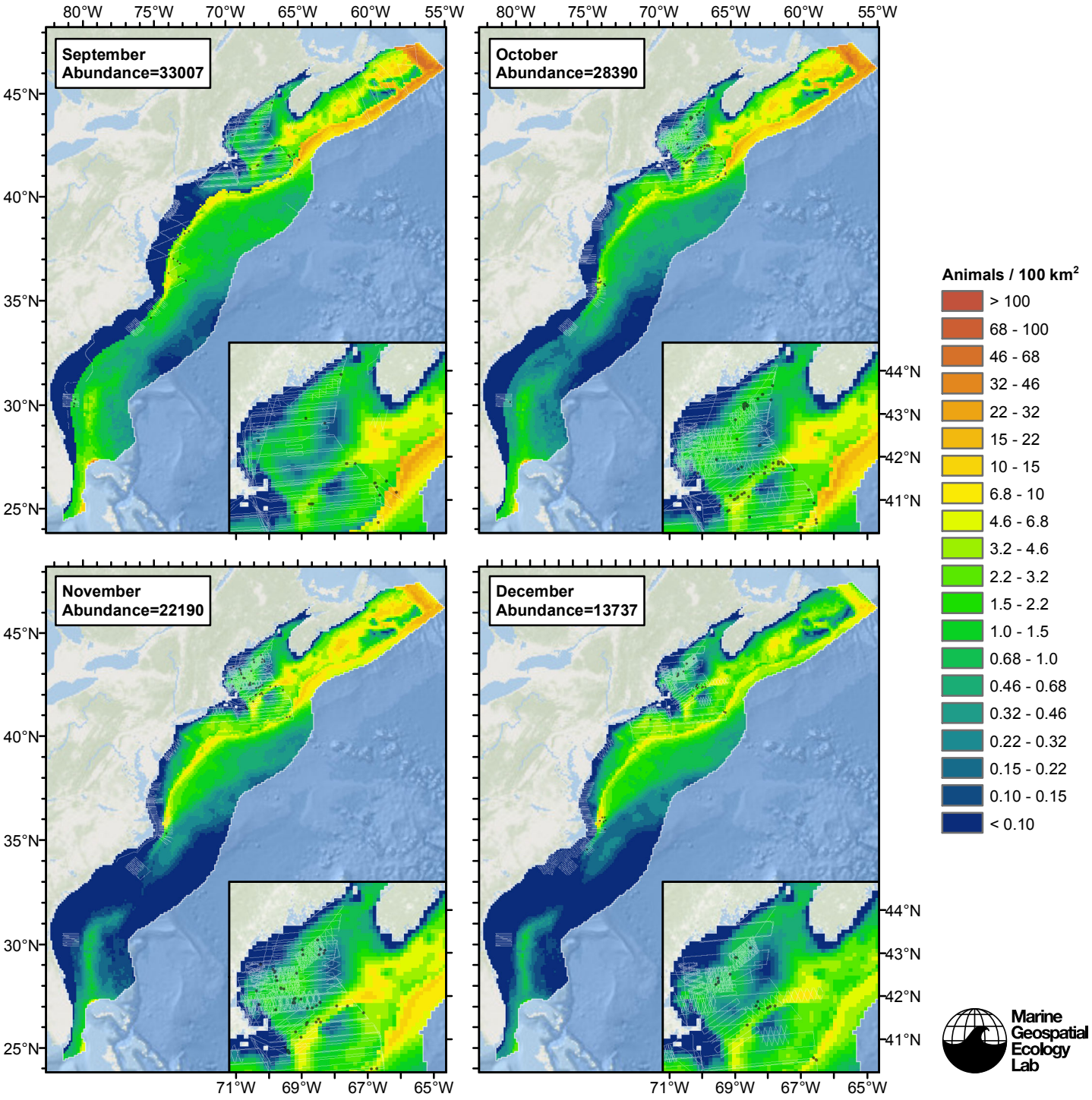

Discussion

In both geographic subregions, the models fitted using contemporaneous predictors explained slightly less deviance than the models fitted to the same segments using climatological predictors, suggesting that climatological predictors had slightly more explanatory power than contemporaneous predictors for this pilot whales guild. On this basis, we selected the models fitted to all segments with climatological predictors as our best estimate of pilot whale distribution and abundance.

Both models retained many predictors, indicative of the large number of segments with sightings and the complex spatial and temporal patterns in distribution. In the Shelf subregion, where there was some survey effort every month of the year in the Gulf of Maine (but a strong bias towards spring and summer), pilot whales were predicted to be present in the Gulf of Maine in low densities in January-March, then move progressively north through U.S. waters from April-August, with U.S. Gulf of

Maine abundance peaking in June and then diminishing to a low in September, followed by a return in October and then a decrease through December. This is in rough concordance with Payne and Heinemann's (1993) description of a seasonal clockwise progression around the Gulf of Maine.

The Shelf model also predicted high abundance along the middle of the Scotian Shelf from June-October, although this region was only surveyed in August, for which the model predicted the least abundance during the June-October period–a reason to view these predictions with caution. However, the predictions of high abundance on the Scotian Shelf in summer are supported by results from the Canadian TNASS survey conducted in July 2007, which reported sightings of 36 pilot whale groups along the Scotian Shelf (Lawson and Gosselin 2009). We believe our models could be improved by incorporating the Canadian TNASS survey. We made several attempts to contact J. Lawson regarding this survey, in the hope of incorporating it into our models, but received no response. We remain hopeful that a collaboration can be established in the future, and the Canadian TNASS data may be incorporated into a new version of our models.

The model for the Slope and Abyss subregion predicted strong seasonal changes in density, with a low in January-March and a peak in May-July. Although several sections of the shelf break from Florida to Virginia were surveyed year-round, surveying in the north occurred almost exclusively in the June-August period. Also, deep-water areas far from the shelf break were only surveyed fully in July, with a few transects in the southeast in June, August, February, and March.

Although the Shelf model's predictions were in concordance Payne and Heinemann's (1993) description of seasonal shifts in long-finned pilot whale distribution along the northeast shelf and slope, comparatively little was available in the literature for deep-water areas far from the shelf. Our Slope and Abyss model's predictions of strong seasonal variability in density were based on survey effort that was seasonally sparse. We are not comfortable recommending that monthly predictions of such strong seasonal variability be used without incorporating additional data. We will revisit this possibility in our next model update, when we expect to incorporate the NOAA Atlantic Marine Assessment Program for Protected Species (AMAPPS) surveys for 2010-2014, which NOAA did not make available for the current study. The AMAPPS surveys include two additional years of off-shelf surveying in summer (June-September), and one survey of the northeast shelf break in March-April 2014. Until that update, we recommend that our average year-round pilot whale density prediction be used.

Our models predicted a mean year-round abundance of 18,977 pilot whales across the study area, with a peak of 35,715 in June and a low of 6245 in February. Although we recommend our year-round average density prediction be used, the year-round abundance estimate derived from it does not compare well to NOAA's summertime abundance estimates. As of this writing, NOAA designated its August 2006 estimate of 26,535 long-finned pilot whales as its best estimate, from an aerial survey of the southern Gulf of Maine to the Bay of Fundy and Gulf of St. Lawrence (Waring et al. 2014). For short-finned pilot whales, NOAA designated its June-August 2011 estimate of 21,515 from combined surveys of Florida to lower Bay of Fundy region. Added together, NOAA's best estimate of the two species together, in summer, was 48,050 pilot whales, substantially more than our June estimate of 35,715.

We can suggest two explanations for this result. First, NOAA's pilot whale abundance estimates show substantial year-to-year variability. For the Florida to Bay of Fundy region, NOAA estimated 36,784 pilot whales (both species together) in 2004 and 27,151 in 2011, a difference of 21%. If this represents typical year-to-year variance, it may not be surprising that our estimate, based on many years of surveying, would differ substantially from NOAA's estimates taken from two particular years.

Second, in its 2006 estimate, NOAA utilized a lower g(0) value (0.43) for aerial surveys that was 41% lower than our g(0) estimate (0.607). Had NOAA utilized our higher g(0) estimate instead, their 2006 abundance estimate would have been roughly 29% lower, at about 18,800 long-finned pilot whales, a difference of about 7700. Subtracting this from their combined 48,050 estimate yields 40,350, which is much closer to our peak estimate of 35,715. We based our aerial g(0) estimate on percent-time-at-surface data, rather than NOAA's 2006 g(0) estimate for small cetaceans (Palka 2006), based on reports that short-finned pilot whales spend significant bouts of time resting or socializing at the surface often during the daytime, interspersed with bouts of diving to forage, often at night (Alves et al. 2013). This behavior would make pilot whales more available to be seen at the surface than other cetaceans that were included in Palka's (2006) g(0) estimate.

In conclusion, our models predict a realistic density surface for the combined pilot whales guild. The density surface represents mean year-round density, which is likely to be lower than typical summer density. It may be higher than typical winter density, but this is less certain. With more data, it may be possible offer predictions confidently at monthly temporal resolution. Until then, model users should be mindful that density may be higher in summer months and lower in winter than indicated by our year-round density surface.

Finally, we note high pilot whale density was predicted throughout the year at an area of the shelf break and continental slope north of where the Gulf Stream separates from the shelf at Cape Hatteras. Sightings were reported in this vicinity in nearly every month of the year. Marine spatial planners seeking to site activities that are potentially harmful to pilot whales would be well advised to avoid this area at all times.

References

Alves F, Dinis A, Ribeiro C, Nicolau C, Kaufmann M, Fortuna CM, et al. (2013) Daytime dive characteristics from six short-finned pilot whales Globicephala macrorhynchus off Madeira Island. Arquipelago - Life and Marine Sciences 31: 1-8.

Barlow J (2006) Cetacean abundance in Hawaiian waters estimated from a summer/fall survey in 2002. Marine Mammal Science 22: 446-464.

Barlow J, Forney KA, Von Saunder A, Urban-Ramirez J (1997) A report of cetacean acoustic detection and dive interval studies (CADDIS) conducted in the southern Gulf of California. NOAA Technical Memorandum NOAA-TM-NMFS-SWFSC-250. 48 p.

Heide-Jorgensen MP, Bloch D, Stefansson E, Mikkelsen B, Ofstad LH, Dietz R (2002) Diving behaviour of long-finned pilot whales Globicephala melas around the Faroe Islands. Wildlife Biology 8: 307-313.

Hooker SK, Fahlman A, Moore MJ, Soto NA de, Quiros YB de, Brubakk AO, et al. (2012) Deadly diving? Physiological and behavioural management of decompression stress in diving mammals. Proc R Soc B 279: 1041-1050.

Lawson JW, Gosselin J-F (2009) Distribution and preliminary abundance estimates for cetaceans seen during Canada's Marine Megafauna Survey-A component of the 2007 TNASS. DFO Can. Sci. Advis. Sec. Res. Doc. 2009/031. 28 p. Available online: http://biblio.uqar.qc.ca/archives/30125408.pdf

Olson PA (2008) Pilot whales: Globicephala melas and G. muerorhynchus. In: Encyclopedia of Marine Mammals, 2nd ed. (Perrin WF, Wursig B, Thewissen JGM, eds.) Academic Press, San Diego, California. pp. 847-852.

Palka DL (2006) Summer Abundance Estimates of Cetaceans in US North Atlantic Navy Operating Areas. US Dept Commer, Northeast Fish Sci Cent Ref Doc. 06-03: 41 p.

Payne PM, Heinemann DW (1993) The distribution of pilot whales in shelf/shelf edge and slope waters of the northeastern United States, 1978-1988. Report of the International Whaling Commission (Special Issue 14): 51- 68.

Waring GT, Josephson E, Maze-Foley K, Rosel PE, eds. (2014) U.S. Atlantic and Gulf of Mexico Marine Mammal Stock Assessments – 2013. NOAA Tech Memo NMFS NE 228; 464 p.

Wells RS, Fougeres EM, Cooper AG, Stevens RO, Brodsky M, Lingenfelser R, et al. (2013) Movements and Dive Patterns of Short-Finned Pilot Whales (Globicephala macrorhynchus) Released from a Mass Stranding in the Florida Keys. Aquatic Mammals 39: 61-72.